NASA/CR—2000-209921/VOL1

DHC-6 Twin Otter Tailplane Airfoil Section Testing in the Ohio State University 7x10 Wind Tunnel

Dale Hiltner, Michael McKee, Karine La Noé, and Gerald Gregorek
Ohio State University, Columbus, Ohio

September 2000

The NASA STI Program Office . . . in Profile

Since its founding, NASA has been dedicated to the advancement of aeronautics and space science. The NASA Scientific and Technical Information (STI) Program Office plays a key part in helping NASA maintain this important role.

The NASA STI Program Office is operated by Langley Research Center, the Lead Center for NASA's scientific and technical information. The NASA STI Program Office provides access to the NASA STI Database, the largest collection of aeronautical and space science STI in the world. The Program Office is also NASA's institutional mechanism for disseminating the results of its research and development activities. These results are published by NASA in the NASA STI Report Series, which includes the following report types:

- TECHNICAL PUBLICATION. Reports of completed research or a major significant phase of research that present the results of NASA programs and include extensive data or theoretical analysis. Includes compilations of significant scientific and technical data and information deemed to be of continuing reference value. NASA's counterpart of peer-reviewed formal professional papers but has less stringent limitations on manuscript length and extent of graphic presentations.

- TECHNICAL MEMORANDUM. Scientific and technical findings that are preliminary or of specialized interest, e.g., quick release reports, working papers, and bibliographies that contain minimal annotation. Does not contain extensive analysis.

- CONTRACTOR REPORT. Scientific and technical findings by NASA-sponsored contractors and grantees.

- CONFERENCE PUBLICATION. Collected papers from scientific and technical conferences, symposia, seminars, or other meetings sponsored or cosponsored by NASA.

- SPECIAL PUBLICATION. Scientific, technical, or historical information from NASA programs, projects, and missions, often concerned with subjects having substantial public interest.

- TECHNICAL TRANSLATION. English-language translations of foreign scientific and technical material pertinent to NASA's mission.

Specialized services that complement the STI Program Office's diverse offerings include creating custom thesauri, building customized data bases, organizing and publishing research results . . . even providing videos.

For more information about the NASA STI Program Office, see the following:

- Access the NASA STI Program Home Page at ***http://www.sti.nasa.gov***

- E-mail your question via the Internet to help@sti.nasa.gov

- Fax your question to the NASA Access Help Desk at (301) 621-0134

- Telephone the NASA Access Help Desk at (301) 621-0390

- Write to:
  NASA Access Help Desk
  NASA Center for AeroSpace Information
  7121 Standard Drive
  Hanover, MD 21076

NASA/CR—2000-209921/VOL1

DHC-6 Twin Otter Tailplane Airfoil Section Testing in the Ohio State University 7x10 Wind Tunnel

Dale Hiltner, Michael McKee, Karine La Noé, and Gerald Gregorek
Ohio State University, Columbus, Ohio

Prepared under Grant NAG3–1574

National Aeronautics and
Space Administration

Glenn Research Center

September 2000

Acknowledgments

The authors would like to thank the NASA Glenn Research Center Icing Branch for sponsoring this wind tunnel test through the grant NAG3–1574 to the Ohio State University. We also would like to acknowledge the project advocacy and support that the FAA William J. Hughes Technical Center provided throughout this research effort.

Available from

NASA Center for Aerospace Information
7121 Standard Drive
Hanover, MD 21076
Price Code: A06

National Technical Information Service
5285 Port Royal Road
Springfield, VA 22100
Price Code: A06

Table of Contents

List of Figures

List of Symbols

AOA,α	angle of attack
c	chord
C_D	section drag coefficient
C_{Do}	section drag coefficient at a = 0o
C_H	section hinge moment coefficient
$C_{H\alpha}$	section hinge moment slope versus α at constant δ_e
$C_{H\delta}$	section hinge moment slope with δ_e at constant α
C_L	section lift coefficient
C_{Lmax}	peak section lift coefficient
$C_{L\alpha}$	section lift curve slope at constant δ_e
$C_{L\delta}$	section lift coefficient slope with δ_e at constant α
$C_{M,CM1/4}$	section moment about ¼ chord
C_P	pressure coefficient
P_{total}	total pressure
P_{static}	static pressure
q,Q	dynamic pressure
Re	Reynolds Number
V	velocity
α,AOA	angle of attack
α_{stall}	angle of attack at stall
δ_e	elevator deflection

SUMMARY

Ice contaminated tailplane stall (ICTS) has been found to be responsible for 16 accidents with 139 fatalities over the last three decades, and is suspected to have played a role in other accidents and incidents. The need for fundamental research in this area has been recognized at three international conferences sponsored by the FAA since 1991. In order to conduct such research, a joining NASA/FAA Tailplane Icing Program was formed in 1994; the Ohio State University has played an important role in this effort. The program employs icing tunnel testing, dry wind tunnel testing, flight testing, and analysis using a six-degrees-of-freedom computer code tailored to this problem. A central goal is to quantify the effect of tailplane icing on aircraft stability and control to aid in the analysis of flight test procedures to identify aircraft susceptibility to ICTS. This report contains the results of testing of a full scale 2D model of a tailplane section of NASA's Icing Research Aircraft, with and without ice shapes, in an Ohio State wind tunnel in 1994. The results have been integrated into a comprehensive database of aerodynamic coefficients and stability and control derivatives that will permit detailed analysis of flight test results with the analytical computer program. The testing encompassed a full range of angles of attack and elevator deflections, as well as two velocities to evaluate Reynolds number effects. Lift, drag, pitching moment, and hinge moment coefficients were obtained. In addition, instrumentation for use during flight testing was verified to be effective, all components showing acceptable fidelity. Comparison of clean and iced airfoil results show the ice shapes causing a significant decrease in the magnitude of CLmax (from –1.3 to –0.64) and associated stall angle (from –18.6° to –8.2°). Furthermore, the ice shapes caused an increase in hinge moment coefficient of approximately 0.02,the change being markedly abrupt for one of the ice shapes. A noticeable effect of elevator deflection is that magnitude of the stall angle is decreased for negative (upward) elevator deflections. All these result are consistent with observed tailplane phenomena, and constitute an effective set of data for comprehensive analysis of ICTS.

1. INTRODUCTION

This wind tunnel test is part of the NASA, FAA and The Ohio State University, Tailplane Icing Program. The purpose of the program is to quantify the effect of tailplane icing on aircraft stability and control to aid in the development of a flight test procedure that will identify aircraft susceptible to tailplane icing. As a first step in this program, wind tunnel testing of the 2-Dimensional aerodynamics of the tailplane of the NASA Glenn Research Center Icing Research Aircraft, a DeHavilland DHC-6 Twin Otter (Fig. 1) was undertaken. Pressure data from surface taps and belt taps were acquired and integrated to obtain lift, drag, pitching moment, and hinge moment coefficients. The belt taps consisted of precise holes punched into each tube of a series of strip-a-tube belts wrapped around the airfoil section. Belt taps were included in the testing as the aircraft will have belt taps installed during flight testing. Tests were conducted on the clean, or uniced, airfoil and the airfoil with two representative ice shapes at a full range of angle of attack (AOA), from large negative to beyond stall, and the full range of elevator deflections. Reynolds number effects were obtained by testing at two velocities. As shown in Figure 1, the Twin Otter tailplane is composed of two separate airfoil sections. Basic data for the clean secondary airfoil section were also acquired. In addition, data were taken from a 5-hole probe mounted on the airfoil leading edge. This data will be used to determine tailplane AOA from similar probes in future flight testing.

The representative ice shapes were called S&C (for stability and control) and LEWICE (because it was generated by the code of the same name). The S&C ice shape has been used in several stability and control programs on the Twin Otter. This ice shape was determined using a combination of in-flight photographs of icing on the Twin Otter's tailplane, and the FAA ADS-4 report "Engineering Summary of Airframe Icing Technical Data", by Bowden, et al. The LEWICE ice shape was predicted using the LEWICE 1.3 computer program. (Specific input conditions were: velocity = 120 kts, liquid water content = 0.5 g/m^3, median volumetric diameter = 20μm, icing time = 45 min, AOA = 0°, total temperature = -4° C.) The ice shape was determined in five equal time steps. Each step consisted of a 9 minute accretion time, a redefining of the iced airfoil geometry, and a recalculation of the airflow over the new geometry. The 45 minute accretion time was chosen to be conservative while aligning with the FAA requirement of demonstrating capability with 45 minute accretion time on an unprotected surface.

To satisfy program objectives, this 2-D airfoil data will be used to generate separate aircraft and tailplane stability and control derivatives. These data will allow the tailplane effects and flow field environment during maneuvering flight to be explored by a flight path simulation program presently under development. Maneuvers that indicate a tendency for tailplane stall will be examined analytically refined by flight test. Data obtained from the belt taps and the 5-hole probes will be used to quantify the tailplane aerodynamics during these flight test maneuvers.

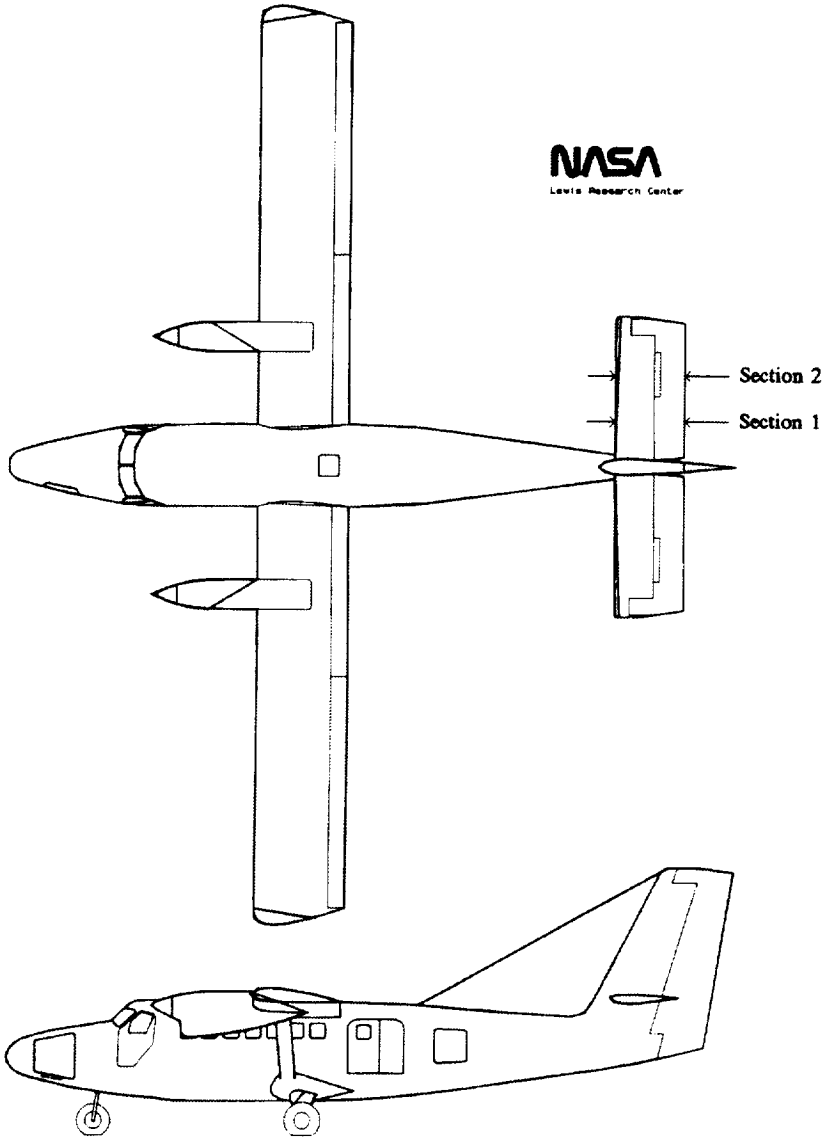

Figure 1 NASA Glenn Research Center Icing Research Aircraft

2. EXPERIMENTAL FACILITY

The Aeronautical and Astronautical Research Laboratory Low-Speed Wind Tunnel Facility (OSU LSWT) is a closed-loop circuit with a 7x10 ft. high-speed test section, and a 14x16 ft. low-speed test section. A 2000 Hp electric motor provides dynamic pressures up to 65 psf in the 7x10 ft. section. (See Fig. 2.) A sting balance mount allows models to be tested at angle of attacks ranging from -15 to +45 degrees, while the rotating tunnel floor has a range of -90 to +270 degrees.

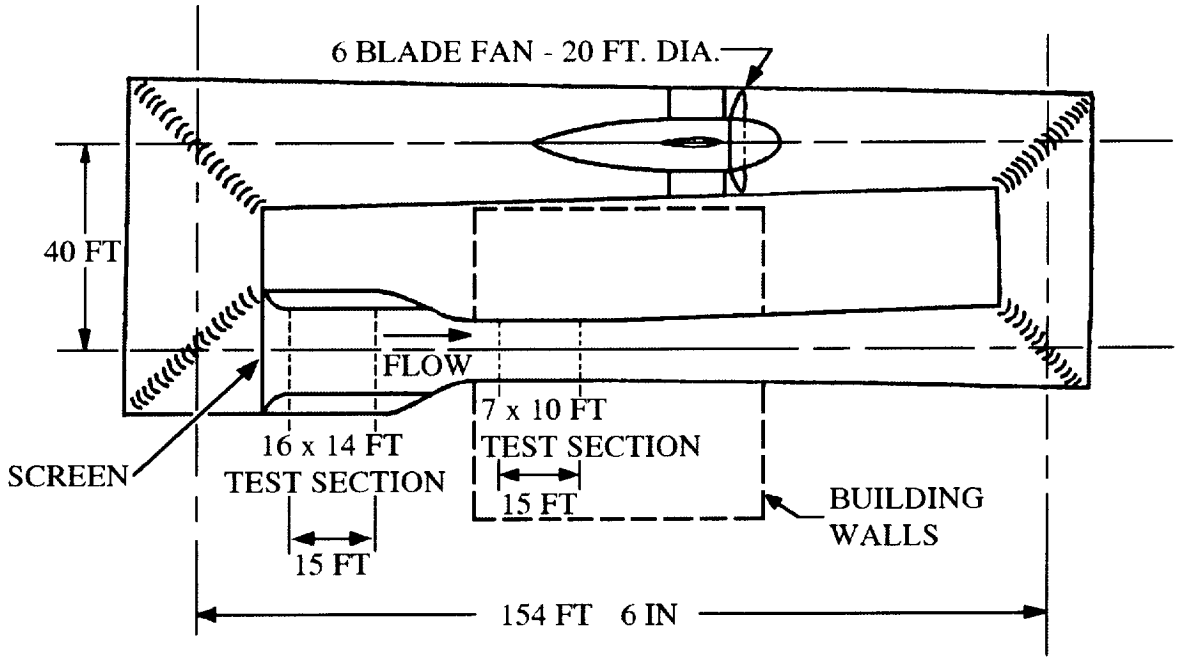

Figure 2 OSU Low-Speed Wind Tunnel Facility

Tunnel speed is manually set based on average values obtained from two dedicated tunnel pitot and static probe sets. A PC-class computer is used to control sting and mounting table angles, and wake probe sweep, as well as data acquisition tasks. Up to 14 data channels can be sampled. Signal conditioning and amplification are provided by individual rack mounted units.

Testing of 2-dimensional airfoils is conducted by installing a 7-ft. span model to fill the height of the low speed test section. The model is attached to the floor mounting table, which is then rotated to provide specific AOA's. Surface taps on the model are used to acquire pressure distributions, which are integrated to obtain model forces and coefficients. To determine drag, wake survey probes are installed down stream of the model. By sweeping these probes across the test section, the complete model wake can be measured.

3. MODEL DESCRIPTION

The two airfoil sections tested are shown in Figure 3. As is seen from the 2-view aircraft drawing (Fig.1), the Section 1 airfoil was a significant portion of the tailplane area. Drawings of the two ice shapes are shown in Figure 4. Some minor smoothing of the lofted airfoil shape was required; a 0.020 inch "bump" at the lower leading edge was removed, and a straight line contour from the elevator main spar to the trailing edge was assumed.

The primary factors in the model design were to provide a smooth aerodynamic surface while allowing flexibility in model configuration and low fabrication costs. A highly stiff design was also desired, to maintain model shape under load. The chosen model design consisted of airfoil sections machined in machineable plastic (also known as REN material), supported by metal tubing spars and aluminum ribs. This allowed CNC machining to be used to fabricate the airfoil shape with high accuracy.

A schematic of the model is shown in Figure 5. The 20 inch span Machineable Plastic sections were supported by two internal metal tubing spars on each of the stabilizer and elevator sections. Three ribs and two endplates structurally connected the spar tubes of the stabilizer to the forward spar tube of the elevator. The ribs contained keyways for keys mounted on the stabilizer spar tubes to provide stiffness under model moment loading. The ribs of the elevator overlapped those of the stabilizer, to form a hinge around the forward elevator spar tube. End ribs on the elevator provided attach points to the endplates, which were used for changing the elevator deflection angle. The machineable plastic sections transmitted their loads to the ribs through pins. The endplates contained rods to attach the model to the tunnel yaw table floor supports, and to a ceiling pivot. The model was mounted to the yaw table such that the table center of rotation was at 28% model chord.

Removable plug sections were used to create the two configurations tested. The stabilizer section consisted of the baseline (or Section 1) section. An aft extension plug was then used to create the Section 2 stabilizer section. The elevator section consisted of the Section 2 section with plugs to create the baseline section. Figures 6 through 9 show the model as installed in the tunnel.

Tap locations were chosen to provide high resolution where pressure gradients were large, and low resolution elsewhere to minimize the total number of taps. Taps were labeled starting with #1 on the leading edge of the stabilizer and ending with #86 on the elevator trailing edge. (This included taps for the baseline and Section 2 airfoils.) Odd numbered taps were located on the suction side of the airfoil, with even numbers on the pressure side, except at the boat-tail ends. The tap locations of the ice shapes replaced those on the nominal airfoil, which was reflected in their numbering. The final tap location configurations are listed in Appendix A, which also shows a graphic of their positions on the airfoil sections.

Surface taps were installed in-house prior to the completion of the section assembly. Taps were located on a 12-inch airfoil section using a Bridgeport milling machine with digital distance readout. Tap locations were determined relative to a coordinate system readily indicated using available points on the section. Once the locations were marked along the section moldline, 0.0625-inch holes were drilled normal to the surface 0.5 inches below one edge. Mating holes were then drilled vertically into the milled out end of the section. Stainless steel tubing was then fitted to these mating holes and routed along the section end and through tubing passageway holes. The tubing length was sized so at least 2 inches extended beyond the section. The tubing was glued and sealed to the mating hole using plumbers paste. With the tubing completed, the

milled out end was filled and glued to a mating 8 inch section to complete the 20-inch section. Strip-a-tube tubing was then attached to the stainless steel tubing and routed through the passageways in each section to connect the surface taps to the scanivalve ports. The tubing length was approximately 15 ft.

The belt was installed by first milling a slot into the pressure side of the stabilizer and elevator. Double sided tape and epoxy were then used to secure the belts to the section. The free ends of the belts were then routed through the slot and into the tubing passageways. Tap locations were determined by measuring a surface distance along each side of the belt. A special tap tool was then used to punch a hole in each tube and remove the excess material. Note that each belt was continuous, connecting directly to the scanivalve, and only one tap per belt tube was used. The two outer tubes of the full belt did not contain any taps, since experience has shown that local flow accelerations over these outer tubes cause erroneous pressure measurements.

The 5-Hole Probe is shown in Figure 10. As indicated in the drawing, the probe provides six pressures. P_{total} and P_{static} are used to determine velocity. The difference between the upper and lower static port pressures in the probe head provides an indication of AOA, and the difference between left and right static port pressures provides an indication of sideslip angle.

The probe was attached to the leading edge of the model with a "glove" fixture that wrapped around the leading edge. The alignment tabs of the probe fit into slots in the probe mount on the glove. A set screw in this mount locked the probe in place. The glove was secured to the model by a screw in each corner. The probe pressure tubing was routed through a hole drilled through the model into the front pressure tubing passageway. The probe was mounted at approximately 16 inches above the tunnel floor, at 75% of the lowest model span section. Note that this probe installation duplicated the installation that will be used on the Twin Otter for flight testing.

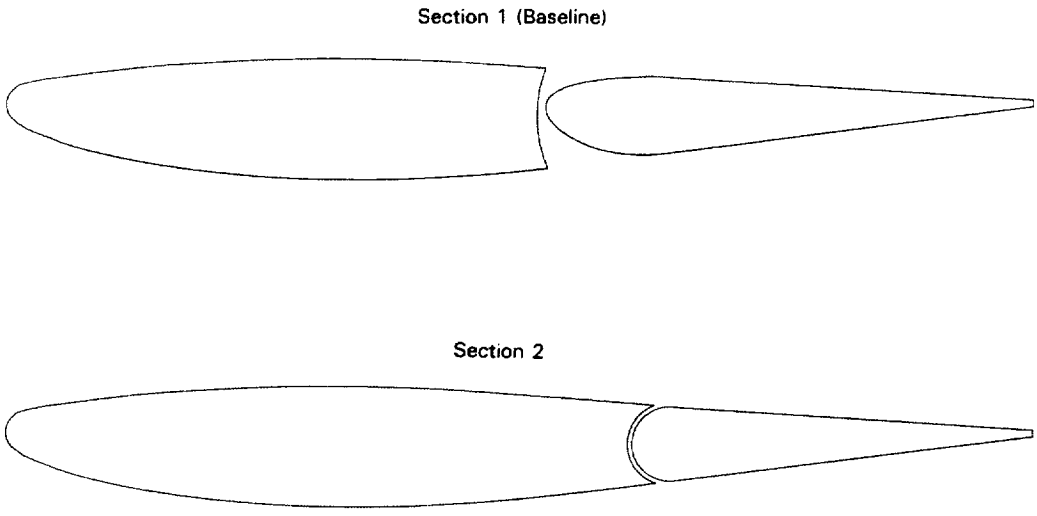

Figure 3 Section 1 (Baseline) and Section 2 Airfoil Sections

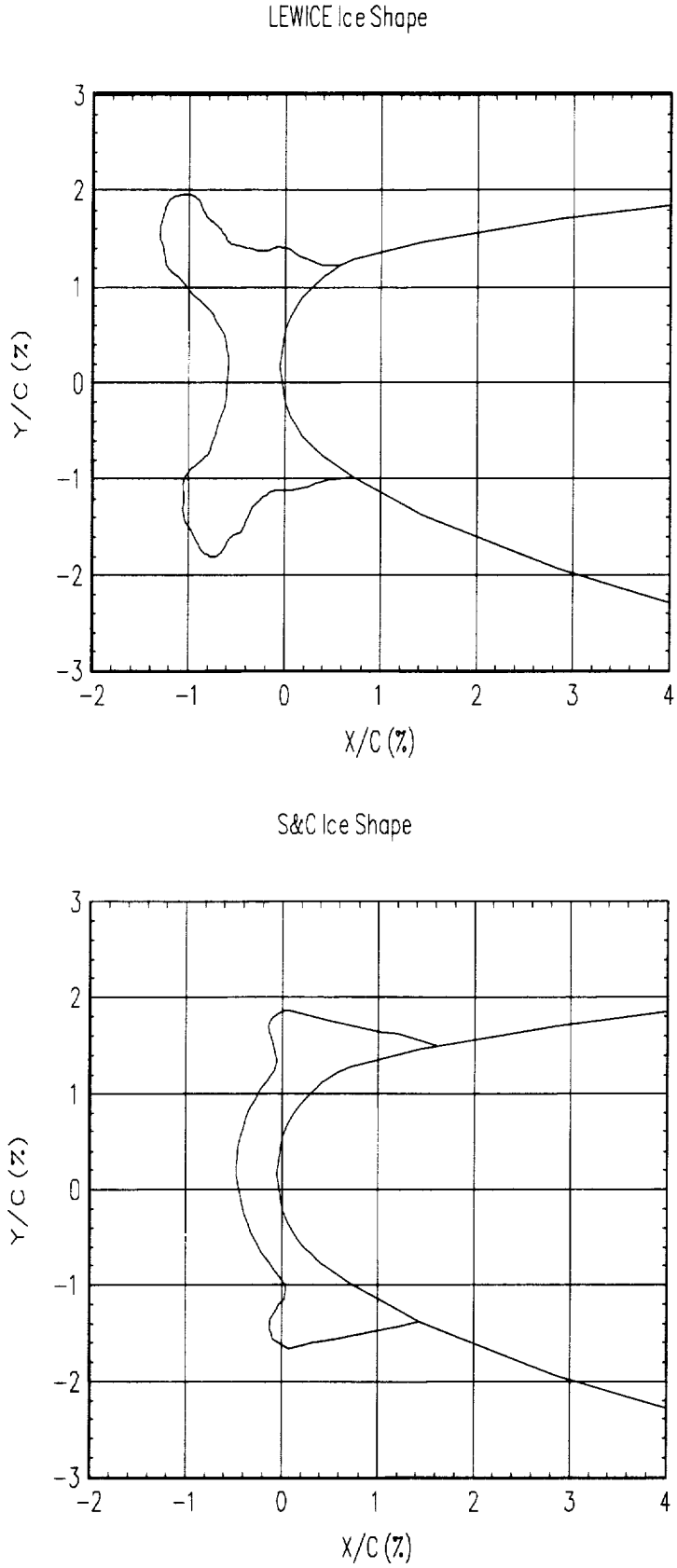

Figure 4 Ice Shape Sections

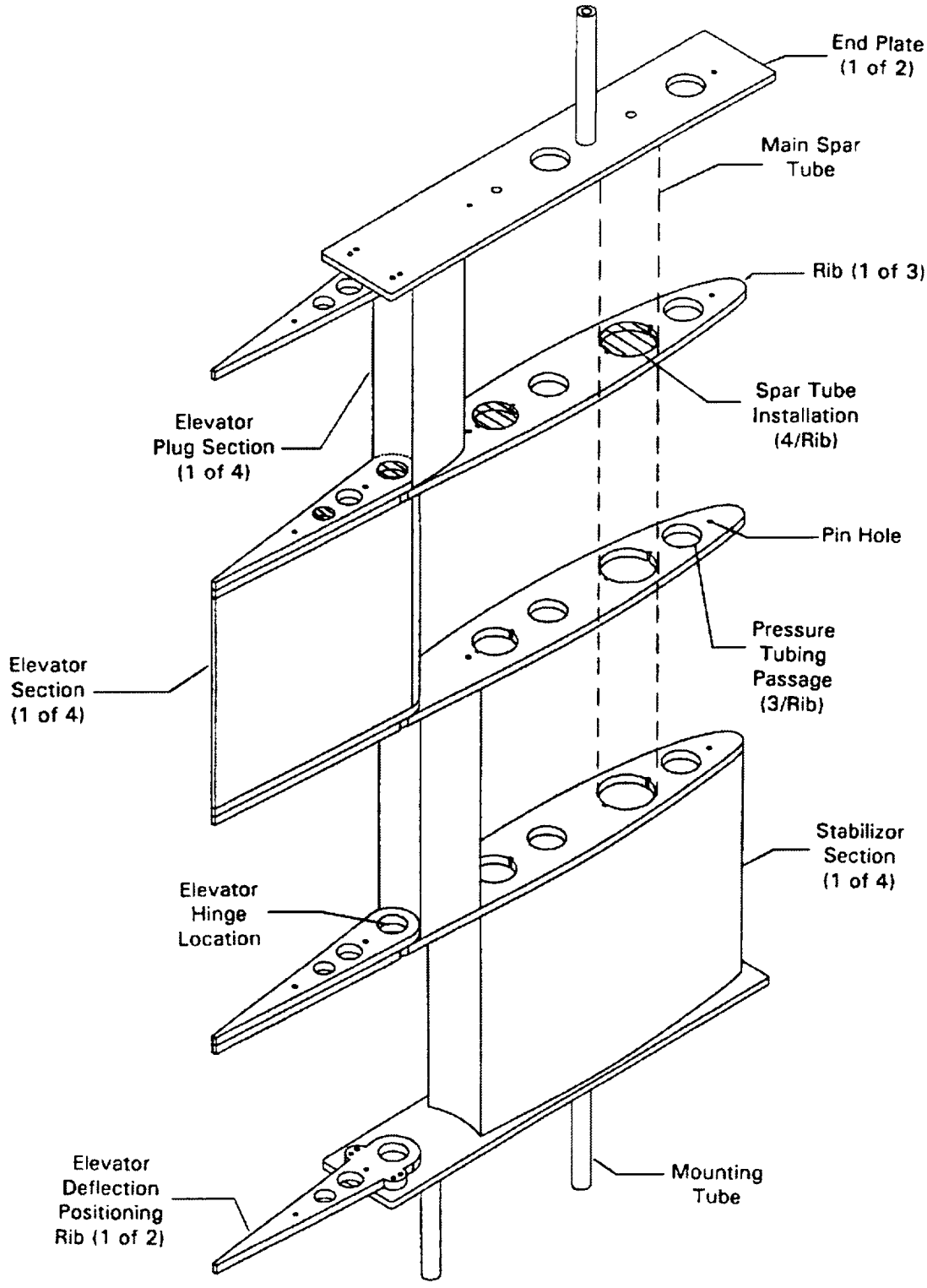

Figure 5 DHC-6 Tailplane Wind Tunnel Model Schematic

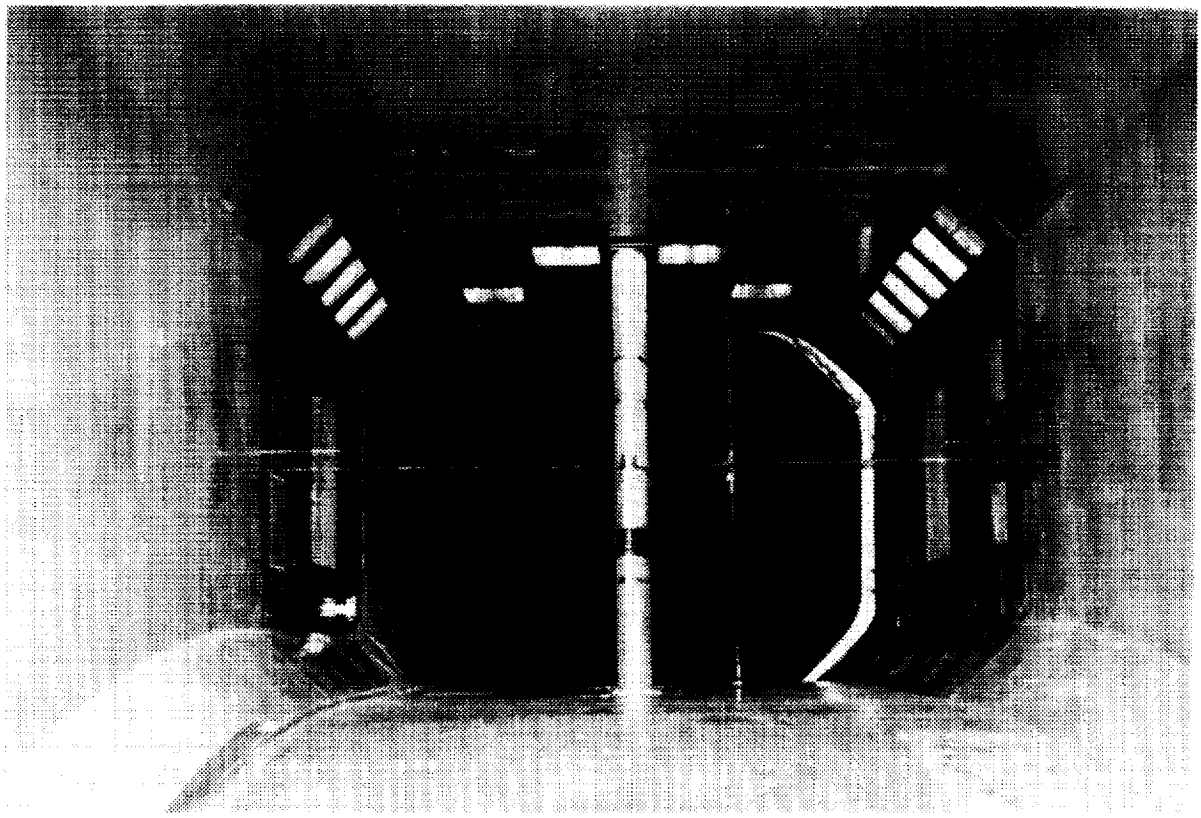

Figure 6 Model Installation, View from Upstream

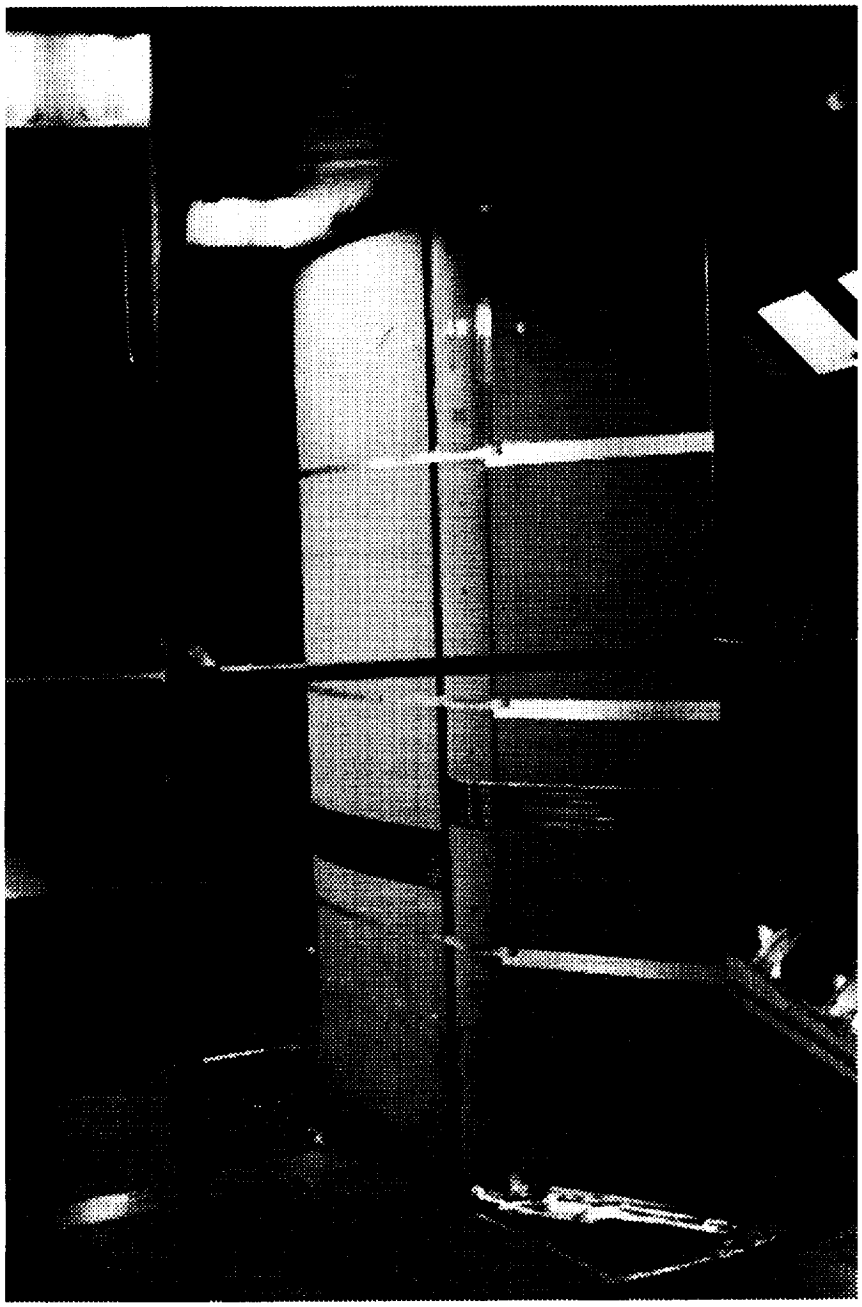

Figure 7 Baseline Installation, δ_e=-26.6° (Wake Probe in Foreground)

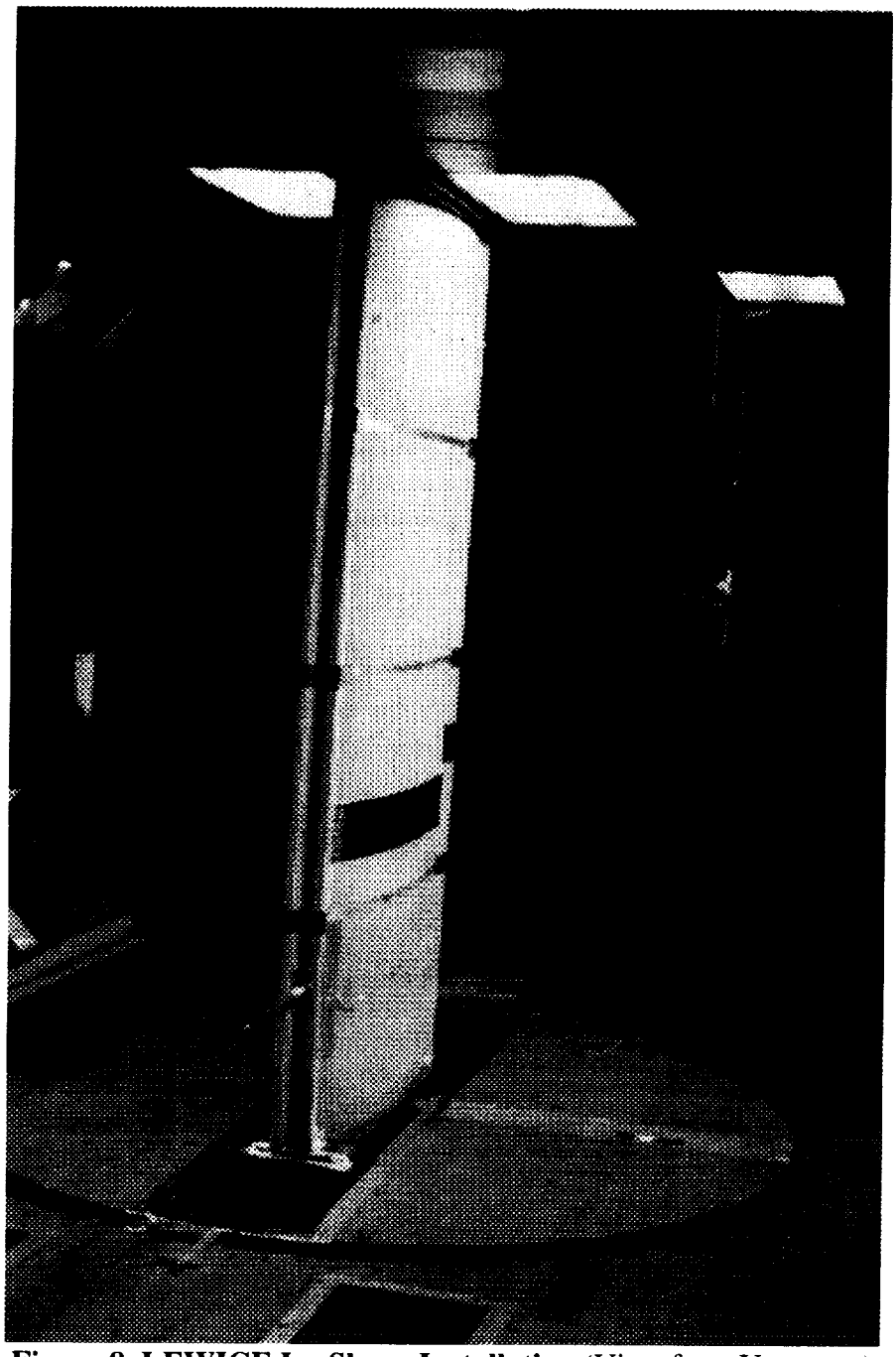

Figure 8 LEWICE Ice Shape Installation (View from Upstream)

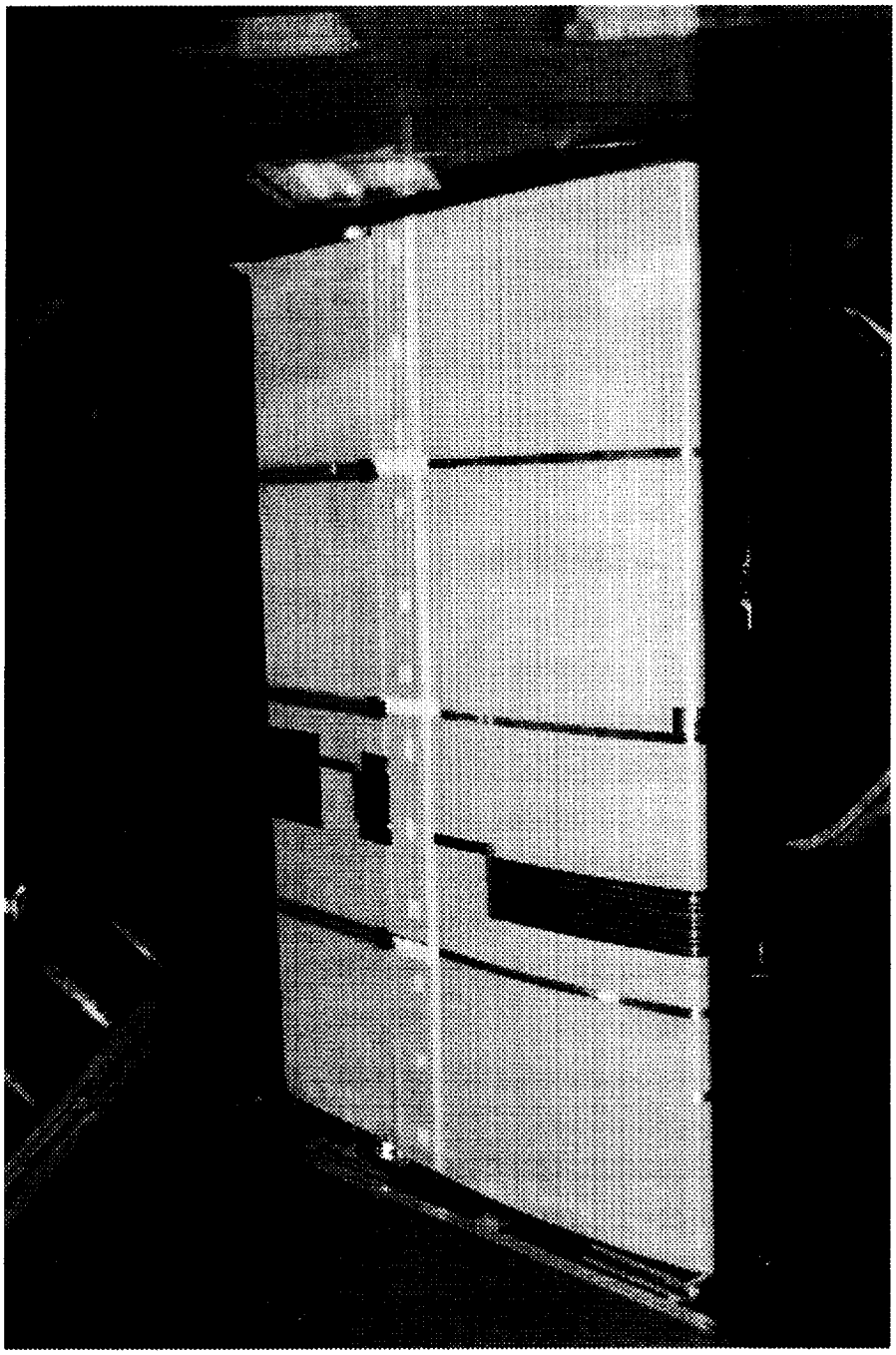

Figure 9 Section 2 Installation

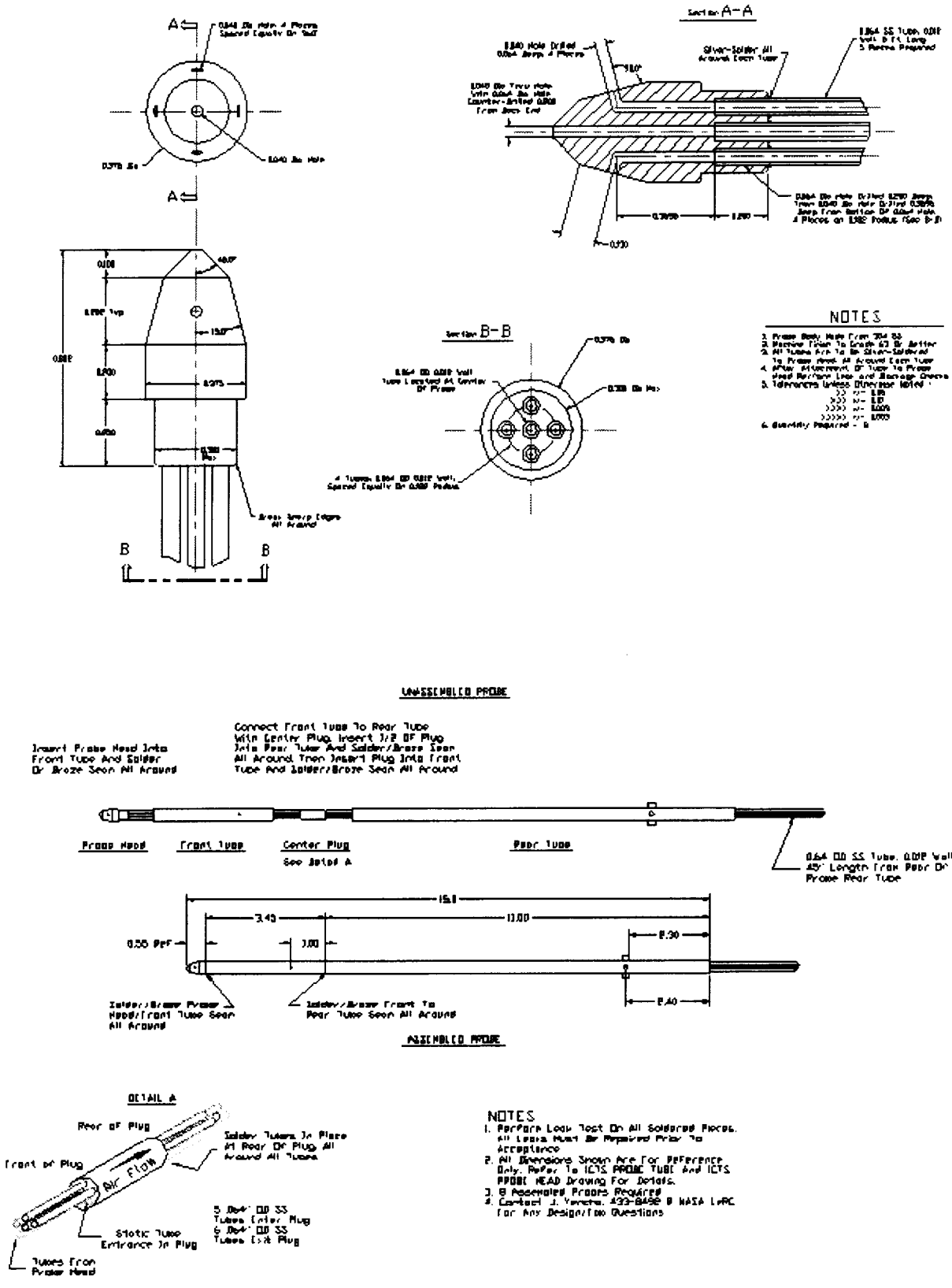

Figure 10 5-Hole Probe

4. DATA ACQUISITION

The scanivalves contained 48 ports and a single Statham 2.5 psi differential transducer, vented to atmospheric pressure. The individual ports were accessed by mechanically rotating a perforated ring to individually pass each port pressure to the transducer. This action was controlled by computer, allowing up to 3 seconds between samples of each port. Four units were used providing up to 192 pressure ports. To provide higher accuracy, tunnel total and static pressures were applied to the first four ports of each unit. During data reduction, these pressures were used to provide tunnel conditions for the pressure coefficients obtained from each respective unit.

The wake measurement system consisted of pressure probes mounted to a 16 ft. length of aerodynamic tubing which spanned the test section. The tubing was supported by roller guides located at each wall exterior, and one roller guide mounted on a vertical section of aerodynamic tubing located at approximately 1/3 of the tunnel width. Three sets of one total and one static pressure probes were attached to the aerodynamic tubing. These probes were 4 inches apart with 32 inches between sets to allow some overlap during the 36-inch sweep across the test section. An individual probe was used for each total and static pressure, allowing measurements to be made at a constant tunnel cross-section location. Both total and static wake probe pressures were measured by 2.5 psi differential transducers.

Tunnel conditions were measured using dedicated 2.0 psi differential transducers for pitot pressures, while 0.5 psi differential transducers were used for the static pressures. All differential transducers were vented to the atmosphere, with atmospheric pressure determined from a sensitive altimeter.

All transducers were calibrated using a manually operated water manometer. Calibrations of the scanivalve transducers over both positive and negative pressure ranges were linear within 0.32% full scale, with a standard deviation within 0.15%. Repeatability of the calibration slopes was within 0.5% full scale. The wake probe transducers were linear within 0.1% with standard deviation less than 0.03%. For the tunnel transducers, linearity was within 0.1% and standard deviation within 0.03%. Similarly, tunnel static transducers were calibrated to 0.2% and 0.12%, respectively.

Power for all transducers was supplied by signal conditioners mounted in the control room. Amplifier banks mounted in the control room amplified the transducer outputs to the proper voltage for the 14 channel A/D converter. The digital outputs were then fed to a 386 class PC. This PC contained all data gathering and data reduction programming, with only tunnel airspeed being manually controlled. Angle of attack positioning, operation of the scanivalves, operation of the wake probe sweep, and recording of all raw data was performed by the run program. During an AOA sweep, the run program displayed current tunnel conditions and model position, as well as the value of each active A/D channel.

5. TEST PROCESS

Appendix B contains a Run Log for the test. (Note that runs prior to run 10 did not generate valid pressure data due to a malfunctioning scanivalve.) Note that repeatability runs of the baseline configuration at 100 kts were taken at δ_e=0.0°, 14.2° and -26.6°. Also, the last data point of each run was taken at AOA=0.0, as a run repeatability check. Only a few runs were taken with the Section 2 configuration, due to test time limitations.

The daily test procedure consisted of first adjusting all signal conditioners and amplifiers to their proper values. This compensated for the small drift associated with the particular electronics used. The barometric pressure in the "balance room" was noted each morning. (All differential transducers were vented to the "balance room" atmosphere.) After the tunnel inspection was completed, the run software was started.

The run software was initially set up for the model characteristics prior to any testing. This included model reference dimensions, as well as any transducer calibrations. The "balance room" pressure and the tunnel temperature were entered each morning. Other specific items entered prior to each run included; run number, run description, the specific set of pressure taps in use, elevator deflection angle, the file name into which the raw data would be saved, status of wake probe usage, and specific AOAs desired during the run. Once these were set, a wind off tare was taken. This numerically zeroed all the pressure transducers to ambient conditions, within 10^{-3} psid.

With the tares completed, the run program was started which positioned the model to the first AOA of the sweep. The tunnel fan was then started and manually set to a specific RPM, which resulted in the desired dynamic pressure, as displayed by the run program. When this dynamic pressure was stabilized, the AOA sweep mode was engaged. The run program then positioned the model and took data for all desired AOA points. A typical AOA sweep of 10 points took approximately 30 minutes to complete. A wake probe sweep, if run, occurred after pressure tap data were taken at each AOA. This sweep added an extra 2 minutes to the time to take data at each AOA. Because of this, only a limited number of wake probe sweeps were accomplished.

Note that once the RPM was set, it was not changed during a run. Large blockage at the higher AOAs caused a reduction in the tunnel velocity and Reynolds Number. Nominally this reduction was on the order of 10 kts (Δq=6 psf and ΔRe=0.5x10^6), during the 100 kts runs. For the runs into the AOA=20° range, the reduction was on the order of 20 kts (Δq=11 psf and ΔRe=0.8x10^6). For the 60 kts runs, the reduction was typically less than 10 kts (Δq=3.5 psf and ΔRe=0.45x10^6), with 15 kts (Δq=4.5 psf and ΔRe=0.55x10^6) being an extreme. This reduction in velocity was allowed because the time required to manually set the velocity at each AOA point would have been excessive. Also, the incremental velocity between each 60 and 100 kts run was kept within a reasonable range, so any Reynolds number effects would be apparent.

With the AOA sweep completed, any desired post run note was entered into the run program, and the raw data were saved to the hard disc. The raw data were the final result generated by the run program. The raw data file included the output voltages of all transducers, and the tap location and calibration data. This method of data storage allowed a run to be modified post-test if errors in the setup were discovered after testing was completed.

Limited tuft flow visualization was also performed. A single row of tufts was installed in the center of the upper and lower model sections. These tufts were briefly video taped at each AOA during most of the AOA sweeps. Correlation to the specific test condition was accomplished by logging the time of each recording. Appendix C contains the timing log for the video. (Note that runs 01 through 07 were applicable for the tuft video.) Additionally, some runs were made with more complete tufting of the model to check for 3-Dimensional effects. Pictures and video were taken of most of these runs. (These runs are indicated as Flow Viz runs in the Run Log of Appendix B.)

6. DATA REDUCTION

Coefficient data were obtained by integrating the pressure coefficient distributions of the stabilizer and elevator separately. A typical pressure distribution is shown in Figure 11. This was accomplished by applying the averaged pressure of adjacent taps to the area between them. When summed, these values gave coefficients defined relative to the local element coordinate system. These local coefficients were then converted to a lift and drag contribution by the appropriate axis transformation. Moment was obtained similarly, using moment arms of the distance from a reference center to the center location of each integration area.

The solid wall correction factors discussed below use drag coefficient as a primary parameter. Due to the limited amount of wake data obtained during the test, all drag coefficient values were estimated from pressure drag coefficients. A C_{Do} bias coefficient was determined by comparing wake drag coefficients to pressure drag coefficients at AOA=0°, and δ_e=0°, for each Section and ice shape configuration tested. These C_{Do} coefficients were then applied to all pressure drag coefficients obtained with the same Section and ice shape configuration. The resulting drag coefficient values were judged to be well within required tolerances for obtaining accurate solid wall corrected coefficients.

With all coefficients thus obtained, solid wall corrections were then applied. The formulas used to obtain the corrected data are shown in Appendix D. An example of typical magnitudes of the corrections is given in Figure 12, which shows corrected and uncorrected data for a baseline run. Note that a buoyancy term was not included in the corrections, which is used in Ref. D1 as a C_D correction. Ref. D1 implies that a buoyancy correction is valid only for large elements of an aircraft configuration, and is not significant for airfoils. Sample calculations verified this implication.

In addition to the corrected coefficient data, the data reduction program also calculated other important data. Five output files were generated containing uncorrected, corrected, wake drag, 5-hole probe pressure, and wall static pressure coefficients. Appendix E contains a description of the file name and data structure conventions of the output files.

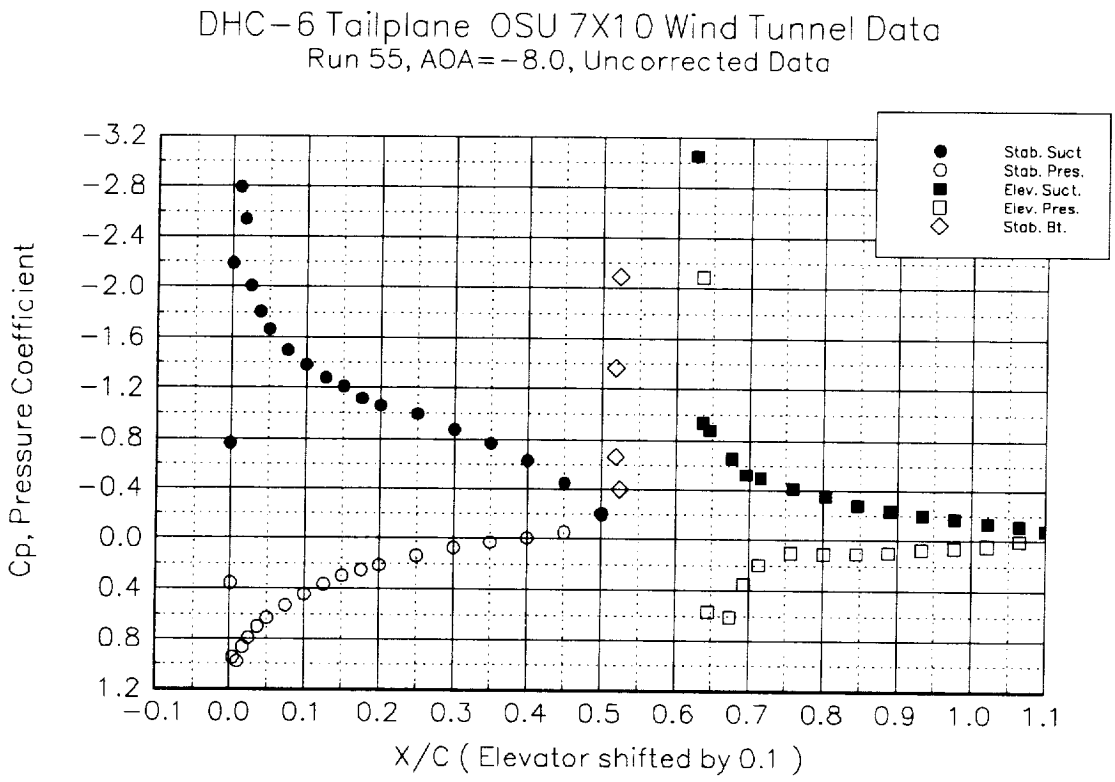

Figure 11 Pressure Distribution Example

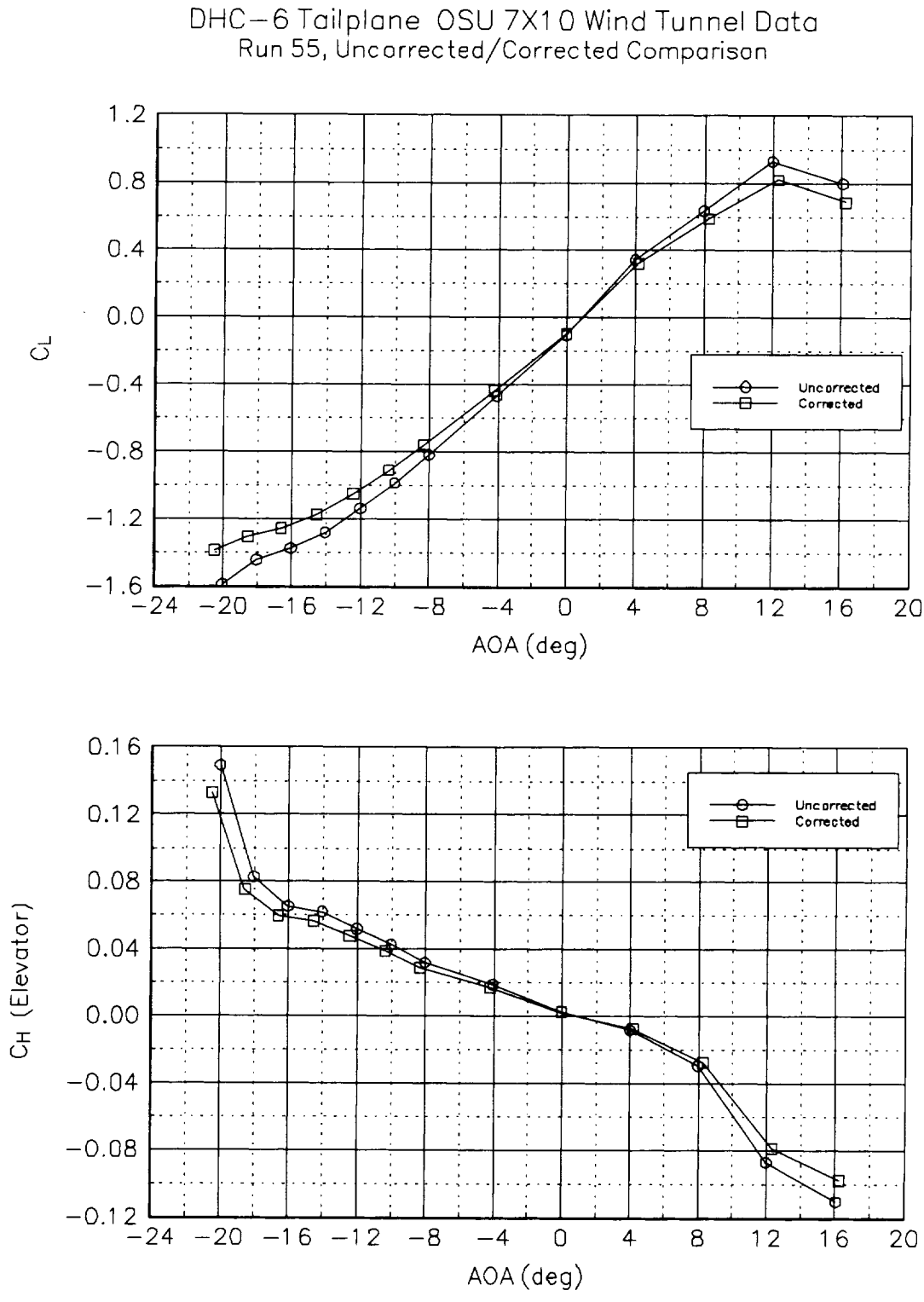

Figure 12 Data Reduction Correction Example

7. RESULTS AND DISCUSSION

The purpose of this test was to quantify the effects of ice shapes on the Twin Otter Tailplane 2-dimensional aerodynamics. This quantification was sought relative to the tailplane stall phenomenon. The two most important phenomena were therefore lift and hinge moment. These are discussed in the following section. Appendix F contains a complete data presentation of all test results of C_L, C_D, C_M, and C_H.

All data are presented with the tailplane as installed on the aircraft, using an aircraft reference system. Therefore, when the airfoil is generating lift relative to the airfoil reference system, this corresponds to negative lift, or positive tailplane down force, in the aircraft reference system. Other sign conventions are AOA positive with the stabilizer leading edge up, moment and hinge moment positive when nose up, and elevator deflection positive with trailing edge down (causing positive lift). Figure 13 presents a schematic describing the axis system and sign conventions.

7.1 Ice Shape Effects

The nominal lift characteristics with zero elevator deflection are shown in Figure 14. (Note that the C_L at AOA=-21° of the baseline configuration was judged to be in error, and indicative of the largely separated flow at this AOA. A more appropriate C_L value was estimated to be C_L=-1.22, based on the characteristics of the 60 kts data.) Here the significant reduction in negative C_{Lmax} and decrease in negative AOA at stall due to the ice shapes is clearly seen. Specifically, negative C_{Lmax} is reduced from C_{Lmax}=-1.3 for the baseline airfoil, to C_{Lmax}=-0.64 for the S&C ice shape, and to C_{Lmax}=-0.60 for the LEWICE ice shape. Negative AOA at stall is decreased from the baseline's AOA=-18.6° to approximately AOA=-8.2° for either ice shape. Nominal hinge moment characteristics are shown in Figure 15. These clearly show the ice shapes causing an approximate ΔC_H=0.02 increase at stall. Note, for the LEWICE ice shape, the transition is not as abrupt as for the S&C ice shape.

The effects of the ice shapes on elevator effectiveness are shown in Figures 16 through 22. (Only the LEWICE ice shape data is shown, as there is little difference in the results with either ice shape.) Figure 20 shows that, in the low AOA linear range used to determine the lift curve slopes, the uniced and LEWICE airfoils have similar trends, with both slopes peaking at δ_e=10°. A noticeable effect of elevator deflection is that negative AOA at stall is decreased for negative elevator deflections and increased for positive tail deflections. For LEWICE data (Fig. 16) at δ_e=-10°, C_{Lmax}=-0.85 at AOA=-6.25°, while at δ_e=+10°, C_{Lmax}=-0.33 at AOA=-10.2°. These trends continue when the negative deflection is increased to δ_e=-20° resulting in C_{Lmax}=-1.21 at AOA=-4.32° (Fig. 17). However, increasing positive deflections result in a smaller increment for C_{Lmax}, of ΔC_L=-0.18 and no change in AOA at stall (Fig. 17). Figure 21 shows that the elevator lift effectiveness is extremely low beyond δ_e=-20°. This indicates that the elevator is saturated, that is, in fully separated flow, at the larger negative deflections.

These stall AOA and effects of flow separation are also seen in the hinge moment, shown in Figures 18 through 20. There is only a small change in C_H due to the LEWICE ice shape between δ_e=+10° and δ_e=+14.2°. However, for both deflections there is a significant shift in C_H starting at AOA=-8°. This shift is significantly trailing edge down, of roughly ΔC_H=+0.040, and is close to the clean δ_e=0.0° values at AOA=-12°. The effect of ice on the δ_e=-10° data shows only a small increase in C_H, at a post stall AOA. However, both the iced and uniced data show a negative steepening of the C_H curve at this deflection. At δ_e=-20° there is a significant ΔC_H=0.02

increase, starting at a negative AOA below stall of AOA=-2.3°. This results in the sharp negative increase in $C_{H\delta}$ for deflections between δ_e=-10° and δ_e=-20° shown in Figure 22. For other deflections, the $C_{H\delta}$ for the LEWICE ice shape shows similar trends to that for the uniced airfoil. Figure 20 shows that, while $C_{H\alpha}$ of the baseline airfoil is negative and relatively constant, $C_{H\alpha}$ for the LEWICE ice shape shows a trend of negatively increasing with increasing positive or negative elevator deflection.

These results match well with observed tailplane stall phenomena. During approach, the elevator would most likely be at a negative deflection. Tailplane stall could more readily occur, since the AOA at which stall would occur would be lowered. Once the stall occurred the AOA would become more negative due to the nose down pitching dynamics. With a negative $C_{H\alpha}$, the trailing edge down (positive) hinge moment would increase, keeping the elevator in a trailing edge down position. The elevator would continue its trailing edge down tendency, until it reached a position limit or the AOA stabilized. Also, in general, the trend in $C_{H\delta}$ is decreasing with increasing positive tail deflection. This would support the typically observed "stick force lightening" phenomenon. However, the trend in $C_{H\delta}$ at the maximum positive tail deflections and largest negative AOA is significantly increasing (Fig. 22). This suggests that any "stick force lightening" would be dependent on the specific AOA and deflection of the maneuvering aircraft.

7.2 Velocity Effects

Representative velocity effects are shown in Figures 23 through 26, for the baseline and LEWICE configurations. Figure 23 indicates that for δ_e=0.0° there is a ΔAOA=2° decrease in negative AOA at stall at 60 kts (Re=2.7x10^6) compared to the 100 kts (Re=4.8x10^6) data. There is also an earlier stall break at the positive AOAs for the +δ_e case. In general, there is an increase in negative lift at the higher speed. At δ_e=-20° there is a significant decrease in negative C_L at about AOA=-4.0°, which is most likely caused by the largely separated flow of this deflection. These results are consistent with typical Reynolds number effects.

Figure 25 shows an indication of the earlier stall break for the δ_e=0.0° case in the hinge moment data. Some slight increase in hinge moment is seen for the lower speed, but this is nominally in the repeatability range and so is not considered to be significant.

The LEWICE ice shape data of Figures 24 and 26 show little differences due to the speed variation. Except for some noticeable larger differences at the most positive AOA, such differences that are seen are within nominal repeatability.

7.3 Comparison of Surface Taps and Belt Taps

In general the agreement between the surface tap and belt tap results can be qualified as good. However, significant differences seem to occur at conditions of largely separated flow. Figures 27 and 28 show lift characteristics for the baseline and LEWICE cases. Agreement is good for the baseline data, until near stall at δ_e=0.0°, and at the low negative AOAs for δ_e=-20°. In the later case, the shift is roughly ΔC_L=0.2, which is relatively large. (Note, however, from Appendix F, Figs. F.27 and F.28, that the drag at low AOA seems to be erroneously large. Applying solid wall corrections using the drag from the surface taps reduces this shift to ΔC_L=0.1, which is still significantly large.) Also, a reduction in negative AOA at stall of about ΔAOA=2° is seen at δ_e=0° and negative δ_es. The LEWICE ice shape data shows a lowering of negative C_L of about ΔC_L=0.06 at δ_e=-20°, and a slight increase in negative C_L of ΔC_L=-0.05 post stall for δ_e=0°. Note that the stall AOAs agree.

The hinge moment data of Figures 29 and 30 show some shifts in C_H at δ_e=0.0° and δ_e=-20° for the baseline case. The ΔC_H=0.04 shift with δ_e=-20° near AOA=-4.0° is large, however, agreement is good near the stall at roughly AOA=-14°. The constant shift of the baseline data with δ_e=0° of about ΔC_H=0.015 is significant, but the trends are more closely followed. There is no indication of a lowering of the negative AOA at stall for the belt data. The LEWICE data follows the trends of the baseline data, but the differences are of much smaller magnitude.

Overall, as tested, the belt is considered to be a good data source for predicting trends. However, care must be taken in using the belt results. The trend of the better agreement of the ice shape data is encouraging. However, for the clean airfoil, the lowering of the negative stall AOA and the shift in C_H and negative δ_e must be taken into account. Also, there are noticeable belt effects starting at approximately AOA=-4° with δ_e=-20° for both the iced and uniced airfoils. These effects indicate that the belt data is more suspect in areas of large flow separation, possibly due to span-wise flow over the belt. As such span-wise flows are more likely to occur on the Twin Otter tailplane in flight, the belt data could be more significantly effected. Therefore, the flight test data obtained from the belt will need to be carefully evaluated.

7.4 Repeatability

In order to quantify repeatability of the coefficient data, repeat runs were made at 100 kts and δ_e=0.0°, δ_e=-26.6°, and δ_e=14.2°. Except for a few AOAs where there is significant separation, the repeatability is good. Figures 31 and 32 show repeatability comparisons for the baseline and LEWICE ice shape.

From these figures it is seen that nominal differences in C_L for the baseline case using surface taps are within ΔC_L=+/-0.03 and ΔC_H=+/-0.007. At some extremes for the δ_e=-26.6° data, the differences are within ΔC_L=+/-0.1 and ΔC_H=+/-0.03. The LEWICE ice shape data agreement using surface taps was better than that for the baseline case. Nominal differences in C_L are within ΔC_L=+/-0.02 with extremes to ΔC_L=+/-0.04. Nominal differences in C_H repeatability are within ΔC_H=+/-0.007. All are good values.

In order to quantify more precisely these levels of repeatability, standard deviation values were calculated for all corrected coefficients obtained with surface taps at each target AOA. (No correction to any coefficient was made for shifts in AOA away from the target values.) Nominal standard deviation for C_L was judged to be within C_L=0.015. This nominal value neglected about 10% of the data points, which was typical for the assessment of all nominal values. The largest standard deviation value was C_L=0.18, for the baseline airfoil at target AOA=12.0° and δ_e=14.2°. Nominal standard deviation for C_D was C_D=0.05, with extremes to C_D=0.10. Both C_M and C_H had nominal standard deviations of 0.003, with extremes to C_M=0.03, and C_H=0.21 at target AOA=12.0° and δ_e=14.2° for the baseline airfoil. Applying the 2-sigma level of uncertainty resulted in repeatability within ΔC_L=+/-0.03, ΔC_D=+/-0.01, ΔC_M=+/-0.006, and ΔC_H=+/-0.006. These are considered to be good overall repeatability levels, which also agree with the above assessment obtained by viewing the repeatability plots.

Repeatability for the baseline configuration using belt taps showed similar nominal values. However, at the extremes, the differences in coefficient values could be up to 3 times larger than those for the surface data. Repeatability of the LEWICE data using belt taps was the same as that of the surface tap data.

Also, note that, due to model twist under load, it is judged that AOA is measured to within $\Delta AOA=+/-0.5^{\circ}$. This size of error, along with the size of coefficient errors defined above, results in the symbol size of the plots of Appendix F representing the approximate nominal error range of the data.

7.5 Section 2 Comparison

The Section 2 airfoil was tested at 60 kts with $\delta_e=0.0^{\circ}$, 14.2°, and -20.0°. The 5-Hole probe was not installed during this testing, as it had been removed earlier with no change in the baseline results. (No other deflections or ice shapes were tested due to time limitations.) Lift and hinge moment comparison plots are shown in Figures 33 and 34.

The most distinctive characteristics of the Section 2 airfoil, compared to the baseline, are its higher $C_{Lmax}=-1.36$, approximately $\Delta AOA=2.0^{\circ}$ lower negative AOA at stall, and the sharpness of the stall break. Section 2 has a longer chord for the main element, significantly smaller gap, and no extension of the elevator leading edge. All of these configuration differences contribute to this higher C_{Lmax}. The hinge moment behaves as expected, with a larger $C_{H\delta}$, caused by the lack of the moment balancing elevator extension of the baseline elevator.

7.6 Flow Visualization

Additional tufts were added to the model at run 60 to provide more complete flow visualization. Overall, 2-Dimensional flow quality can be characterized as good for all airfoil configurations. For the baseline with $\delta_e=0.0^{\circ}$ the tufts showed some spanwise flow towards model centerline near the tunnel floor and ceiling due to the tunnel boundary layer interference. Additionally, a slight flow angle away from the ribs towards the centerline of the tapped airfoil sections was seen. This could be described as a "rib interference" phenomenon. Also, in general, the flow over the belt section appeared to separate later than the surface tap section. The most significant flow field phenomenon observed with $\delta_e=-26.6^{\circ}$ was separated flow on the elevator at all AOAs tested. The S&C ice shape with $\delta_e=0.0^{\circ}$ and $\delta_e=-26.6^{\circ}$ showed little 3-Dimensional flow effects. The "rib interference" phenomenon was not as apparent, and separation of the elevator occurred along a constant chordline.

Comparing the observed flowfield to the surface to belt comparisons of c) above, shows that most of the flowfield phenomena, while visible, did not cause significant differences in coefficients. Baseline coefficient data showed significant differences only when the flowfield was completely separated. This was most noticeable at $\delta_e=-26.6^{\circ}$ and post stall.

Figures 35 and 36 show examples of tuft photographs for the baseline and S&C ice shape at $AOA=-8.0^{\circ}$ and V=100 kts with $\delta_e=0.0^{\circ}$. The corresponding C_p distributions are shown in Figures 37 and 38. The figures show clearly the large amount of separation that occurs with the ice shapes at low AOA. In general, they also show the constant chord line of the flow separation across the span, except near the tunnel floor and ceiling where boundary layer interference has an influence on the flow. The separation line of the ice shape is indicated in the C_p distribution plot to be at approximately 40% chord, which has fully enveloped the tufts at approximately 45% chord. (Note that the line of tufts near the ceiling is judged to be influenced by the ceiling boundary layer interference, and so is not indicative of the actual 2-D airfoil stall location.) The characteristic bluntness of the C_p distribution caused by the ice shape is clearly evident. The baseline airfoil has attached flow over most of its chord, with only beginnings of separation indicated near the trailing edge. This is indicated in the Figure 37 by the classic shape of the C_p distribution, except where the start of separation causes a flattening of the upper surface

pressures starting at approximately 80% chord. Overall, the tuft flow visualization shows well defined 2-D flow and good agreement with the C_p distributions.

7.7 5-Hole Probe Results

Plots of the 5-Hole probe data from the 100 kts baseline run are shown in Figures 39 through 41. In Figure 39, the dynamic pressure indication of the probe is shown to be lower than tunnel conditions by approximately 6 to 10 kts. (Note, the indicated runs were within +/-10 kts of the target of 100 kts.) Also, there is a tendency for lower indications of dynamic pressure at the larger positive and negative AOAs tested. The AOA ports show good fidelity in indicating AOA (Fig. 40). Assuming a reasonably linear probe calibration, the reduction in upwash angle that occurs when the iced airfoil is stalled is clearly seen. The sideslip ports show a small constant bias in Figure 41, which may be due to a slight tunnel angularity, or the probe itself.

The figures also indicate differences in the probe response with airfoil configuration. This suggests that each airfoil configuration will need its own probe calibration. However, the magnitude of the noted differences on the probe output values is currently not known, as a probe calibration has not been accomplished. An assessment of all aspects of the data fidelity of the probe will be accomplished when the probe calibration is available.

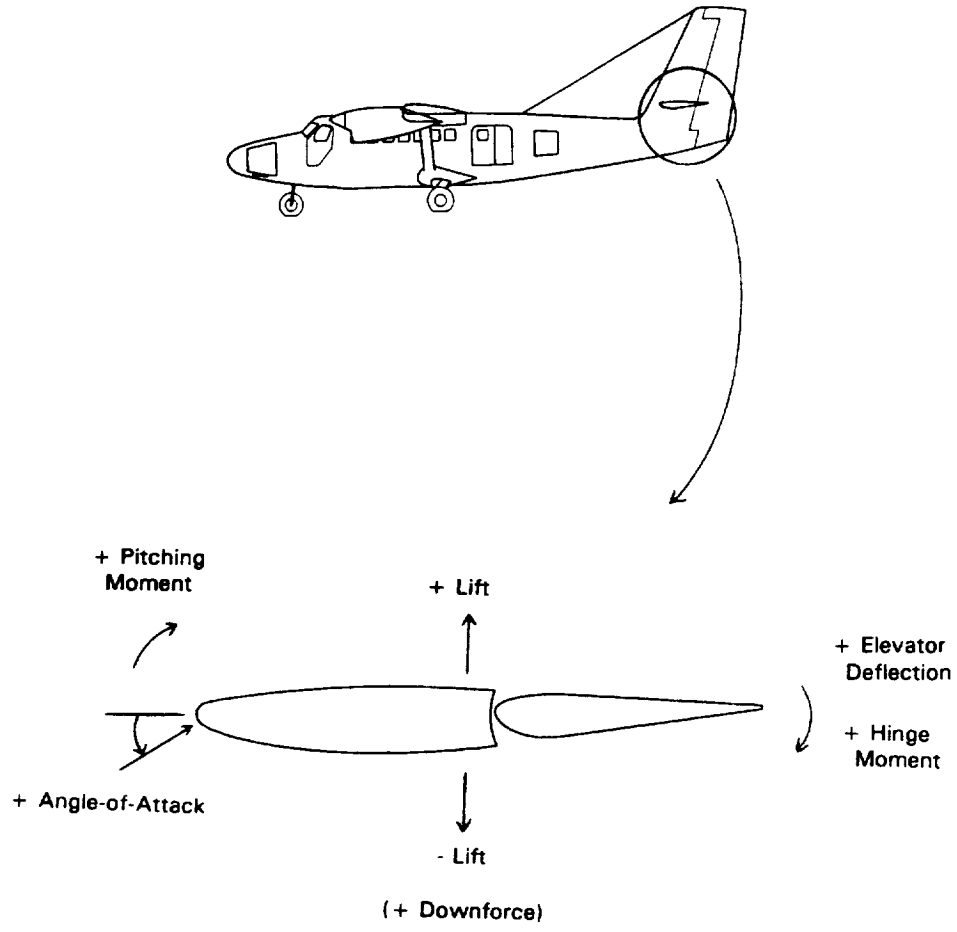

Figure 13 Axis Systems and Sign Conventions

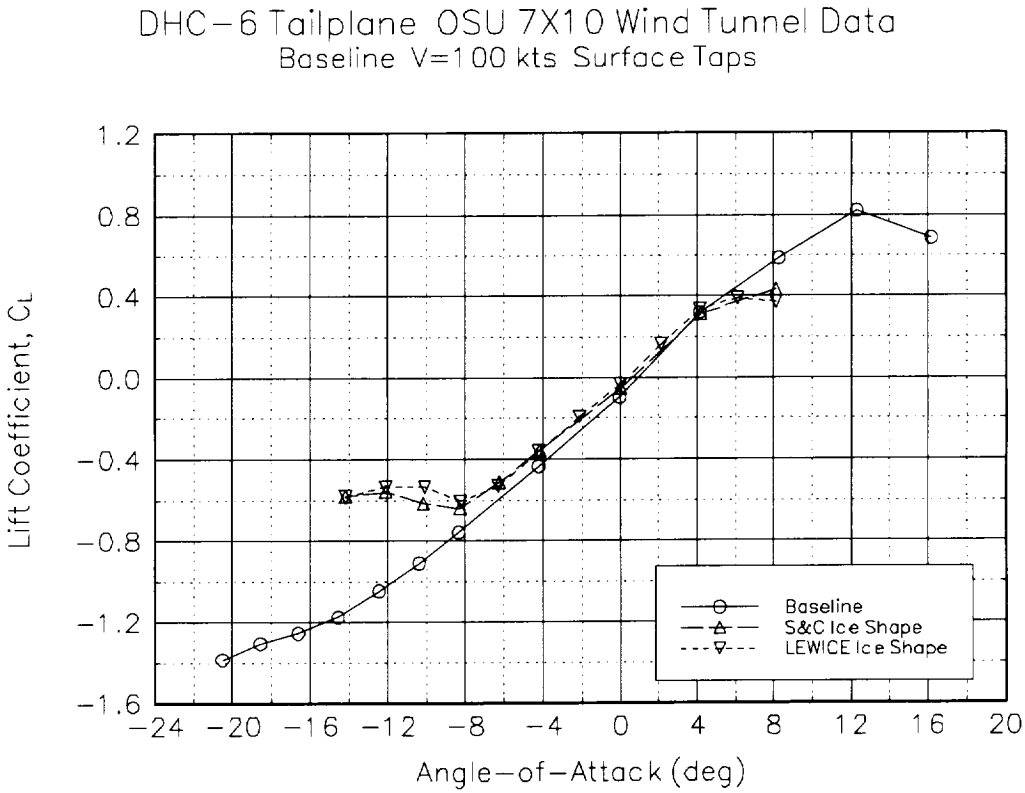

Figure 14 Lift Characteristics, δ_e=0.0

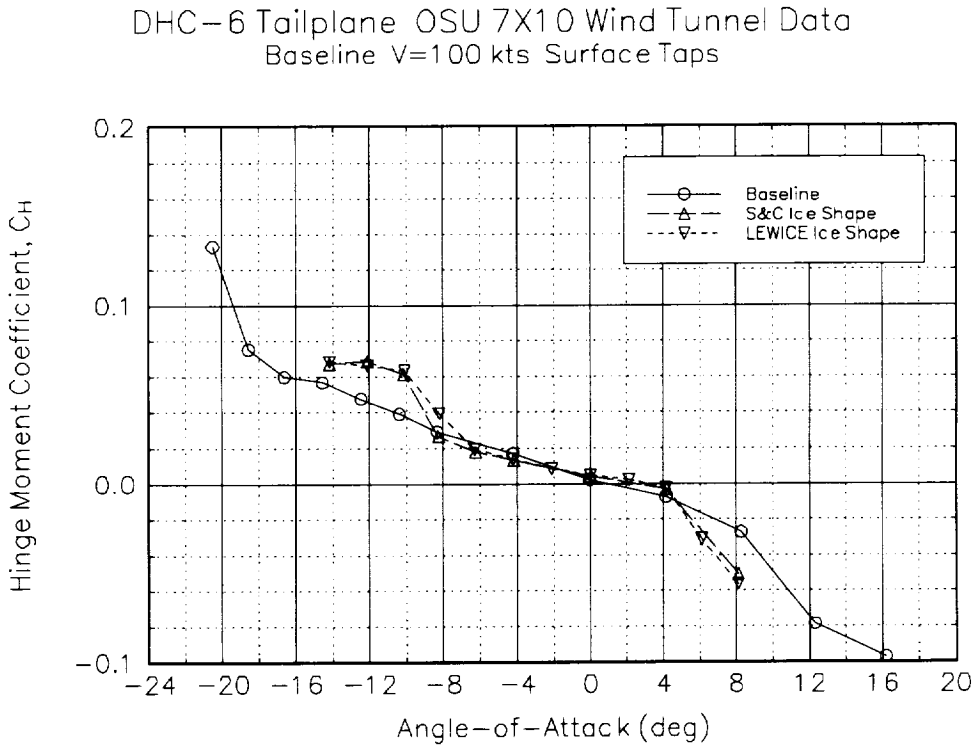

Figure 15 Hinge Moment Characteristics, δ_e=0.0

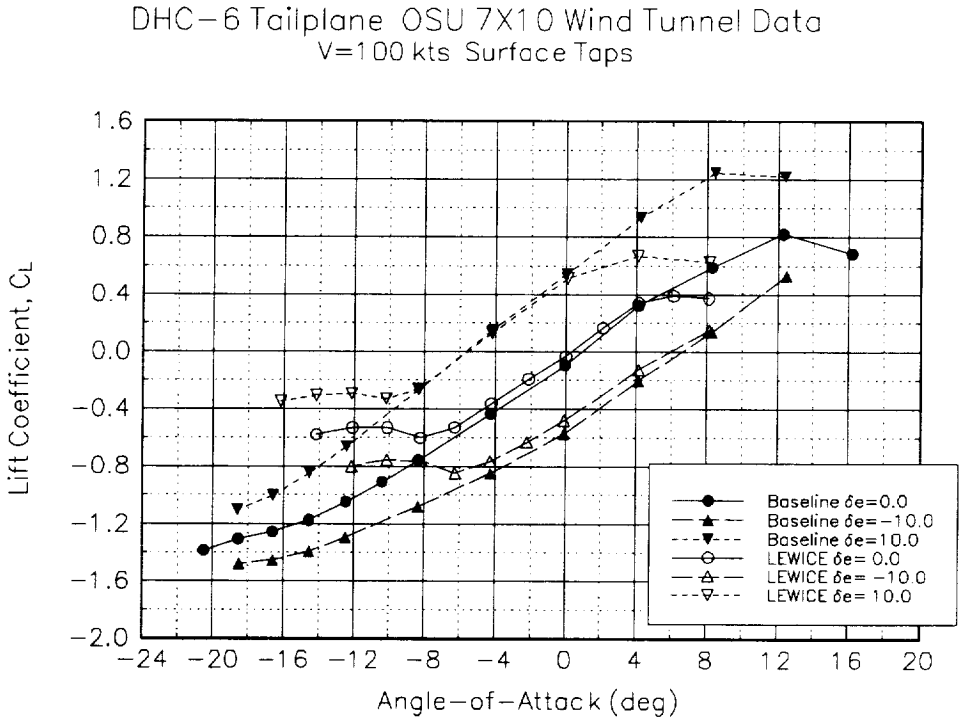

Figure 16 Lift Characteristics, Minimum Deflections

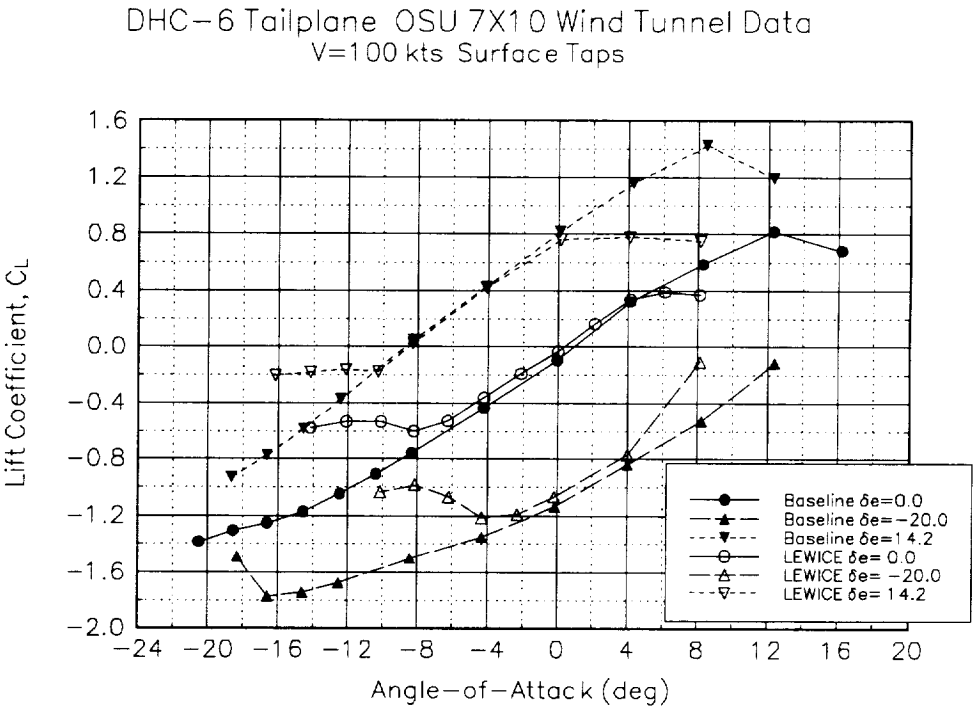

Figure 17 Lift Characteristics, Large Deflections

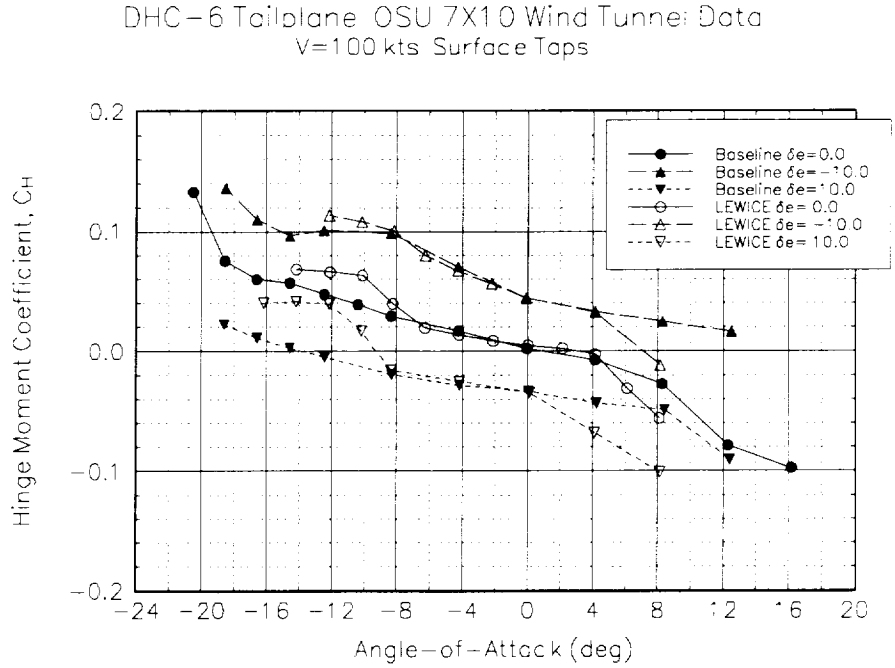

Figure 18 Hinge Moment Characteristics, Minimum Deflections

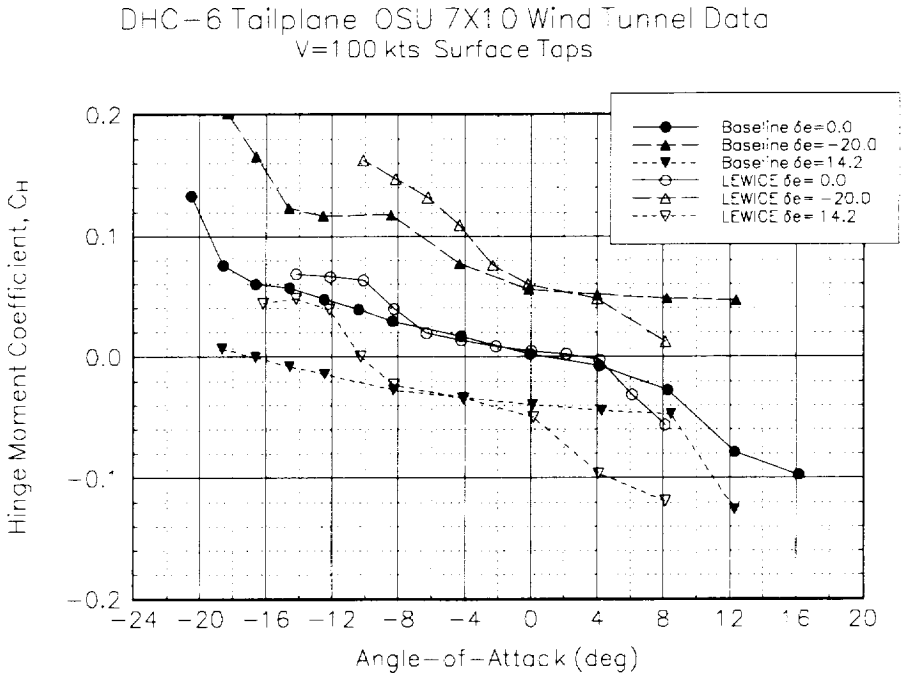

Figure 19 Hinge Moment Characteristics, Large Deflections

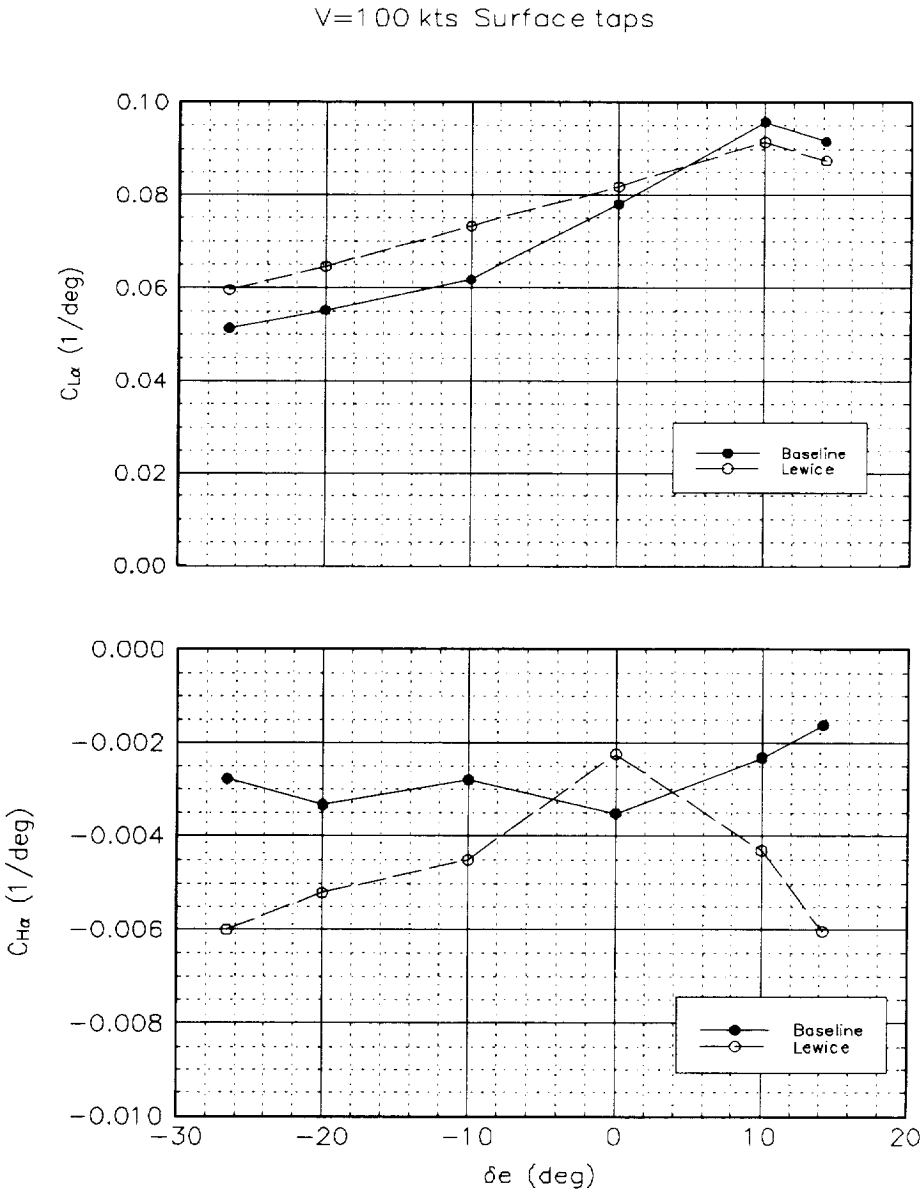

Figure 20 Lift Curve and Hinge Moment Slopes

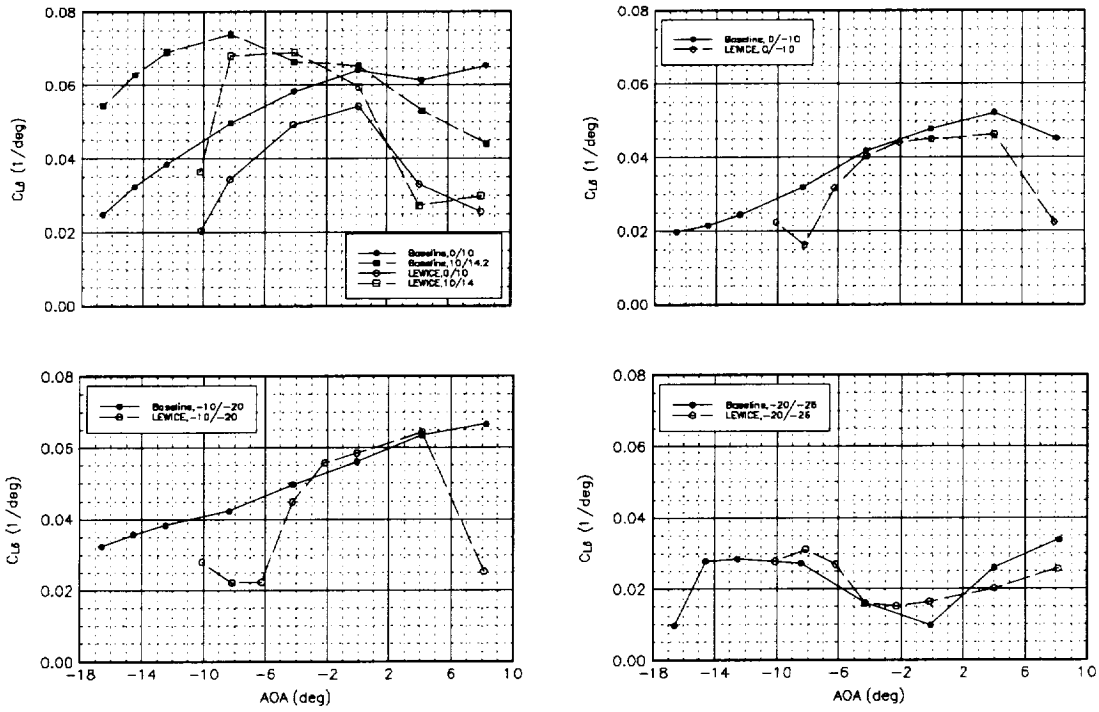

Figure 21 Elevator Lift Effectiveness (V=100 kts, Surface Taps)

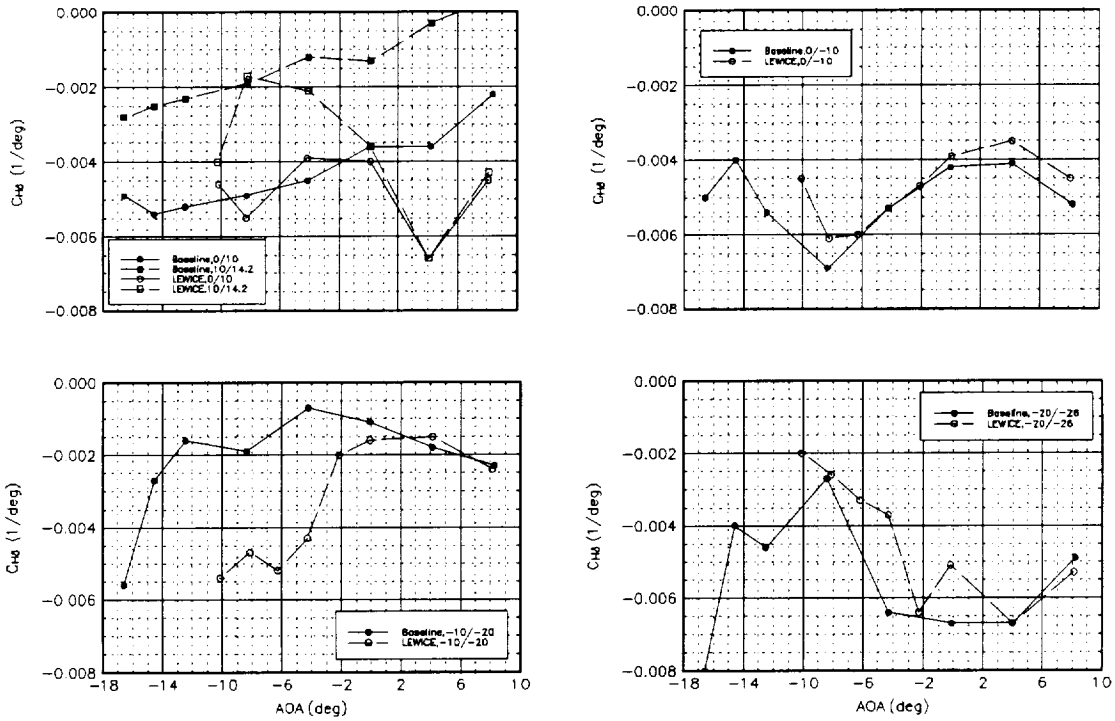

Figure 22 Elevator Hinge Moment Effectiveness (V=100 kts, Surface Taps)

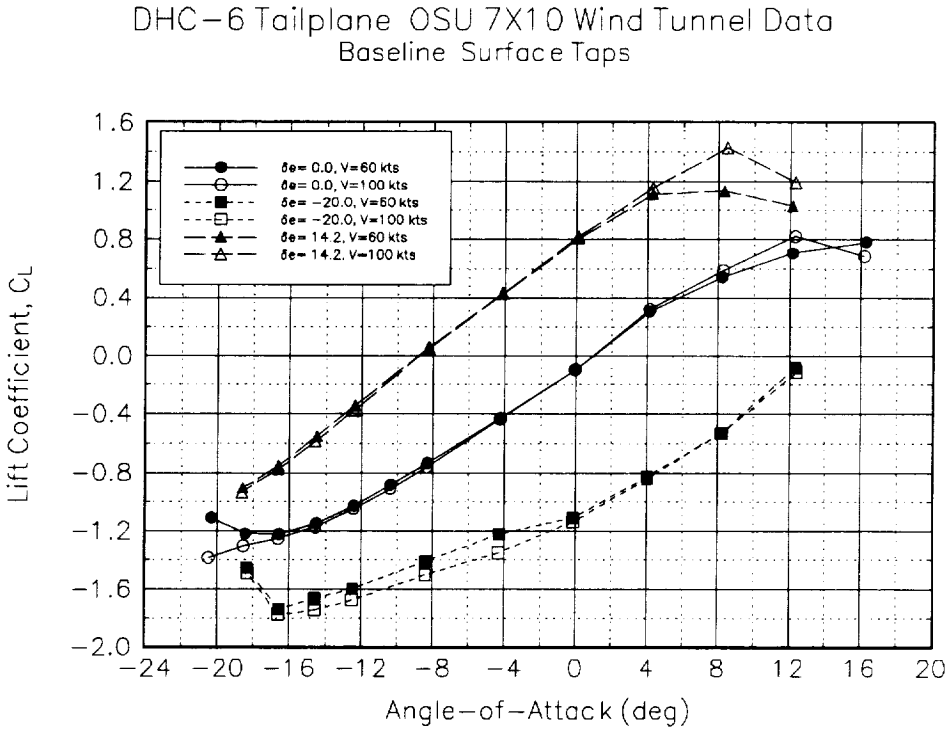

Figure 23 Velocity Effects, Baseline, Lift Characteristics

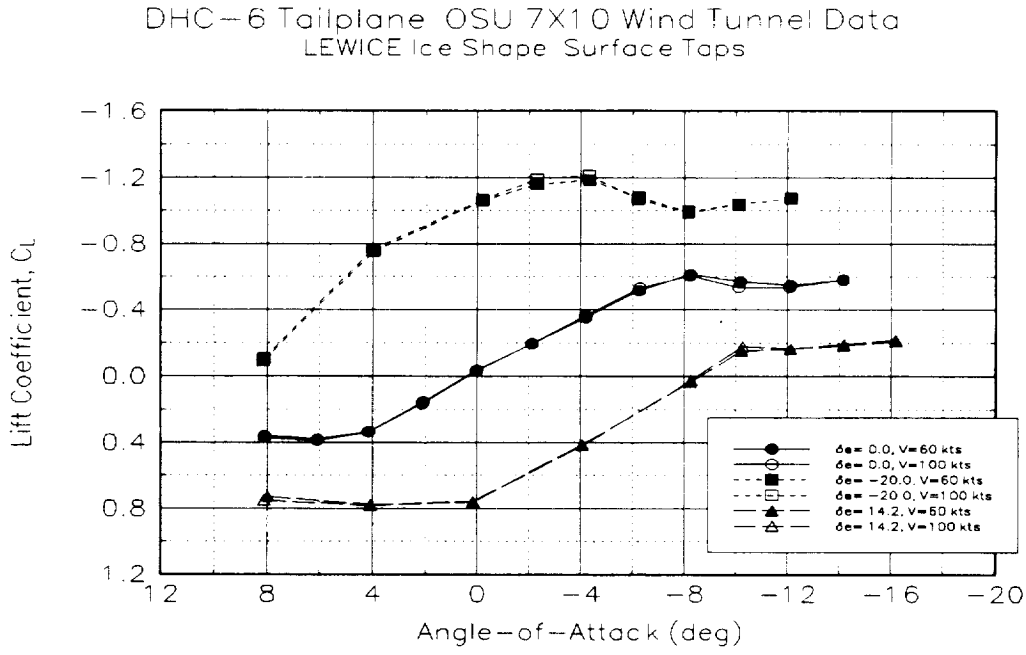

Figure 24 Velocity Effects, LEWICE Ice Shape, Lift Characteristics

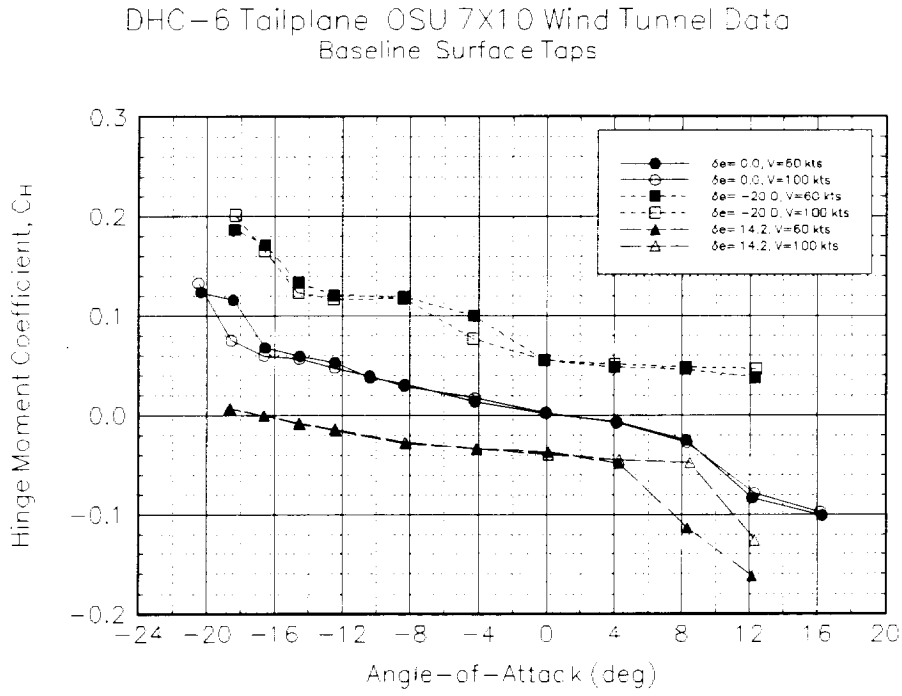

Figure 25 Velocity Effects, Baseline, Hinge Characteristics

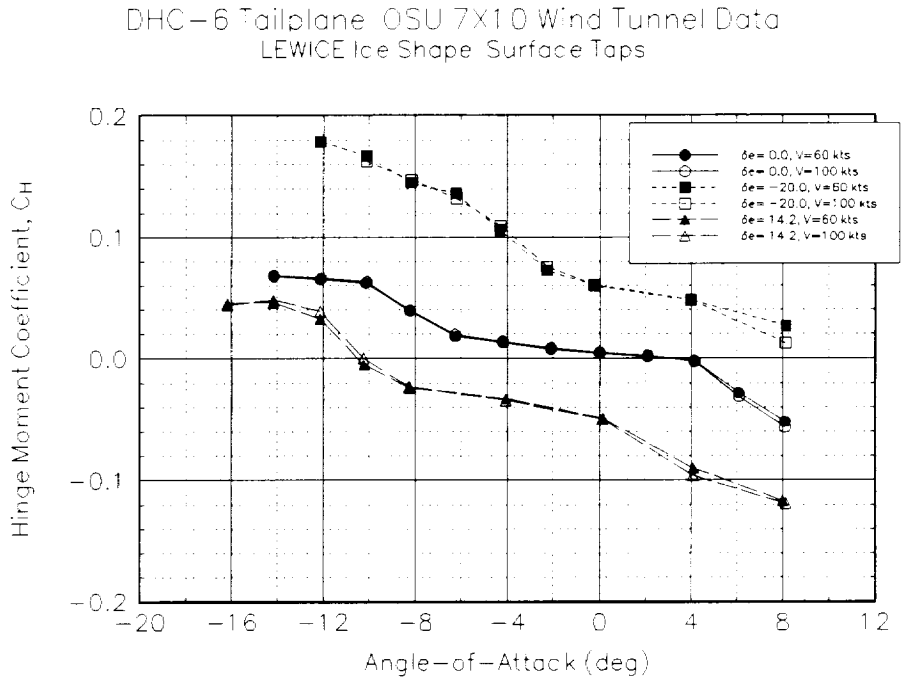

Figure 26 Velocity Effects, LEWICE Ice Shape, Hinge Moment Characteristics

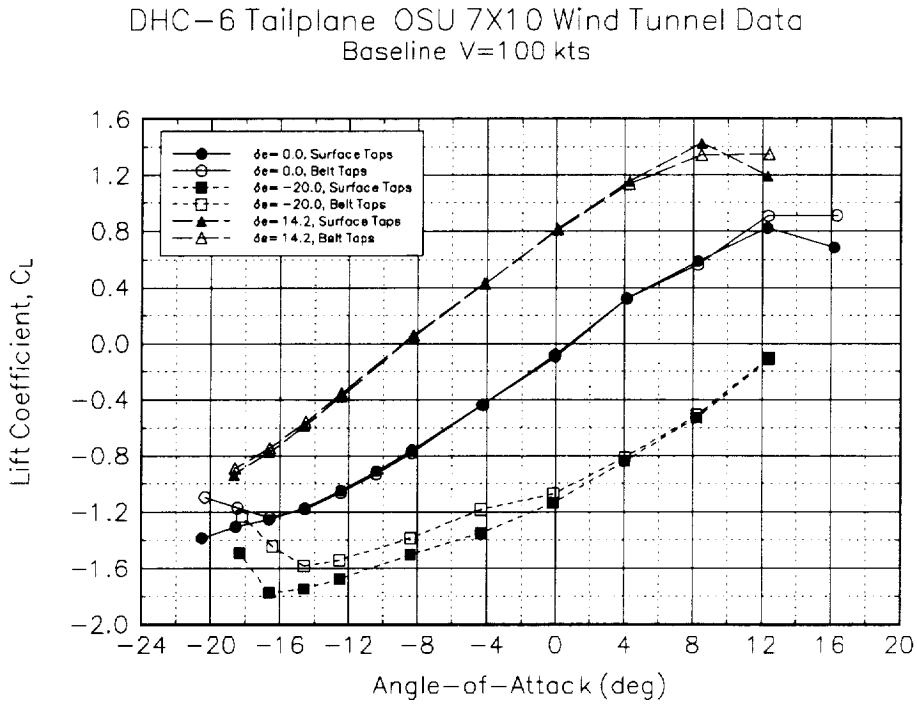

Figure 27 Tap Line Comparison, Baseline, Lift Characteristics

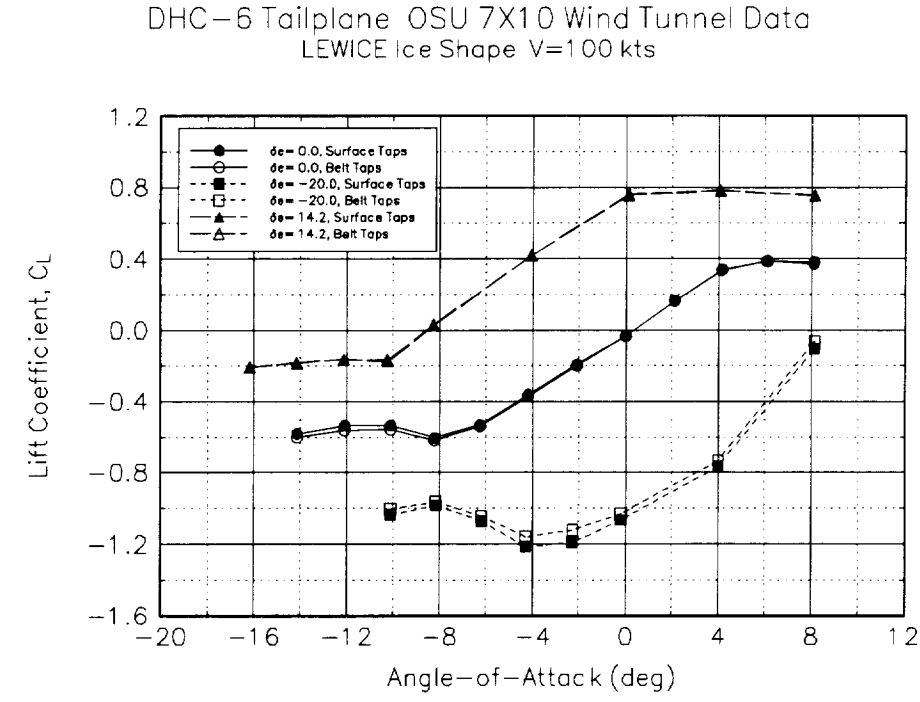

Figure 28 Tap Line Comparison, LEWICE Ice Shape, Lift Characteristics

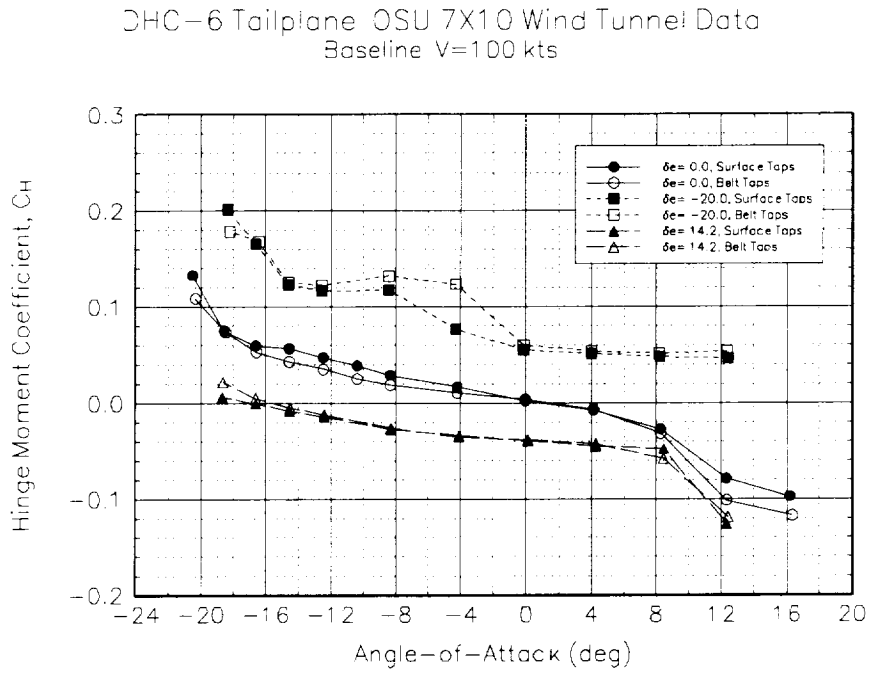

Figure 29 Tap Line Comparison, Baseline, Hinge Moment Characteristics

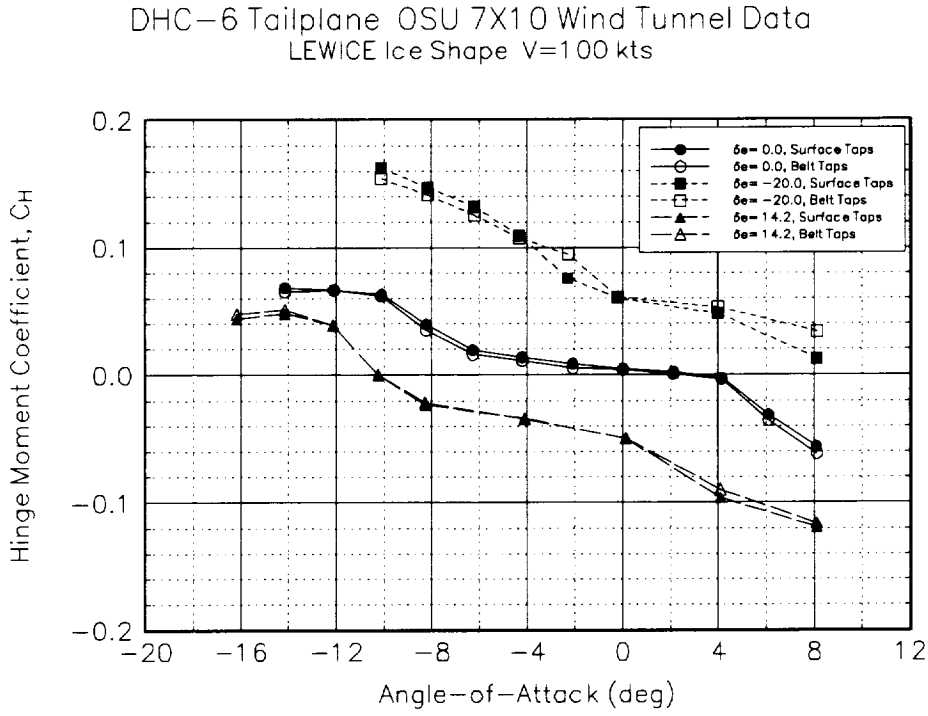

Figure 30 Tap Line Comparison, LEWICE Ice Shape, Hinge Moment Characteristics

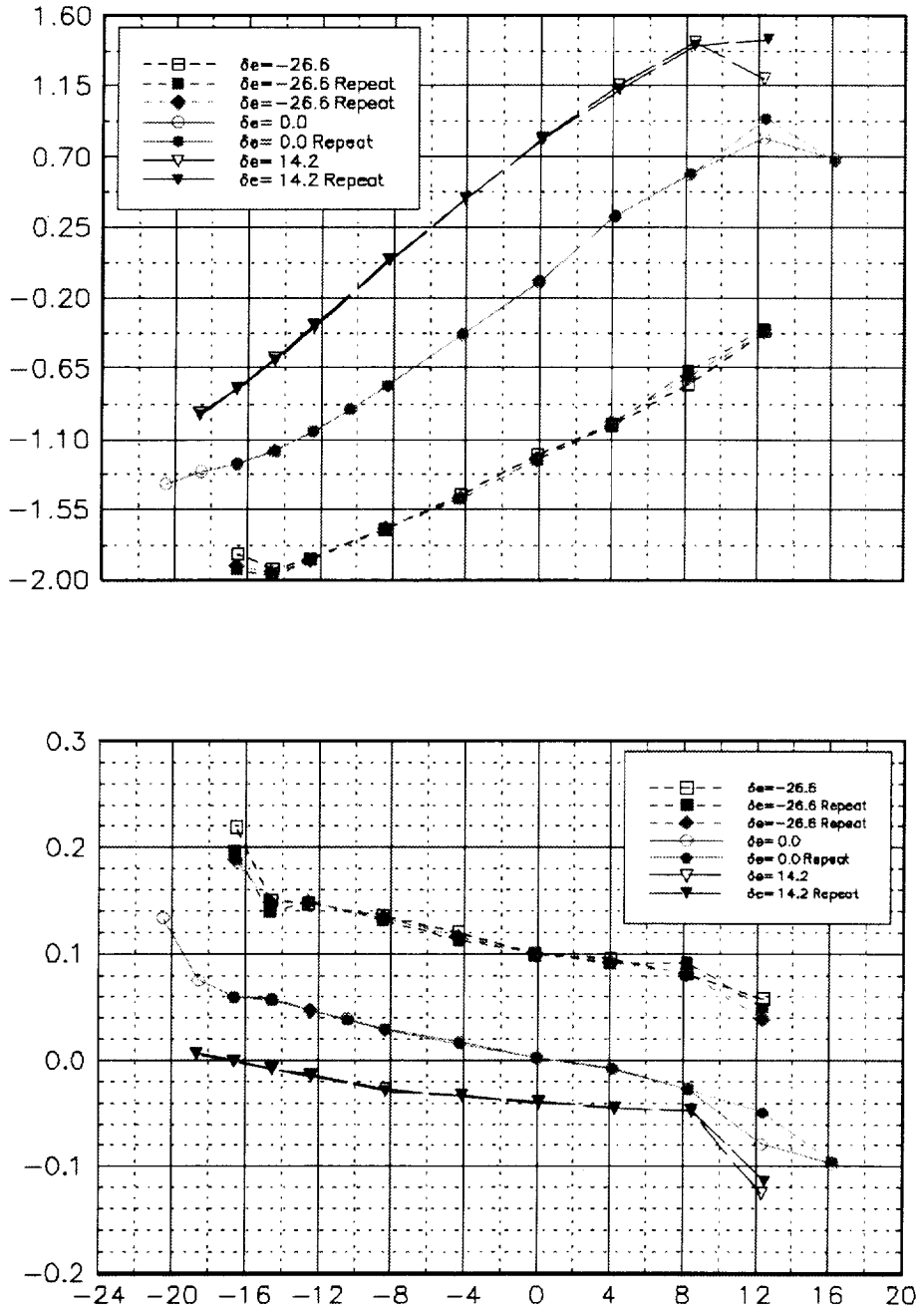

Figure 31 Baseline Repeatability, V=100 kts, Surface Taps

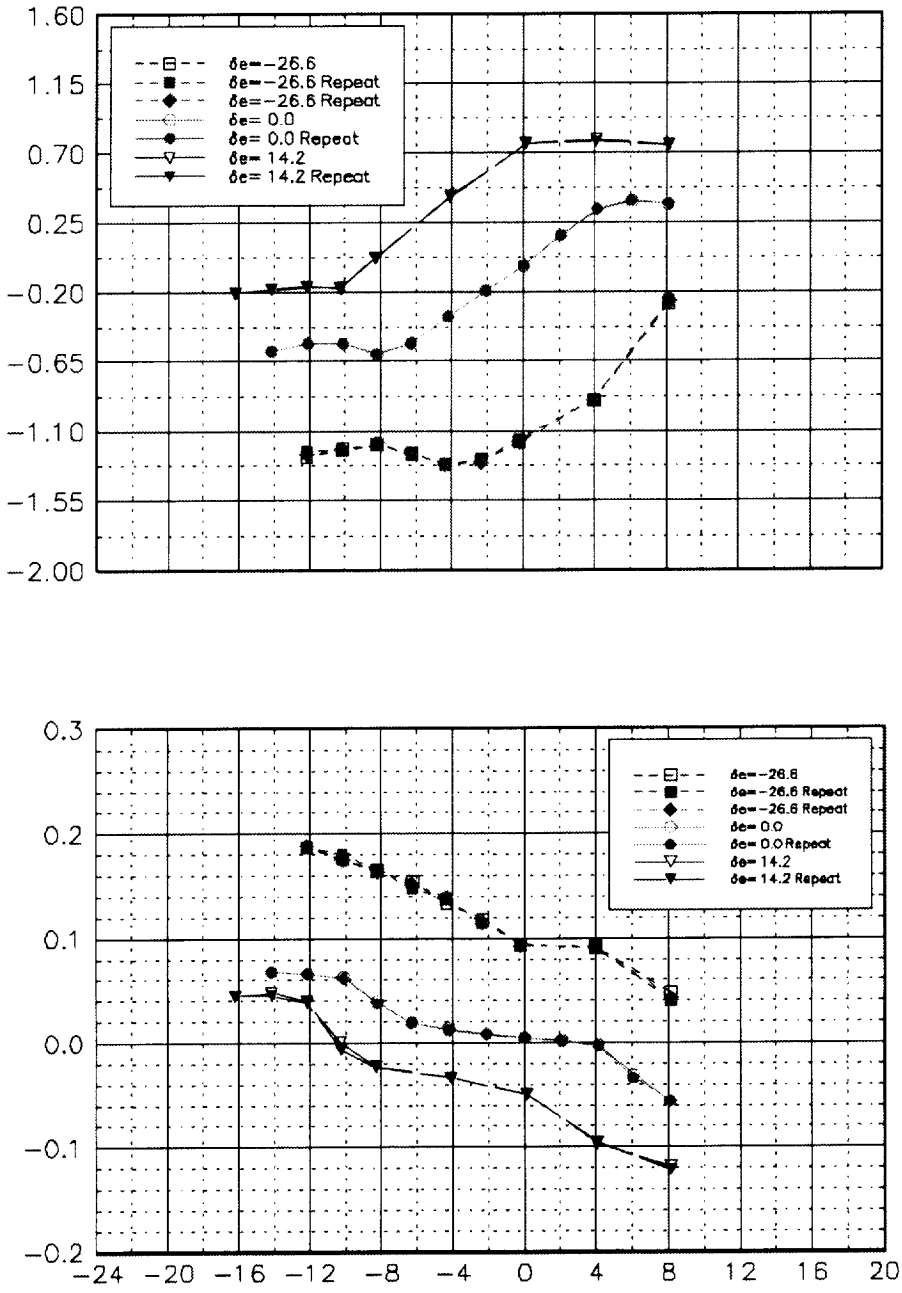

Figure 32 LEWICE Ice Shape Repeatability, V=100 kts, Surface Taps

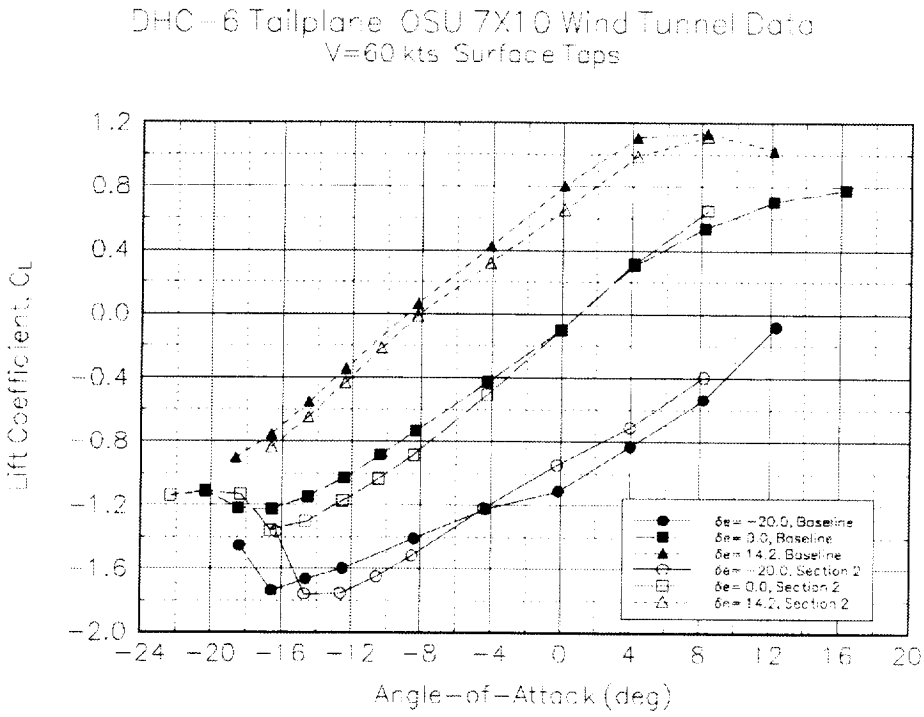

Figure 33 Section 2 Lift Characteristics Comparison

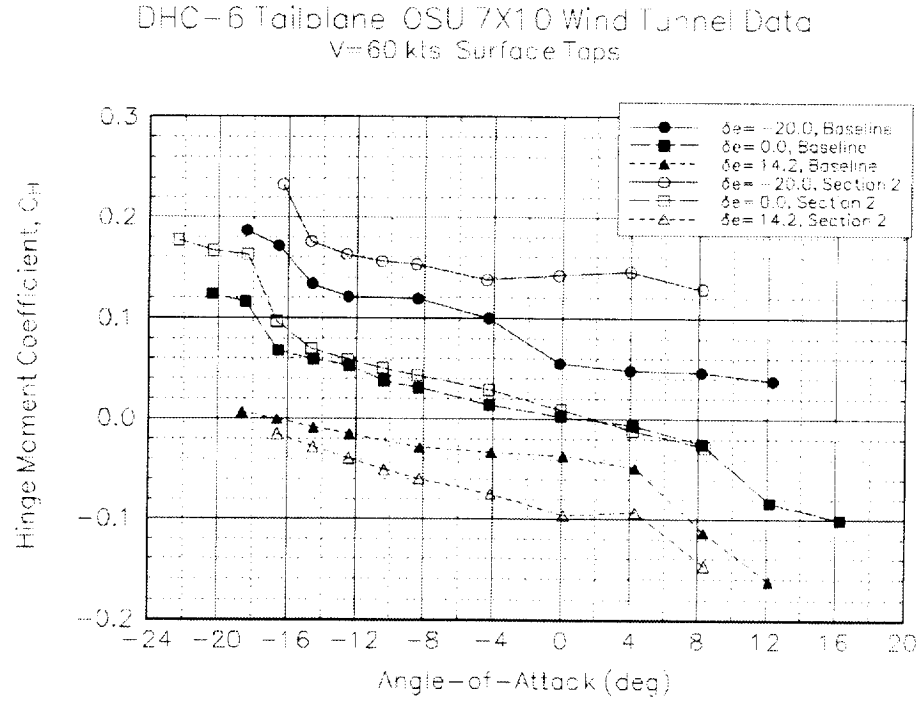

Figure 34 Section 2 Hinge Moment Comparison

Figure 35 Baseline Tuft Flow Visualization, $\alpha = -8.0°$, $\delta_e = 0.0°$

Figure 36 S&C Ice Shape Tuft Flow Visualization, α =-8.0°,δ_e=0.0°

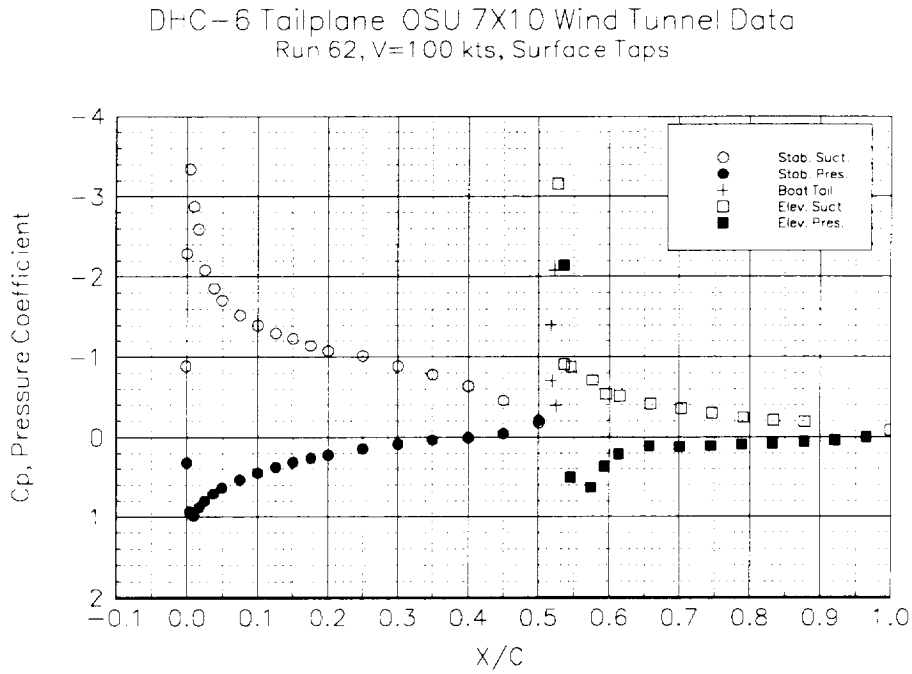

Figure 37 Baseline C_p Distribution, α =-8.0°, δ_e=0.0°

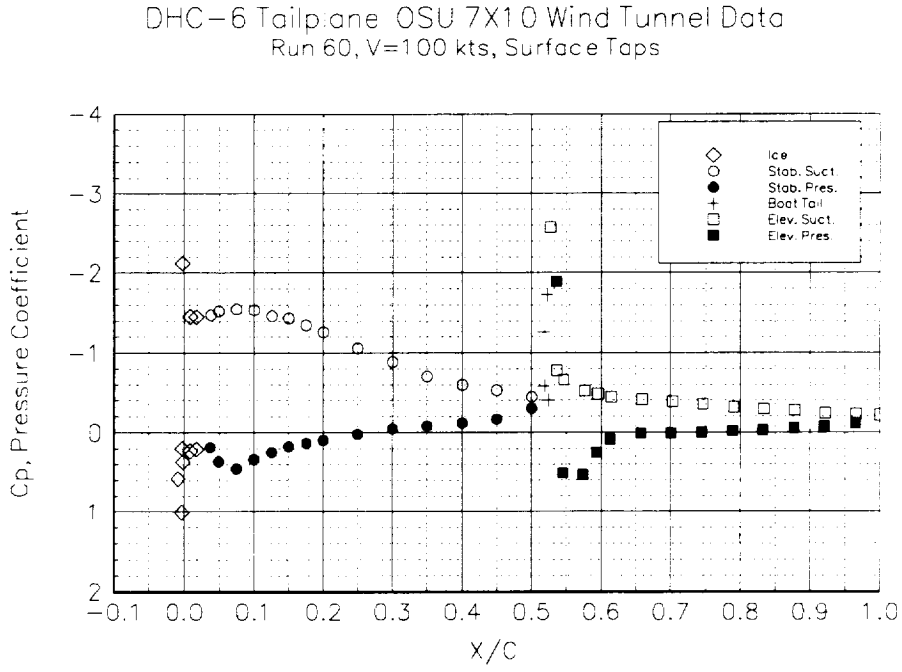

Figure 38 S&C Ice Shape C_p Distribution, α =-8.0°, δ_e=0.0°

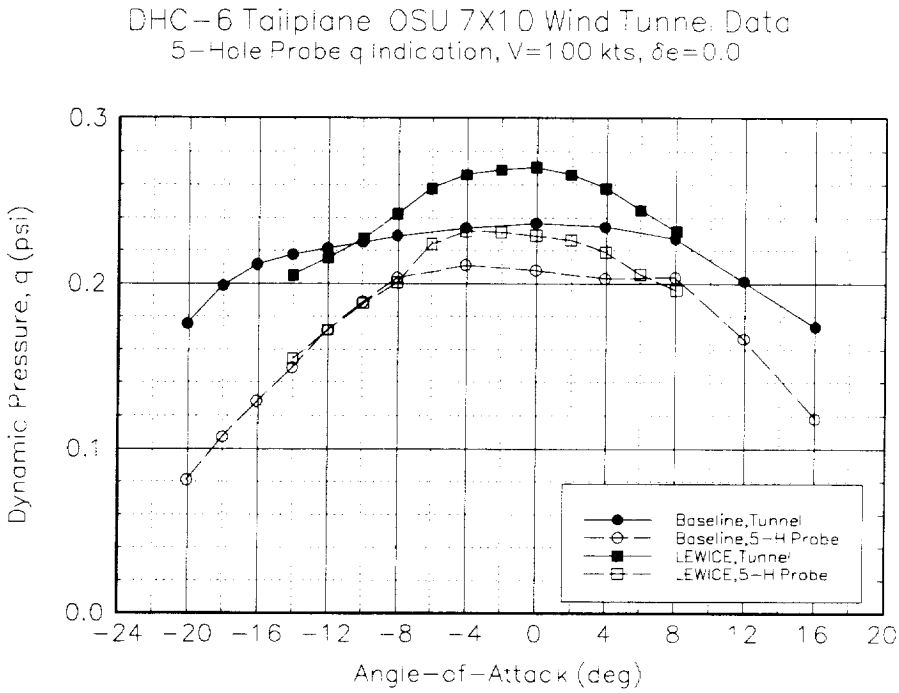

Figure 39 5-Hole Probe Dynamic Pressure Comparison

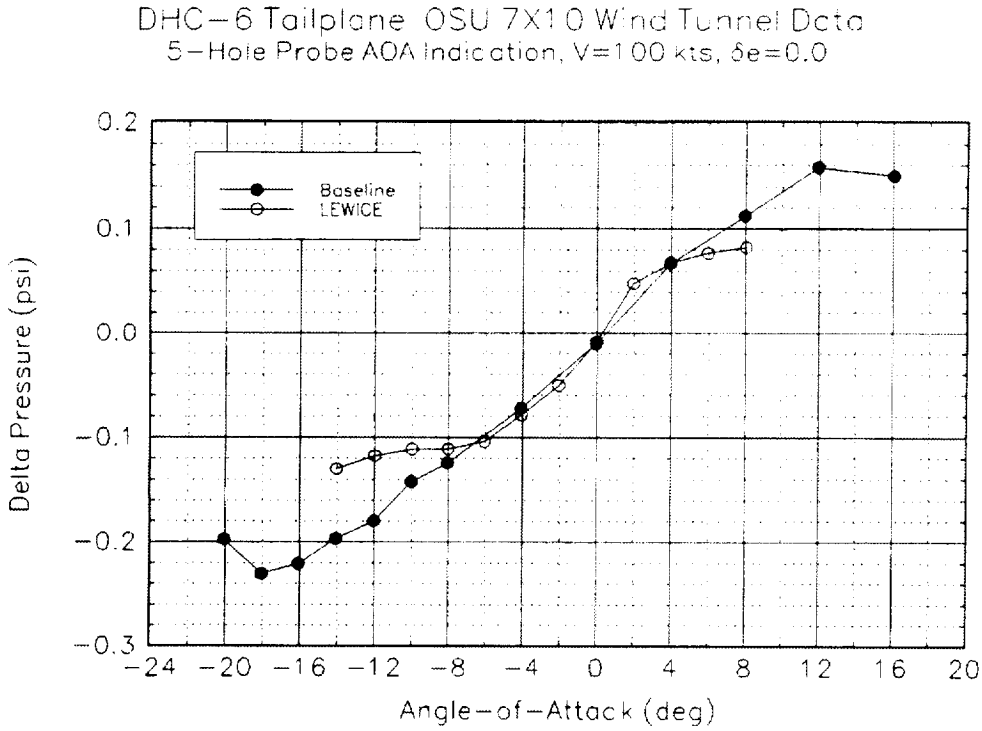

Figure 40 5-Hole Probe Pressure Differential due to Angle-of Attack

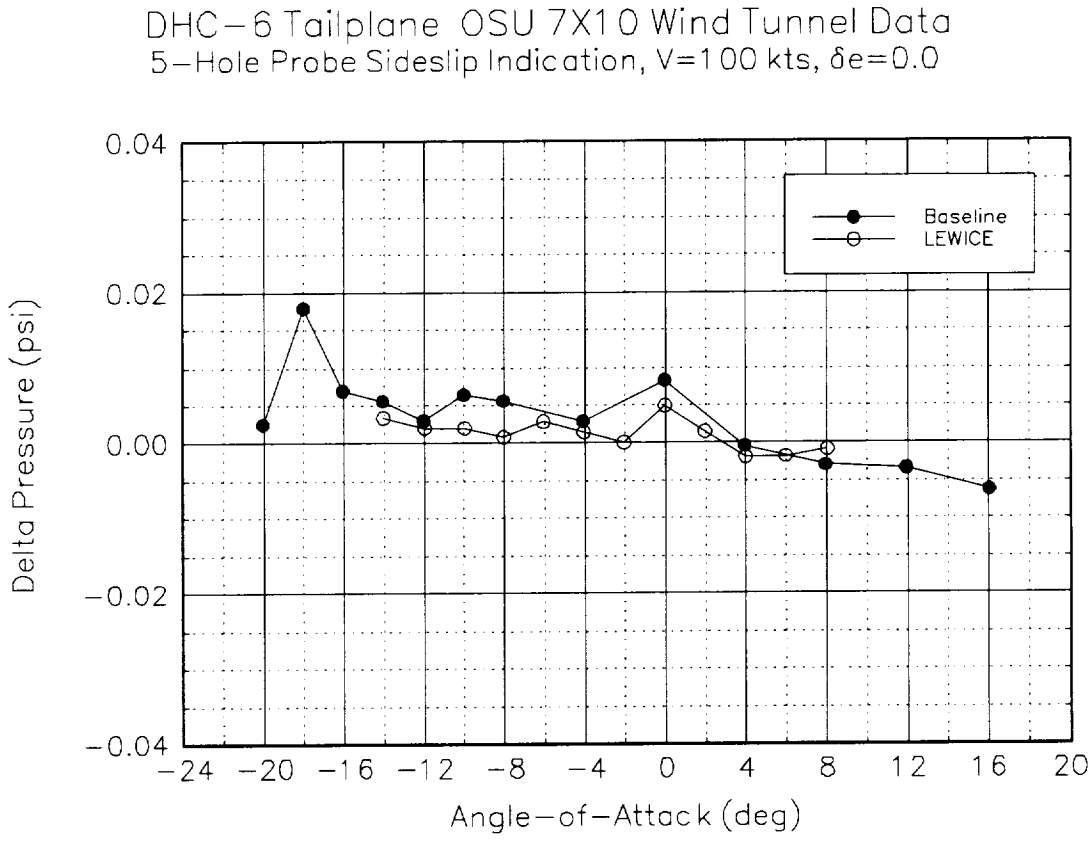

Figure 41 5-Hole Probe Pressure Differential due to Sideslip

8. CONCLUSIONS

A set of data quantifying the 2-D aerodynamics of the DHC-6 Twin Otter tailplane, uniced, and with representative ice shapes, has been obtained. Instrumentation that will be used during future flight testing has been verified to be effective. The results obtained are consistent with expected aerodynamic trends and observed responses during typical pushover maneuvers.

The effects of icing that would have the greatest effect on aircraft stability and control were shown in the changes in lift and hinge moment. For the uniced airfoil with δ_e=0° elevator deflection, C_{Lmax}=-1.3 and AOA_{Stall}=-18.6°. With the LEWICE ice shape, these values were reduced to C_{Lmax}=-0.64 and AOA_{Stall}=-8.2°. Hinge moment data for the LEWICE ice shape at δ_e=-20° showed that C_H increased by ΔC_H=0.02 (trailing edge down) about ΔAOA=2.3° before the stall. These results supported observed responses during typical pushover maneuvers.

Reynolds number variation did not result in any strong characteristic differences in the coefficient data with either ice shape installed. Reynolds number effects were seen for the uniced baseline airfoil, with a lowering of stall AOA by approximately ΔAOA=2° and a decrease in lift coefficient at the slower 60 kts velocities.

The elevator extension and large slot of the baseline airfoil section had a significant effect on the pressure distributions. This was verified by testing of the secondary airfoil section, which showed increased lift, C_{Lmax}=1.35, and a decreased negative angle of attack at stall, AOA=-16.5°. Hinge moment also increased, approximately ΔC_H=0.04 for δ_e=0.0° and -20.0° near stall. All of the components that will be used in future flight testing showed acceptable fidelity. The pressure belt should be a good source of data, however, care must be taken when evaluating these results, as coefficient values can be lowered if the belt is immersed in largely separated flow. The 5-Hole Probe data showed the expected trends with velocity, angle of attack, and sideslip. Differences in dynamic pressures were seen between the tunnel and the probe values, as well as between the baseline and LEWICE configuration data. Calibration of the probe, at a later date, will allow more complete assessment of the probe accuracy and configuration dependencies.

These results have given an effective set of data with which to begin an analysis of tailplane aerodynamics in icing conditions. The data will allow the tailplane aerodynamics during simulated maneuvering flight to be quantified. The flight test instrumentation will allow verification and refinement of these aerodynamics during flight test maneuvers. This combination of simulation and flight test will allow a more complete understanding of the contribution of the tailplane to the aircrafts motion during maneuvering flight. This understanding will be needed, and fully utilized, in the development of maneuvers to identify aircraft susceptible to tailplane stall in icing conditions.

Appendix A
Tap Locations

Section 1, Clean

TAP #	X/C	TAP #	X/C	TAP #	X/C
1	-.0011	31	.3000	74	.7448
2	.0003	32	.3500	75	.7463
3	.0001	33	.3500	76	.7888
4	.0041	34	.4000	77	.7901
5	.0039	35	.4000	78	.8327
6	.0100	36	.4500	79	.8338
7	.0100	37	.4500	80	.8767
8	.0175	38	.5000	81	.8775
9	.0169	39	.5000	82	.9207
10	.0250	40	.5226	83	.9212
11	.0250	41	.5243	84	.9646
12	.0373	42	.5180	85	.9650
13	.0380	43	.5185	86	1.0000
14	.0500	52	.5261		
15	.0500	53	.5363		
16	.0750	54	.5354		
17	.0750	55	.5462		
18	.1000	56	.5449		
19	.1000	57	.5759		
20	.1256	58	.5741		
21	.1260	59	.5955		
22	.1500	60	.5936		
23	.1500	61	.6152		
24	.1753	62	.6131		
25	.1750	63	.6346		
26	.2000	64	.6326		
27	.2000	70	.6569		
28	.2500	71	.6589		
29	.2500	72	.7009		
30	.3000	73	.7026		

Notes:

1) Stabilizer taps are #1–43, elevator taps are #52–86
2) Surface Taps do not include #63, and #64.
3) Belt Taps do not include #42, #43, #57, #63, #74, #78, and #82.

Section 2, Clean

TAP #	X/C	TAP #	X/C	TAP #	X/C
1	-.0011	31	.3000	78	.8327
2	.0003	32	.3500	79	.8338
3	.0001	33	.3500	80	.8767
4	.0041	34	.4000	81	.8775
5	.0039	35	.4000	82	.9207
6	.0100	36	.4500	83	.9212
7	.0100	37	.4500	84	.9646
8	.0175	38	.5000	85	.9650
9	.0169	39	.5000	86	1.0000
10	.0250	44	.5500		
11	.0250	45	.5500		
12	.0373	46	.6000		
13	.0380	47	.6000		
14	.0500	48	.6173		
15	.0500	49	.6086		
16	.0750	50	.6084		
17	.0750	51	.6089		
18	.1000	65	.6119		
19	.1000	66	.6164		
20	.1256	67	.6174		
21	.1260	68	.6297		
22	.1500	69	.6314		
23	.1500	70	.6569		
24	.1753	71	.6589		
25	.1750	72	.7009		
26	.2000	73	.7026		
27	.2000	74	.7448		
28	.2500	75	.7463		
29	.2500	76	.7888		
30	.3000	77	.7901		

Notes:

1) Stabilizer taps are #1–51, elevator taps are #65–86
2) Surface Taps do not include #76.
3) Belt Taps do not include #63 through #86.

S&C Ice Shape Taps

TAP #	X/C	Y/C
1	-.0084	.0030
2	-.0027	.0201
3	-.0014	-.0150
4	-.0018	.0315
5	-.0019	-.0264
6	.0088	.0308
7	.0088	-.0275
8	.0175	.0286
9	.0175	-.0258

Notes:

1) These Taps replace Surface Taps #1 through #11.
2) These Taps replace Belt Taps #1 through #9.

LEWICE Ice Shape Taps

TAP #	X/C	Y/C
1	-.0104	.0029
2	-.0207	.0338
3	-.0165	-.0282
4	-.0044	.0239
5	-.0044	-.0213

Notes:

1) These Taps replace Surface Taps #1 through #5, and #7.
2) These Taps replace Belt Taps #1 through #5.

Section 1 (Baseline)

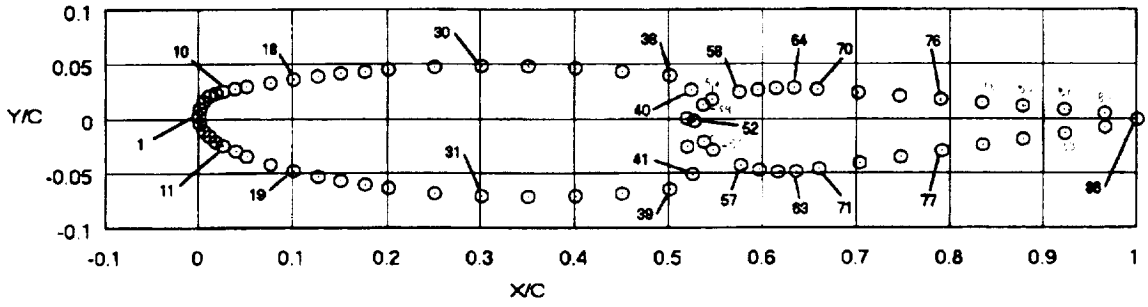

Section 2

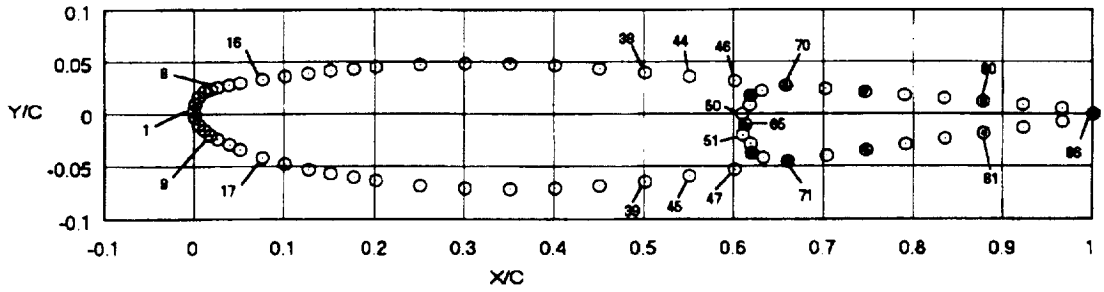

DHC-6 Tailplane Airfoil Section Tap Locations

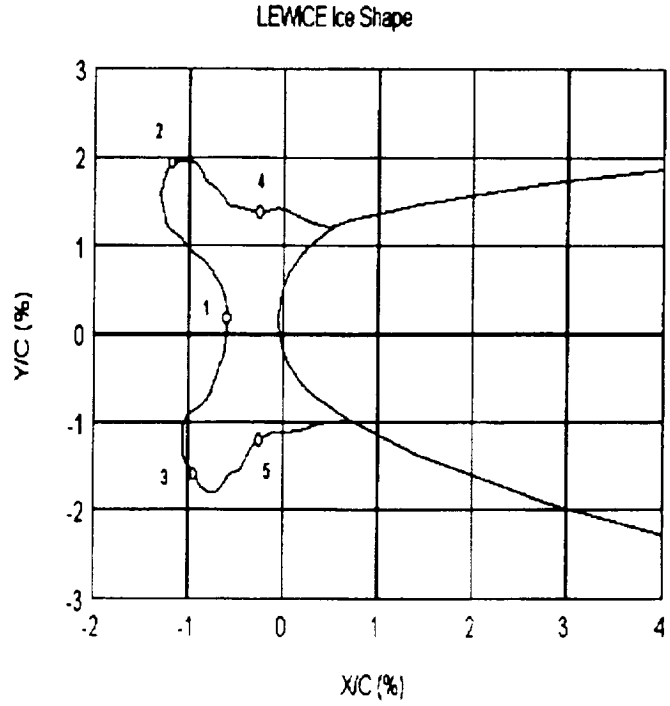

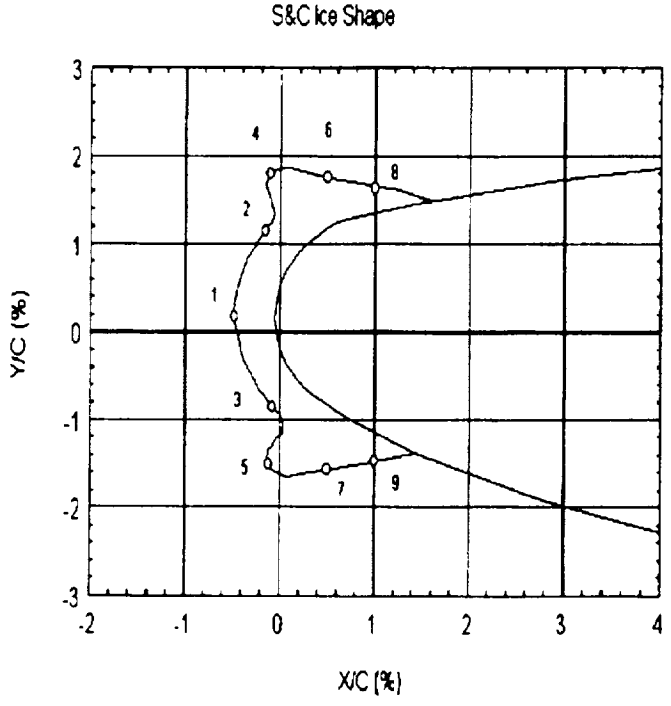

Ice Shape Tap Locations

Appendix B
Run Log

Start of Test 09-01-94, End of Test 09-20-94

Run	Configuration	Velocity (kts)	Elevator (deg)	AOA /Remarks (deg)
01	Baseline	60.0	0.0	18,16,14,12,10,8,6,4,2,0,-2,-4,-6,-8, -10,-12,-14,-16,-18
02	"	100.0	0.0	12,8,4,0,-4,-8,-12,-14,-16,-18
03	"	60.0	-10.0	"
04	"	100.0	"	"
05	"	60.0	"	-18,-20,-22
06	"	"	-20.0	12,8,4,0,-4,-8,-12,-14,-16,-18
07	"	100.0	"	"
08				Check Run
09				Check Run
10	Baseline	60.0	-20.0	12,8,4,0,-4,-8,-12,-14,-16,-18
11	"	100.0	"	"
12	"	60.0	-26.6	12,8,4,0,-4,-8,-12,-14,-16
13	"	100.0	"	12,8,4,0,-4
14	"	100.0	-26.6	-8,-12,-14,-16
15	"	60.0	10.0	12,8,4,0,-4,-8,-12,-14,-16,-18
16	"	100.0	"	"
17	"	60.0	14.2	"
18	"	100.0	"	"
19	S&C Ice Shape	60.0	14.2	12,8,4,0,-4,-8,-10,-12,-14, -16,-18
20	"	100.0	"	8,4,0,-4,-8,-10,-12,-14,-16
21	"	60.0	10.0	8,4,0,-4,-8,-12,-14,-16
22	"	100.0	"	"
23	"	60.0	0.0	8,4,0,-4,-6,-8,-10,-12,-14
24	"	100.0	"	"
25	"	60.0	-10.0	"
26	"	100.0	"	Bad run
27	"	100.0	"	8,4,0,-4,-6,-8,-10,-12,-14
28	"	60.0	-20.0	8,4,0,-2,-4,-6,-8,-10,-12
29	"	100.0	"	"
30	"	60.0	-26.6	"
31	"	100.0	"	"
32	LEWICE Ice Shape	60.0	-26.6	"
33	"	100.0	"	"
34	"	60.0	-20.0	"
35	"	100.0	"	"
36				Bad run

Run	Configuration	Velocity (kts)	Elevator (deg)	AOA /Remarks (deg)
37	LEWICE Ice Shape	60.0	-10.0	8,4,0,-2,-4,-6,-8,-10,-12
38	"	100.0	"	"
39				Not Used
40	"	60.0	0.0	8,6,4,2,0,-2,-4,-6,-8,-10, -12,-14
41	"	100.0	"	"
42	"	60.0	10.0	8,4,0,-4,-8,-10,-12,-14,-16
43	"	100.0	"	"
44	"	60.0	14.2	8,4,0,-4,-8,-10,-12,-14,-16
45	"	100.0	"	"
46	" "	"		Repeat of 045
47	"	100.0	0.0	Repeat of 041
48	" "		-26.6	Repeat of 033
49	"	"	"	Repeat 2 of 033
50	Baseline "	"		Repeat of 013
51	"	"	"	Repeat 2 of 013
52	"	"	-10.0	Repeat of 004
53	"	60.0	"	Repeat of 003
54	"	60.0	0.0	Repeat of 001
55	"	100.0	"	Repeat of 002
56	"	100.0	"	Repeat of 055
57	"	100.0	14.2	Repeat of 018
58	S&C Ice Shape	60.0	"	Repeat of 019
59	"	100.0	"	Repeat of 020
60	"	"	0.0	Repeat of 024
	"	"	"	Flow Viz
61	"	"	-26.6	Repeat of 031, Flow Viz
	Baseline	60.0	"	Flow Viz
	"	60.0	0.0	Flow Viz
62	Baseline, NP	100.0	"	16,12,8,4,0,-4,-8,-12,-14,-16, -18,-20, Flow Viz
63	Section 2, NP	60.0	"	8,4,0,-4,-8,-10,-12,-14,-16,Flow Viz
64	"	"	-20.0	"
65	"	"	14.2	"
66	" "		0.0	-16,-18,-20,-22,Flow Viz

Notes:
1. Runs 01 through 07 had an inoperative scanivalve.
2. Run 19 had the 5-Hole Probe cover installed.
3. Wake probe sweep runs - 0001,0002,0003,0023,0024,0040,0041,0063
4. Wall Statics available for runs 0035 and up, only.
5. Flow Viz indicates more complete tufting and documentation.
6. Post run AOA=0.0° point for all runs after 009 not indicated.
7. NP = No 5-Hole Probe.

Appendix C
Video Log

This log contains a listing of the approximate time for the video taken during testing. To conserve tape, only approximately 15 seconds of each data point were recorded. The times listed below are the approximate start times for each run.

Run 0001
Date 09/08/94

AOA	Time
18	1324
16	1328
14	1334
12	1341
10	1346
8	1352
6	1357
4	1402
2	1407
0	1412
-2	1416
-4	1422
-6	1426
-8	1431
-10	1435
-12	1442
-14	1446
-16	1452
-18	1456

Run 0002
Date 09/08/94

AOA	Time
16	1629
12	1634
8	1639
4	1644
0	1649
-4	1655
-8	1700
-10	1707
-12	1710
-14	1715
-16	1721

Run 0003/5
Date 09/09/94

AOA	Time
12	0931
8	0937
4	0942
0	0947
-4	0952
-8	0958
-12	1004
-14	1009
-16	1013
-18	1018
-18	1153
-20	1156
-22	1200

Run 0004
Date 09/09/94

AOA	Time
12	1103
8	1106
4	1113
0	1114
-4	1117
-8	1120
-12	1123
-14	1127
-16	1130
-18	1133

Run 0006
Date 09/08/94

AOA	Time
12	1242
8	1246
4	1249
0	1253
-4	1256
-8	1259
-12	1303
-14	1306
-16	1309
-18	1313
-20	1316

Run 0007
Date 09/09/94

AOA	Time
12	1328
8	1334
4	1335
0	1339
-4	1342
-8	1346
-12	1350
-14	1354
-16	1356
-18	1359
-20	1403

Run 0010
Date 09/12/94

AOA	Time
12	1553
8	1557
4	1600
0	1605
-4	1606
-8	1610
-12	1613
-14	1616
-16	1620
-18	1623

Run 0011
Date 09/12/94

AOA	Time
12	1639
8	1643
4	1647
0	1650
-4	1653
-8	1656
-12	1700
-14	1704
-16	1707
-18	1711

Run 0012
Date 09/12/94

AOA	Time
12	1758
8	1801
4	1805
0	1808
-4	1812
-8	1815
-12	1818
-14	1182
-16	1825

Run 0013/14
Date 09/12/13/94

AOA	Time
12	1836
8	1840
4	1843
0	1847
-4	1850
-8	0929
-12	0932
-14	0936
-16	0939

Run 0015
Date 09/13/94

AOA	Time
12	1015
8	1019
4	1022
0	1026
-4	1029
-8	1032
-12	1035
-14	1038
-16	1042
-18	1745

Run 0016
Date 09/13/94

AOA	Time
12	1101
8	1105
4	1108
0	1111
-4	1115
-8	1118
-12	1122
-14	1125
-16	1128
-18	1045

Run 0017
Date 09/12/13/94

AOA	Time
12	1220
8	1224
4	1228
0	1232
-4	1235
-8	1238
-12	1241
-14	1244
-16	1247
-18	1251

Run 0018
Date 09/13/94

AOA	Time
12	1305
8	1309
4	1312
0	1316
-4	1319
-8	1322
-12	1326
-14	1329
-16	1332
-18	1336

Run 0019
Date 09/14/94

AOA	Time
12	1006
8	1010
4	1013
0	1017
-4	1020
-8	1024
-12	1027
-14	1030
-16	1037
-18	1040

Run 0020
Date 09/14/94

AOA	Time
8	1110
4	1114
0	1118
-4	1121
-8	1124
-10	1127
-12	1131
-14	1135
-16	1138

Run 0021
Date 09/14/94

AOA	Time
8	1216
4	1220
0	1223
-4	1227
-8	1230
-10	1233
-12	1236
-16	1240
-18	1243

Run 0022
Date 09/14/94

AOA	Time
8	1256
4	1300
0	1304
-4	1307
-8	1310
-10	1313
-12	1317
-16	1320
-18	1323

Run 0023
Date 09/14/94

AOA	Time
8	1400
4	1406
0	1414
-4	1415
-6	1421
-8	1428
-10	1430
-12	1435
-14	1441

Run 0024
Date 09/14/94

AOA	Time
8	1458
4	1505
0	1509
-4	1515
-6	1520
-8	1525
-10	1530
-12	1537
-14	1541

Run 0025
Date 09/14/94

AOA	Time
8	1628
4	1633
0	1635
-4	1639
-6	1642
-8	1645
-10	1649
-12	1652
-14	1655

Run 0026/27
Date 09/14/94

AOA	Time
8	1708
4	1711
0	1715
-4	1718
-6	1722
-8	1725
-10	1728
-12	1731
-14	1849

Run 0028
Date 09/14/94

AOA	Time
8	1929
4	1932
0	1938
-2	1939
-4	1943
-6	1946
-8	1949
-10	1953
-12	1956

Run 0029
Date 09/14/94

AOA	Time
8	2010
4	2013
0	2016
-2	2020
-4	2023
-6	2026
-8	2029
-10	2033
-12	2036

Run 0030
Date 09/15/94

AOA	Time
8	0910
4	0913
0	0918
-2	0921
-4	0923
-6	0927
-8	0930
-10	0934
-12	0937

Run 0031
Date 09/15/94

AOA	Time
8	0955
4	1000
0	1005
-2	1007
-4	1010
-6	1013
-8	1017
-10	1021
-12	1023

Run 0032
Date 09/15/94

AOA	Time
8	1455
4	1459
0	1503
-2	1506
-4	1510
-6	1513
-8	1516
-10	1519
-12	1522

Run 0033
Date 09/15/94

AOA	Time
8	1537
4	1541
0	1545
-2	1548
-4	1551
-6	1554
-8	1558
-10	1601
-12	1605

Run 0034
Date 09/15/94

AOA	Time
8	1658
4	1702
0	1705
-2	1708
-4	1711
-6	1715
-8	1718
-10	1722
-12	1725

Run 0035
Date 09/15/94

AOA	Time
8	1832
4	1836
0	1839
-2	1843
-4	1846
-6	1850
-8	1853
-10	1856

Run 0037
Date 09/15/94

AOA	Time
8	2012
4	2015
0	2018
-2	2021
-4	2025
-6	2028
-8	2031
-10	2034
-12	2037

Run 0038
Date 09/15/94

AOA	Time
8	2053
4	2056
0	2100
-2	2103
-4	2107
-6	2110
-8	2114
-10	2117
-12	2120

Run 0040
Date 09/16/94

AOA	Time
8	0904
6	0910
4	0915
2	0920
0	0925
-2	0930
-4	0934
-6	0940
-8	0945
-10	0950
-12	0955
-14	1000

Run 0041
Date 09/16/94

AOA	Time
8	1159
6	1205
4	1210
2	1215
0	1220
-2	1225
-4	1230
-6	1235
-8	1241
-10	1245
-12	1250
-14	1256

Run 0042
Date 09/15/94

AOA	Time
8	1400
4	1405
0	1409
-4	1412
-8	1415
-10	1418
-12	1421
-14	1425
-16	1428

Run 0043
Date 09/16/94

AOA	Time
8	1610
4	1614
0	1617
-4	1620
-8	1624
-10	1627
-12	1630
-14	1633
-16	1637

Run 0044
Date 09/16/94

AOA	Time
8	1730
4	1735
0	1738
-4	1741
-8	1745
-10	1748
-12	1752
-14	1755
-16	1758

Run 0045
Date 09/15/94

AOA	Time
8	1828
4	1833
0	1835
-4	1838
-8	1842
-10	1845
-12	1848
-14	1852
-16	1855

Appendix D
Solid Wall Correction Calculations

The effect of the walls on the 2-dimensional airfoil data must be considered. Corrections have been applied to the raw wind tunnel data using the methods of Ref. D1. For this test, three phenomena have been taken into account:

Solid Blockage

Solid blockage creates an increase of velocity due to the reduction of the area through which the air must flow. To quantify this effect, computations have been made by considering the two-dimensional model as a cylinder. This cylinder can be simulated as a doublet of strength $\mu = 2\pi V a^2$ (a : cylinder radius), with the walls represented by the streamlines created by matching doublets, on each side of the cylinder. Therefore,

$$\frac{\Delta V}{V_u} = \frac{a^2}{h^2}$$ (The subscript u indicates uncorrected data)

After doing a summation, we obtain,

$$\varepsilon_{sb} = \left(\frac{\Delta V}{V_u}\right)_{tot} = \Lambda\sigma$$

with:

h : tunnel height
c : model chord

$$\sigma = \left(\frac{\pi^2}{48}\right)\left(\frac{c}{h}\right)^2$$

$$\Lambda = \frac{16}{\pi}\int_0^1 \frac{y}{c}\left[(1-P)\left(1+\frac{dy}{dx}\right)\right]^{\frac{1}{2}} d\frac{x}{c}$$

x, y: airfoil coordinates, P its no-camber, symmetrical, pressure distribution.

Usually Λ is given by a graph
In our case, $\Lambda = 0.22$

Wake Blockage

Wake blockage creates a velocity increment at the model because of a pressure gradient due to higher velocity which keeps the flow around the model. In computations, the wake is simulated by a line source and the walls by an infinite vertical row of source-sink combinations. This reduces to:

$$\varepsilon_{wb} = \frac{\Delta V}{V_u} = \frac{c}{4h} C_{du}$$

We can, then, correct the tunnel conditions by these equations:

$$V = V_u(1+\varepsilon) \qquad \text{with :}$$
$$q = q_u(1+2\varepsilon) \qquad \varepsilon = \varepsilon_{sb} + \varepsilon_{wb}$$

$$Re = Re_u(1+\varepsilon)$$

From the dynamic pressure effect and the wake gradient term, we get:

$$C_d = C_{du}(1 - 3\varepsilon_{sb} - 2\varepsilon_{wb})$$

Streamline Curvature

The lift and moment about the quarter chord of an airfoil are too large at a given angle of attack (which is also too large). This is due to the fact that the airfoil seems to have more camber because of the floor and ceiling.

Calculations of this effect are made by assuming that the airfoil can be approximated by a single vortex at its quarter-chord point. The floor and ceiling are represented by a vertical row of vortices, extending to infinity and with alternating signs. The load on the airfoil can be decomposed as a flat plate loading, computed as an angle of attack correction, and an elliptical loading, which gives the lift, pitching-moment and hinge-moment corrections.

It can be shown that the upwash induced at the half chord by the two images is:

$$\Delta\alpha = \frac{1}{8\pi} \frac{c^2}{h^2 + \left(\frac{c}{4}\right)^2} Cl$$

We can consider that $(c/4)^2$ is small compared to h^2, so it gives σ equal to σ previously found, and we have then:

$$\alpha = \alpha_u + \frac{57.3\sigma}{2\pi}\left(C_{lu} + 4C_{m_{\frac{1}{4}u}}\right)$$

$$C_l = C_{lu}(1 - \sigma - 2\varepsilon)$$

$$C_{m_{\frac{1}{4}}} = C_{m_{\frac{1}{4}u}}(1 - 2\varepsilon) + \frac{\sigma C_l}{4}$$

Hinge Moment

To establish a correction for the hinge moment, we follow the same analysis process discussed above, but we consider only the flap, or elevator, instead of the entire airfoil. We are now at a three-quarter-chord point, so we lose accuracy by taking $(3c/4)^2 << h^2$ in the $\Delta\alpha$ expression.
Therefore, including this 3c/4 term results in $\sigma' = 0.9\,\sigma$.

So,

$$C_h = C_{hu}(1 - 2\varepsilon) + \frac{\sigma'}{4}C_{lf} \qquad \text{with:}$$

C_{lf} : lift coefficient of the elevator

References

D1. Rae, W. and Pope, A., Low Speed Wind Tunnel Testing, Wiley-Interscience, 1984.

Appendix E
Data Reduction Output File Formats

Uncorrected Coefficients

File Name: AA500XX.DAT
Run: 00XX

Column	Value
1	AOA (degrees)
2	Elevator Deflection (degrees)
3	Mach Number
4	Reynolds Number (millions)
5	Q (psi)
6	Velocity (kts.)
	From Surface Taps
7	C_L (total)
8	C_D (pressure only)
9	C_M (1/4c)
10	C_L (Elevator only)
11	C_H (Elevator)
	From Belt Taps
12	C_L
13	C_D (pressure only)
14	C_M (1/4c)
15	C_L (Elevator only)
16	C_H (Elevator)
17	Run Number

Corrected Coefficients using Surface Taps

File Name: SC500XX.DAT
Run: 00XX

Column	Value
1	AOA (degrees)
2	Elevator Deflection (degrees)
3	Mach Number
4	Reynolds Number (millions)

5	Q (psi)
6	Velocity (kts.)
7	C_L (total)
8	C_D (pressure only)
9	C_M (1/4c)
10	C_H (Elevator)

Corrected Coefficients using Belt Taps

File Name: BC500XX.DAT
Run: 00XX

Column	Value
1	AOA (degrees)
2	Elevator Deflection (degrees)
3	Mach Number
4	Reynolds Number (millions)
5	Q (psi)
6	Velocity (kts.)
7	C_L (total)
8	C_D (pressure only)
9	C_M (1/4c)
10	C_H (Elevator)

Probe Pressures

File Name: PP500XX.DAT
Run: 00XX

Column	Value
1	AOA (degrees)
2	Elevator Deflection (degrees)
3	Mach Number
4	Reynolds Number (millions)
5	Q (psi)
6	Velocity (kts.)
7	P Total (psi.)
8	P Static (psi.)
9	P AOA 1 (psi.) (for AOA Suction side)

10	P AOA 2 (psi.) (for AOA Pressure side)
11	P Beta 1 (psi.) (for Sideslip R/H side)
12	P Beta 2 (psi.) (for Sideslip L/H side)

Wall Static Pressures
(Available for Runs 0035 and up, only.)

File Name: WS500XX.DAT
Run: 00XX

Column	Value
1	AOA (degrees)
2	Elevator Deflection (degrees)
3	Mach Number
4	Reynolds Number (millions)
5	Q (psi)
6	Velocity (kts.)
7	Ps West Forward (psi.)
8	Ps West Center (psi.)
9	Ps West Aft (psi.)
10	Ps East Forward (psi.)
11	Ps East Center (psi.)
12	Ps East Aft (psi.)

Appendix F
DHC-6 Twin Otter Tailplane Coefficient Data

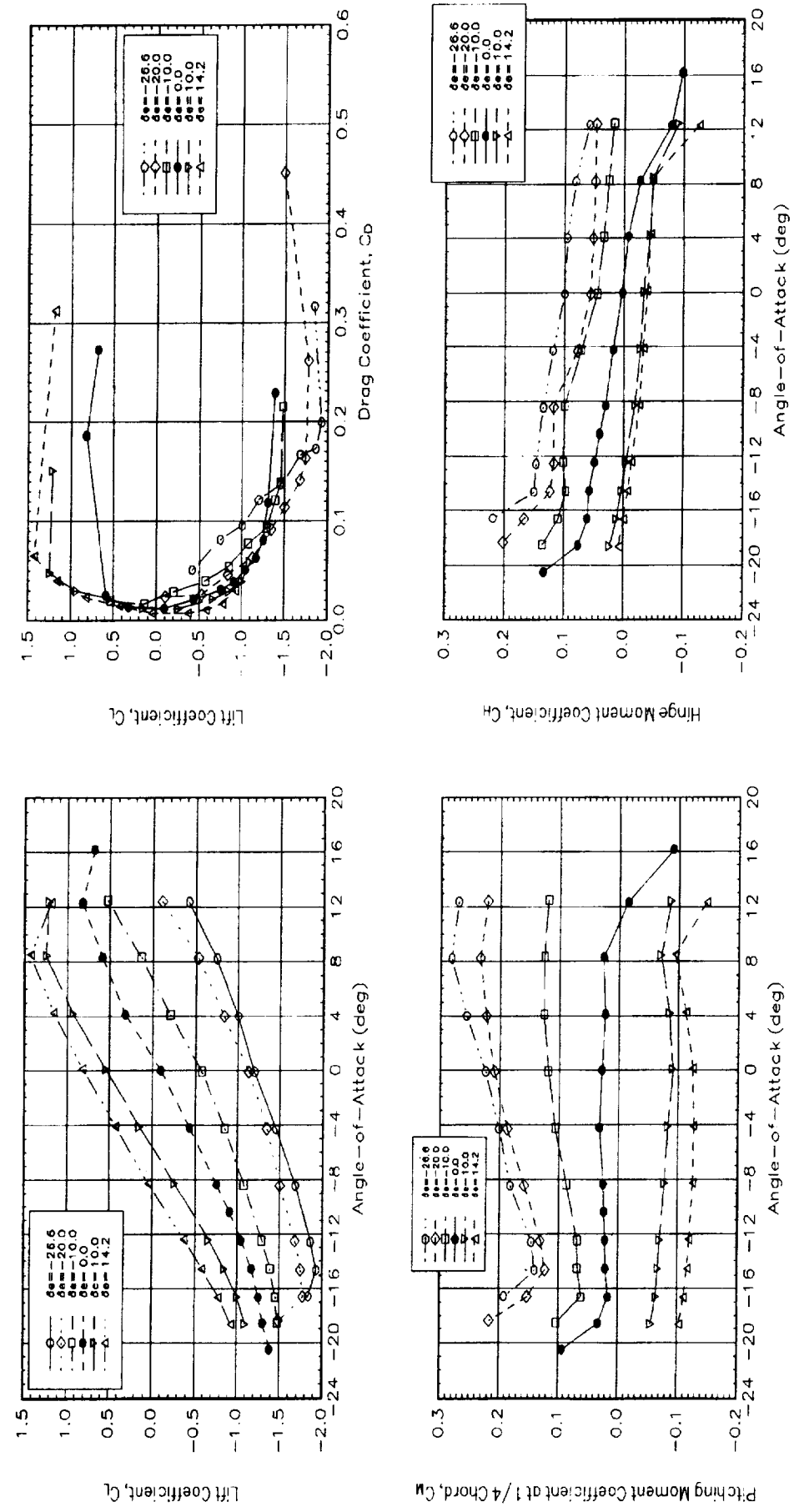

Figure F.01 Baseline, 100 kts

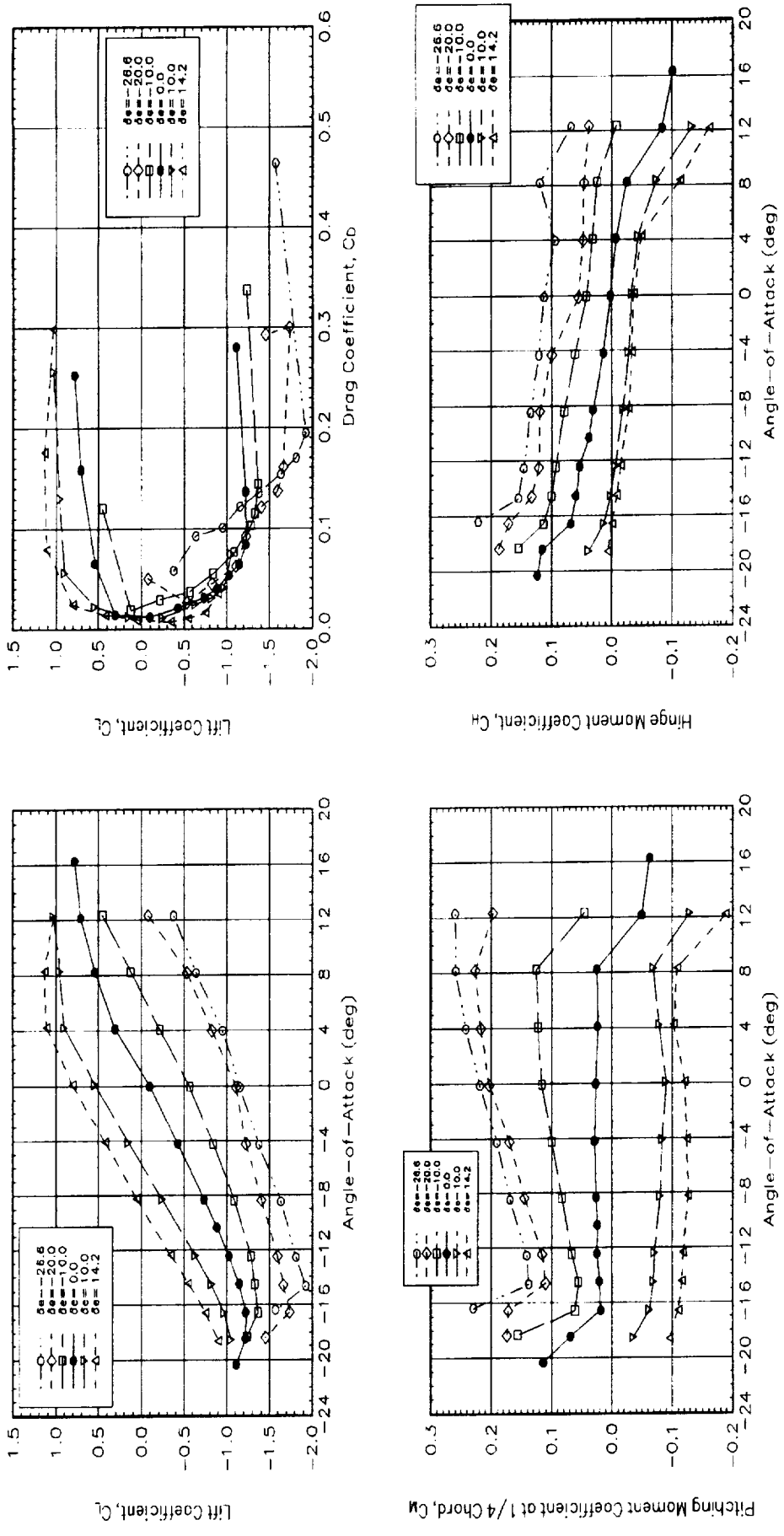

Figure F.02 Baseline, 60 kts

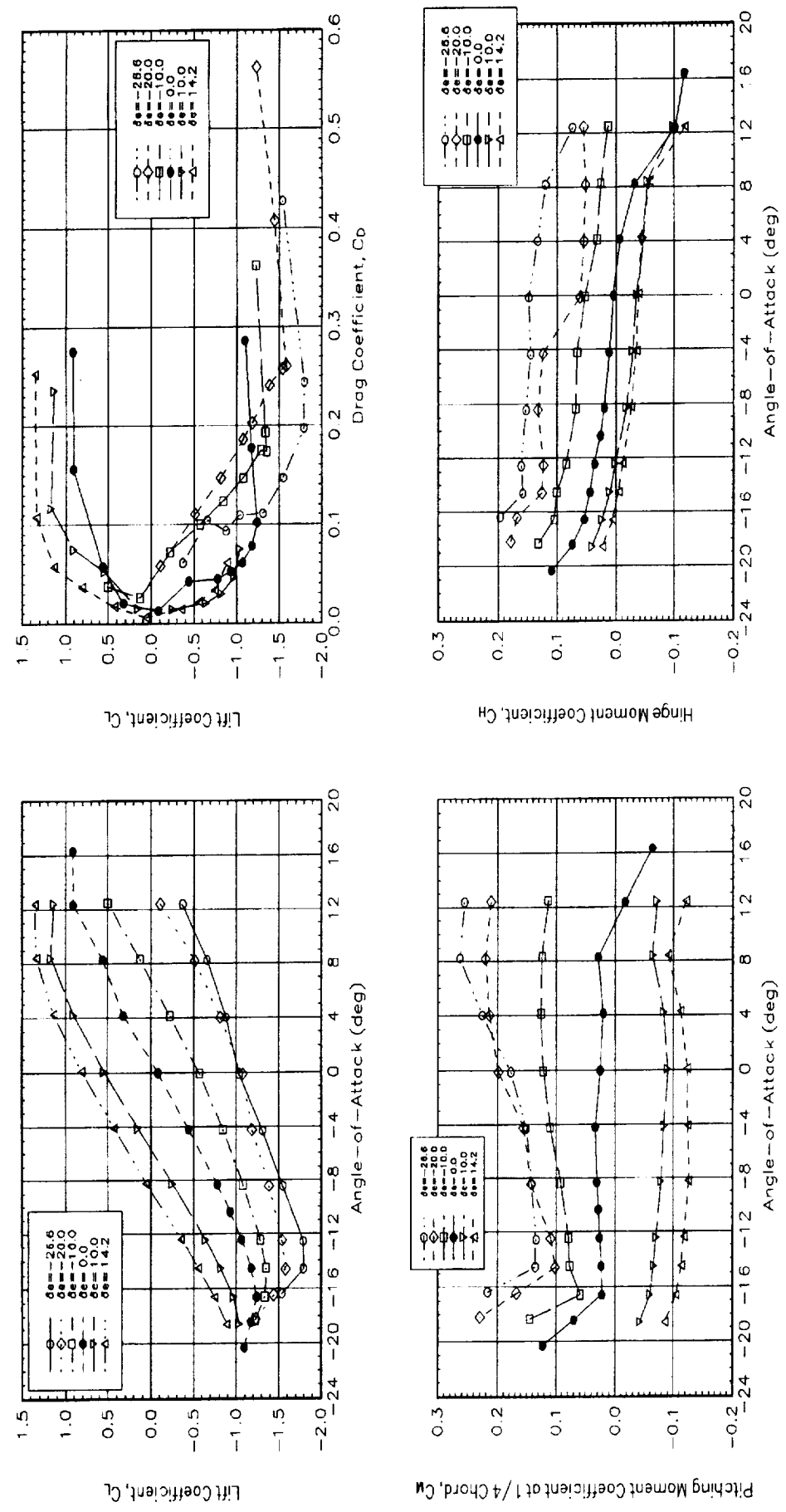

Figure F.03 Baseline, 100 kts, Belt Taps

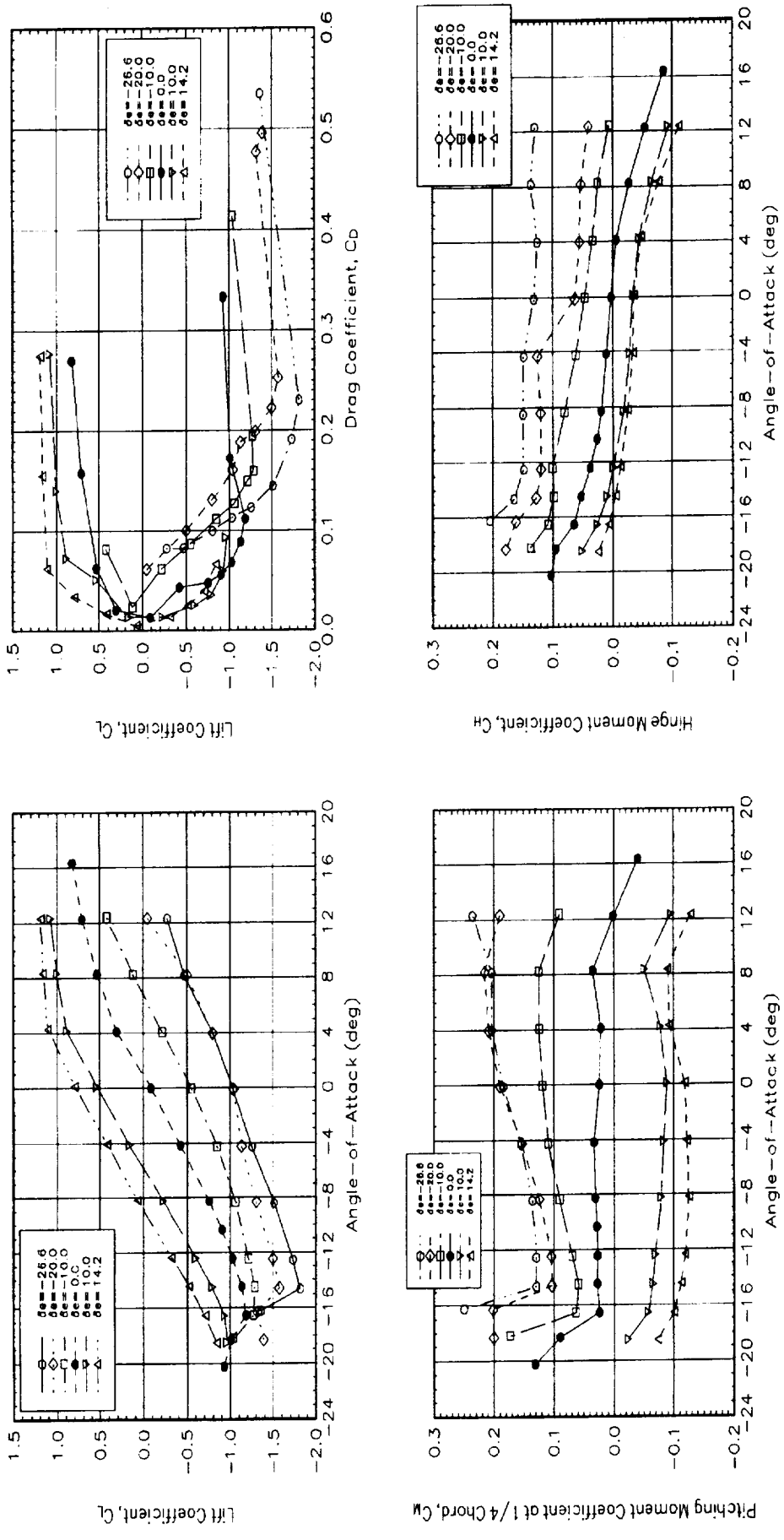

Figure F.04 Baseline, 60 kts, Belt Taps

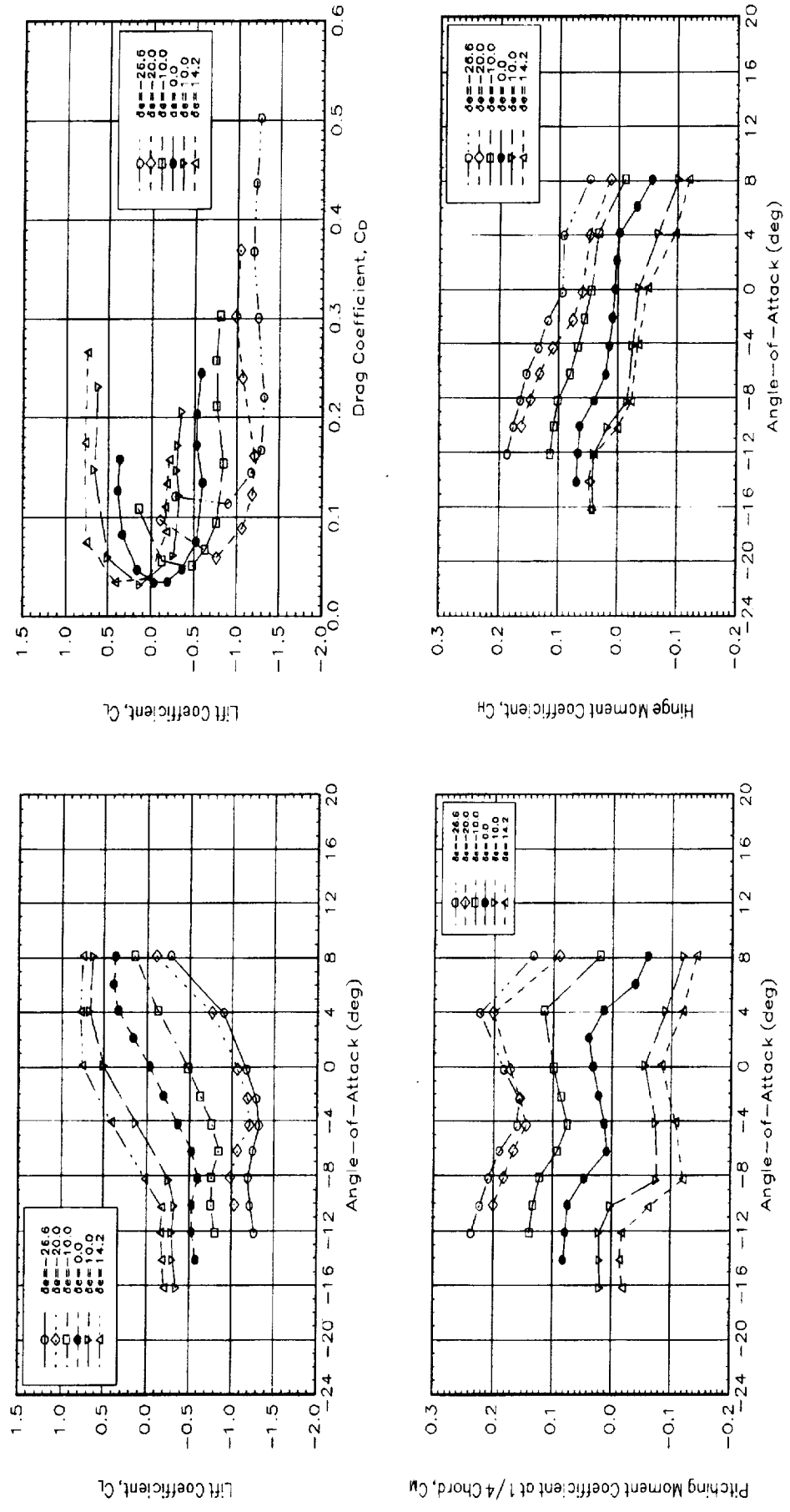

Figure F.05 Lewice Ice Shape 100 kts

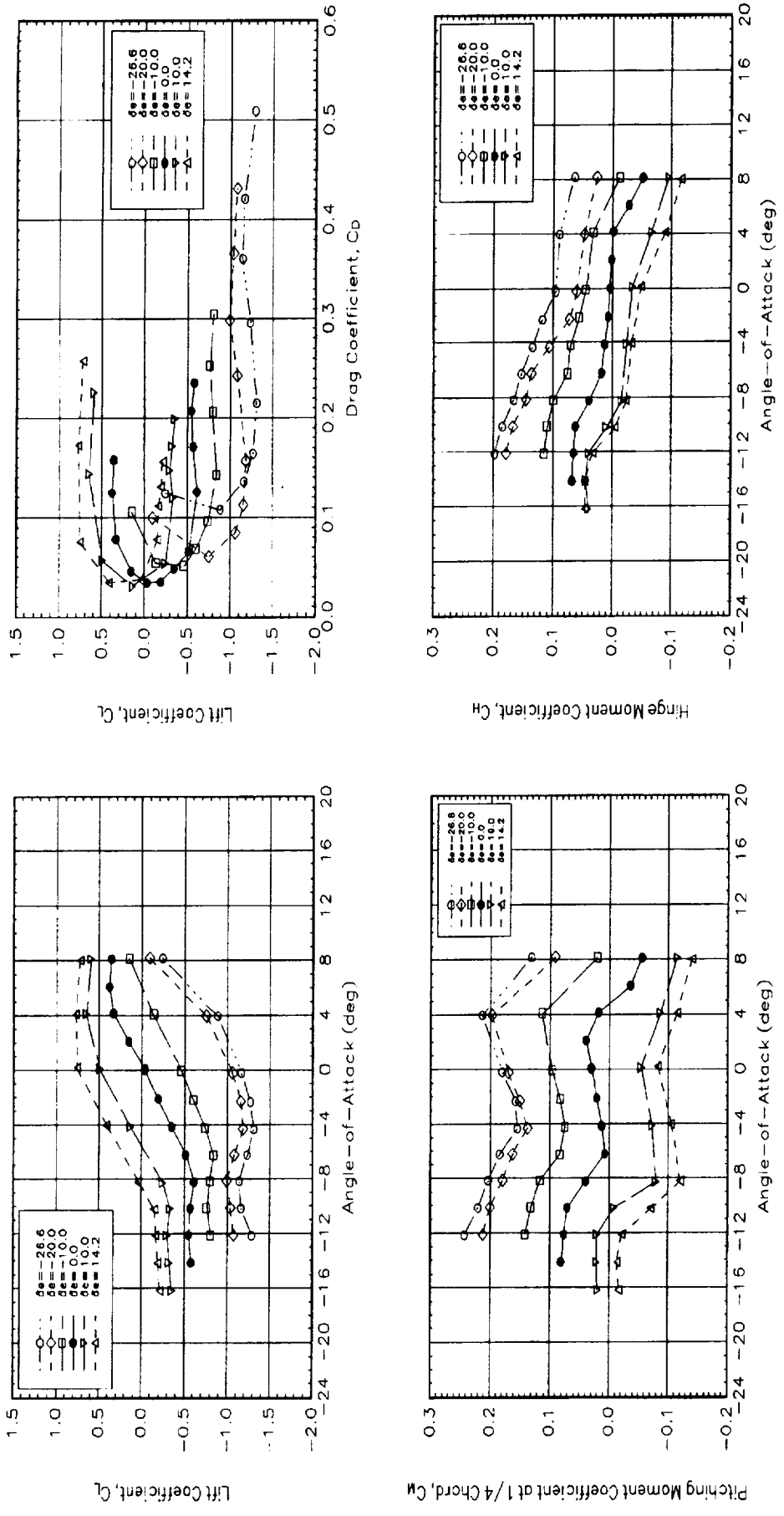

Figure F.06 Lewice Ice Shape 60 kts

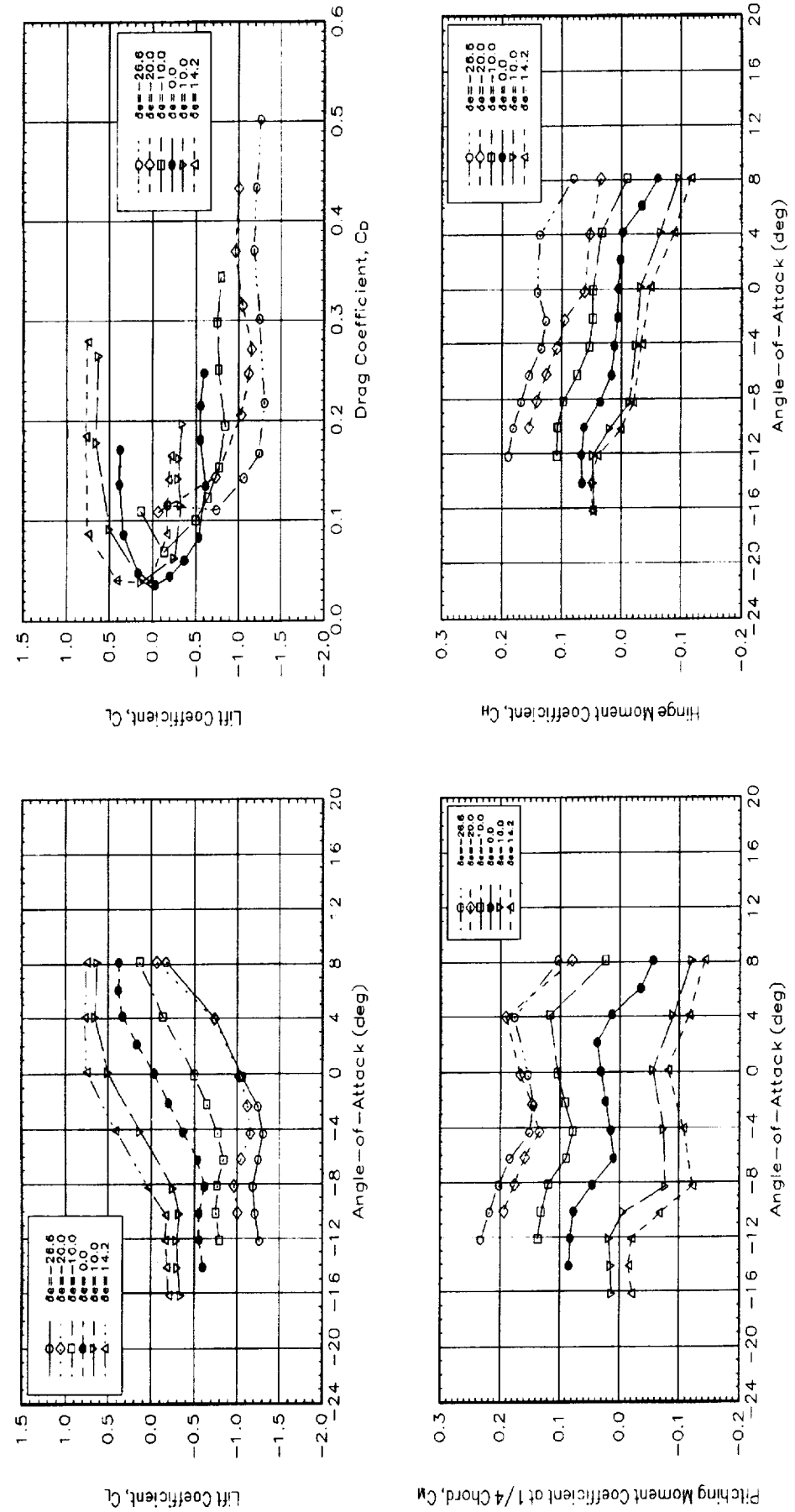

Figure F.07 Lewice Ice Shape, 100 kts, Belt Taps

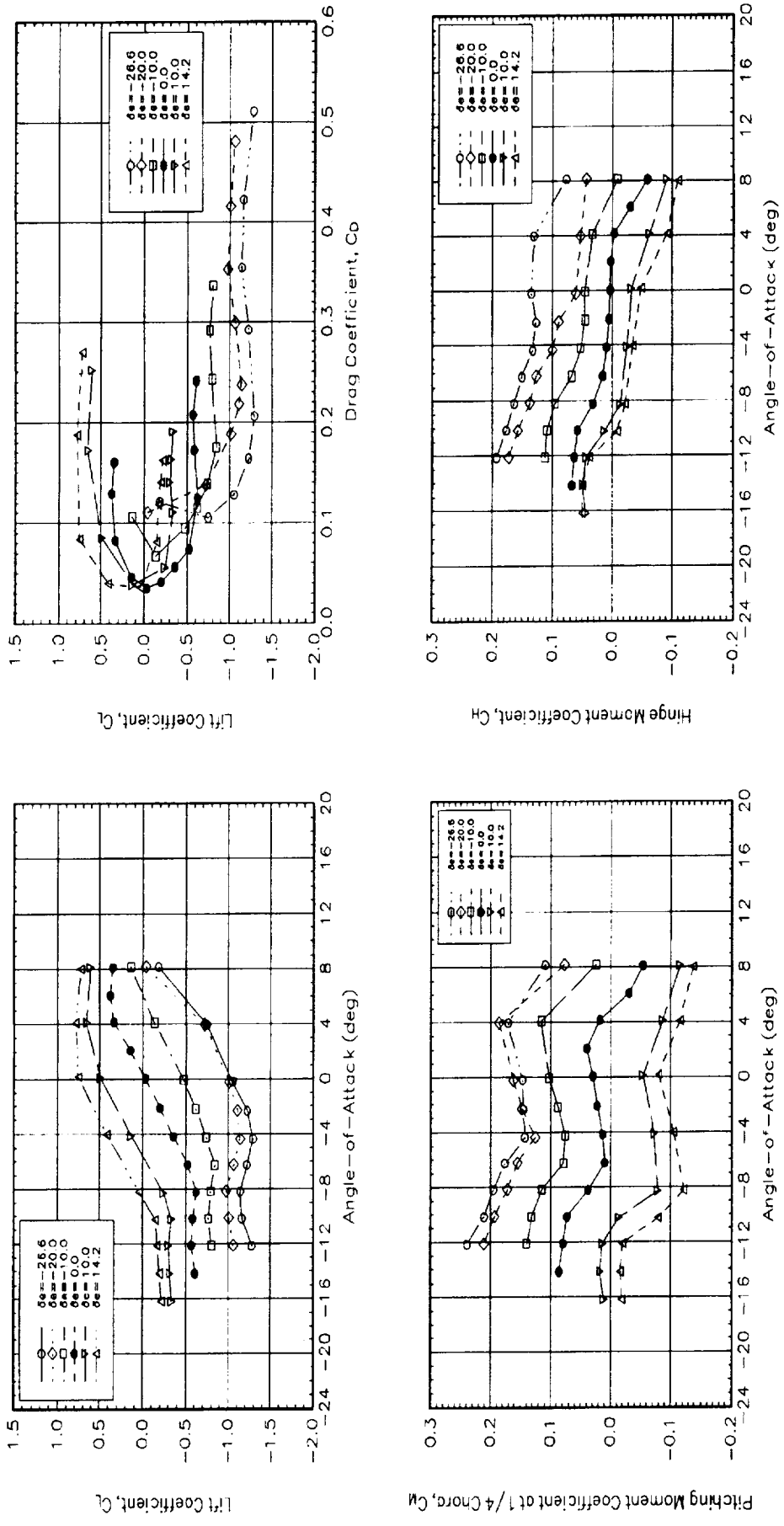

Figure F.08 Lewice Ice Shape, 60 kts, Belt Taps

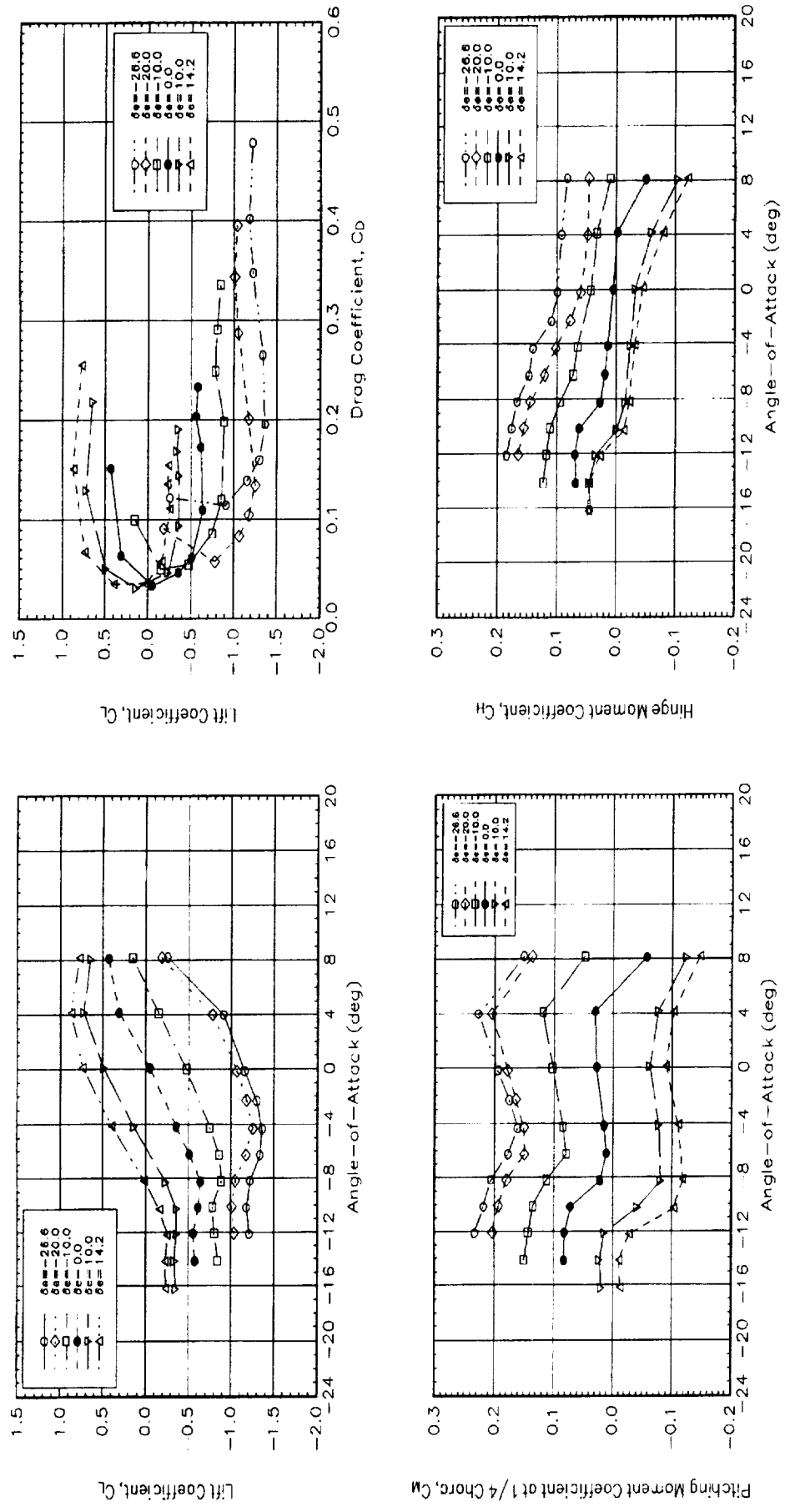

Figure F.09 S&C Ice Shape, 100 kts

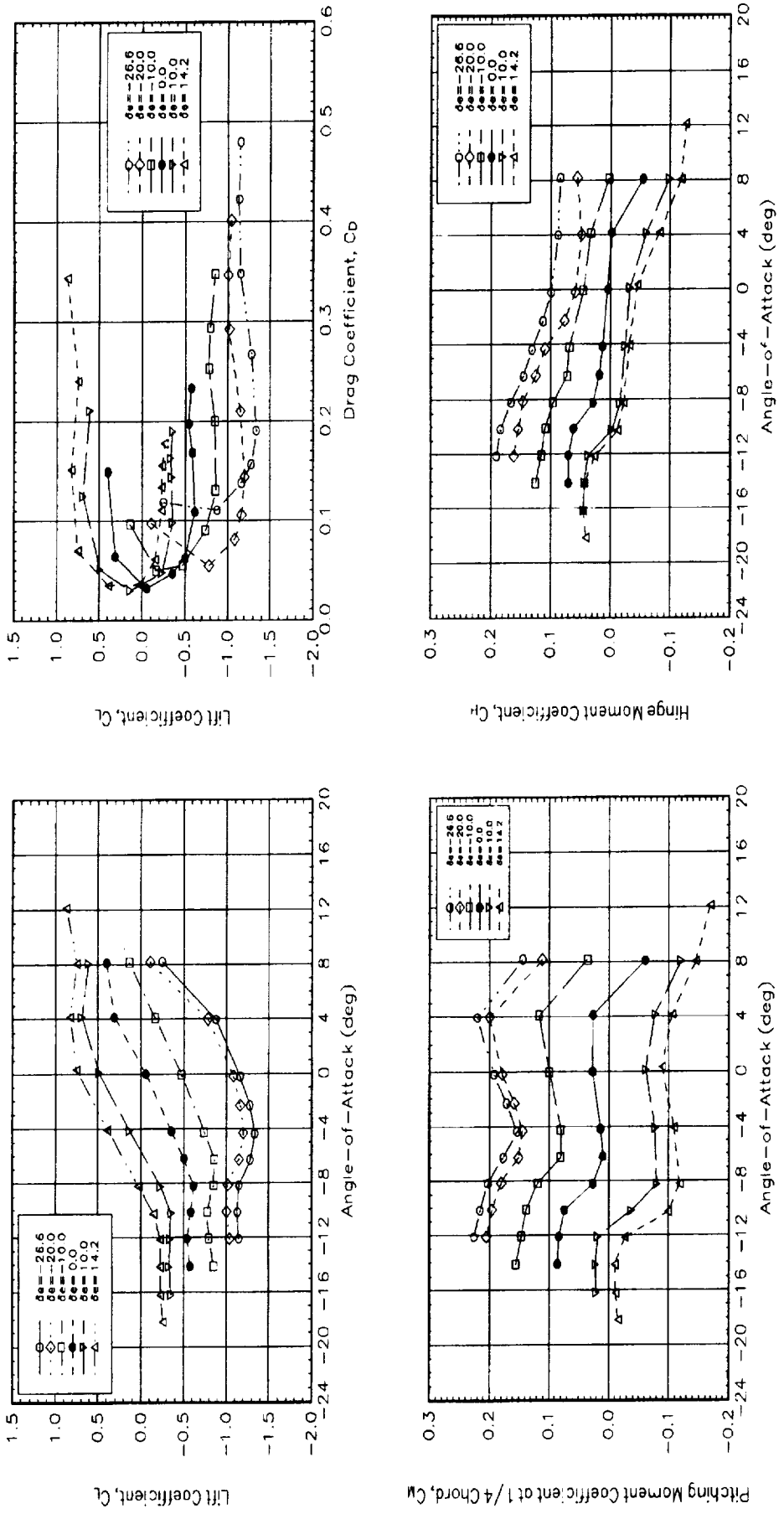

Figure F.10 S&C Ice Shape, 60 kts

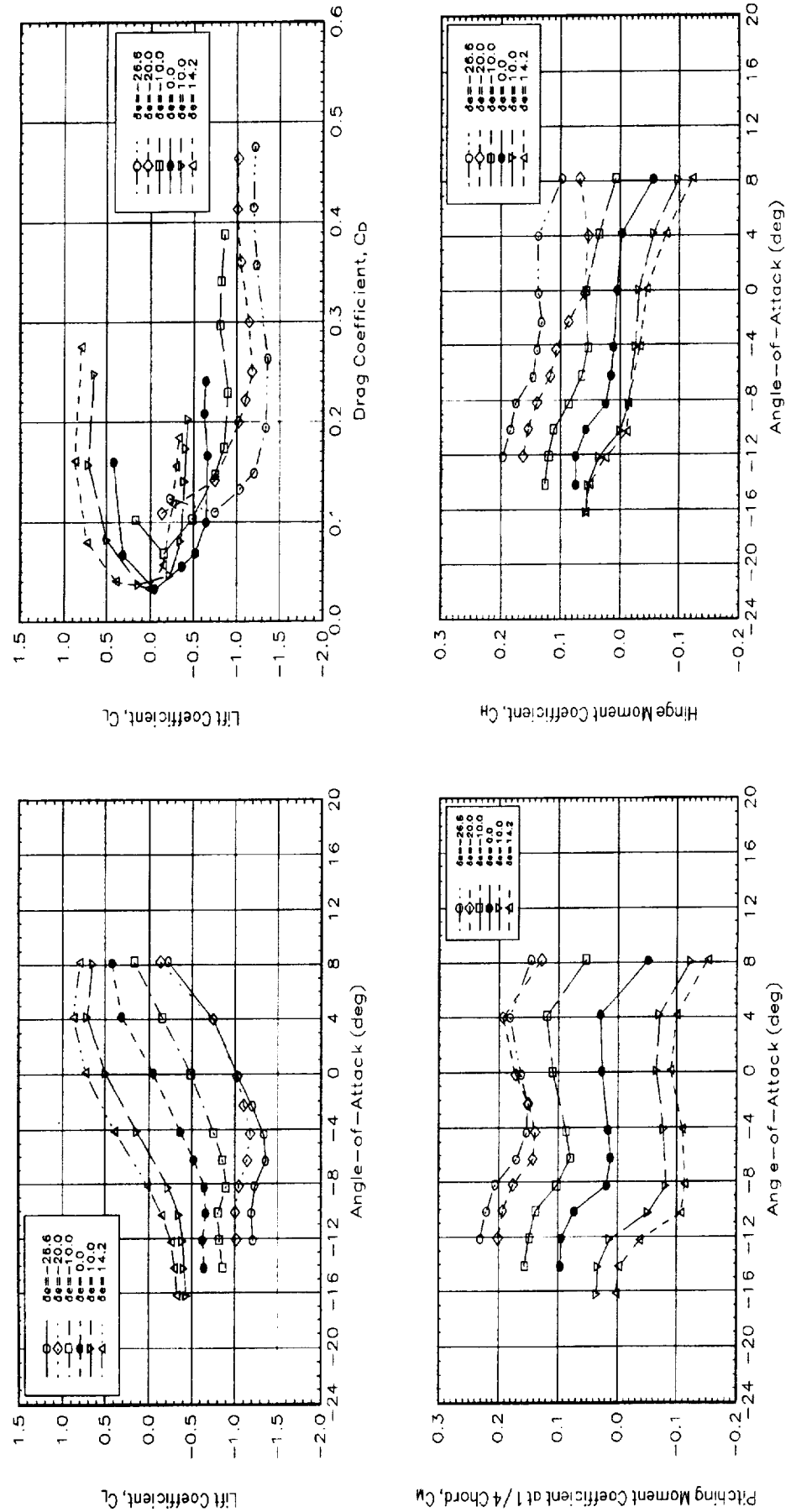

Figure F.11 S&C Ice Shape, 100 kts, Belt Taps

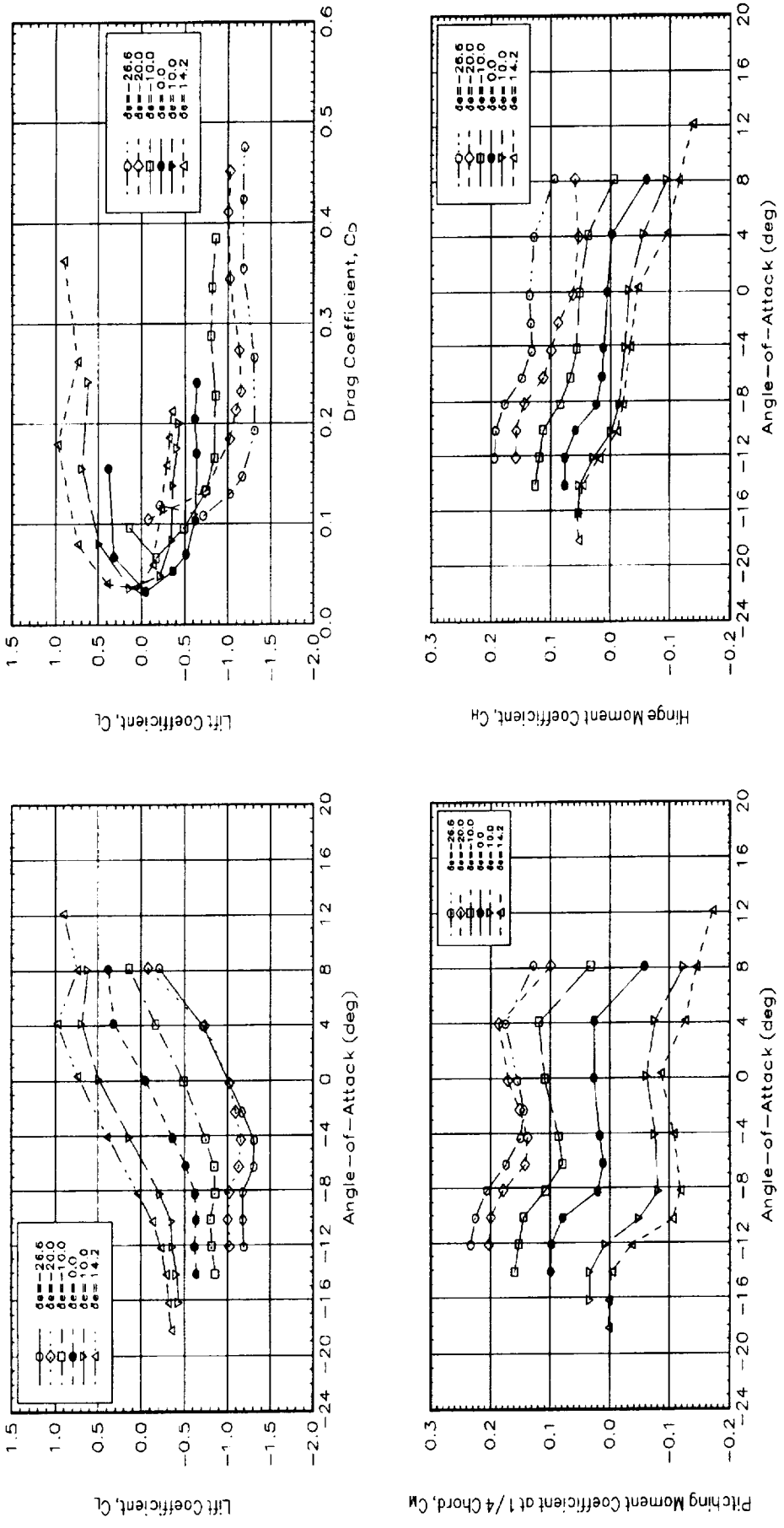

Figure F.12 S&C Ice Shape, 60 kts, Belt Taps

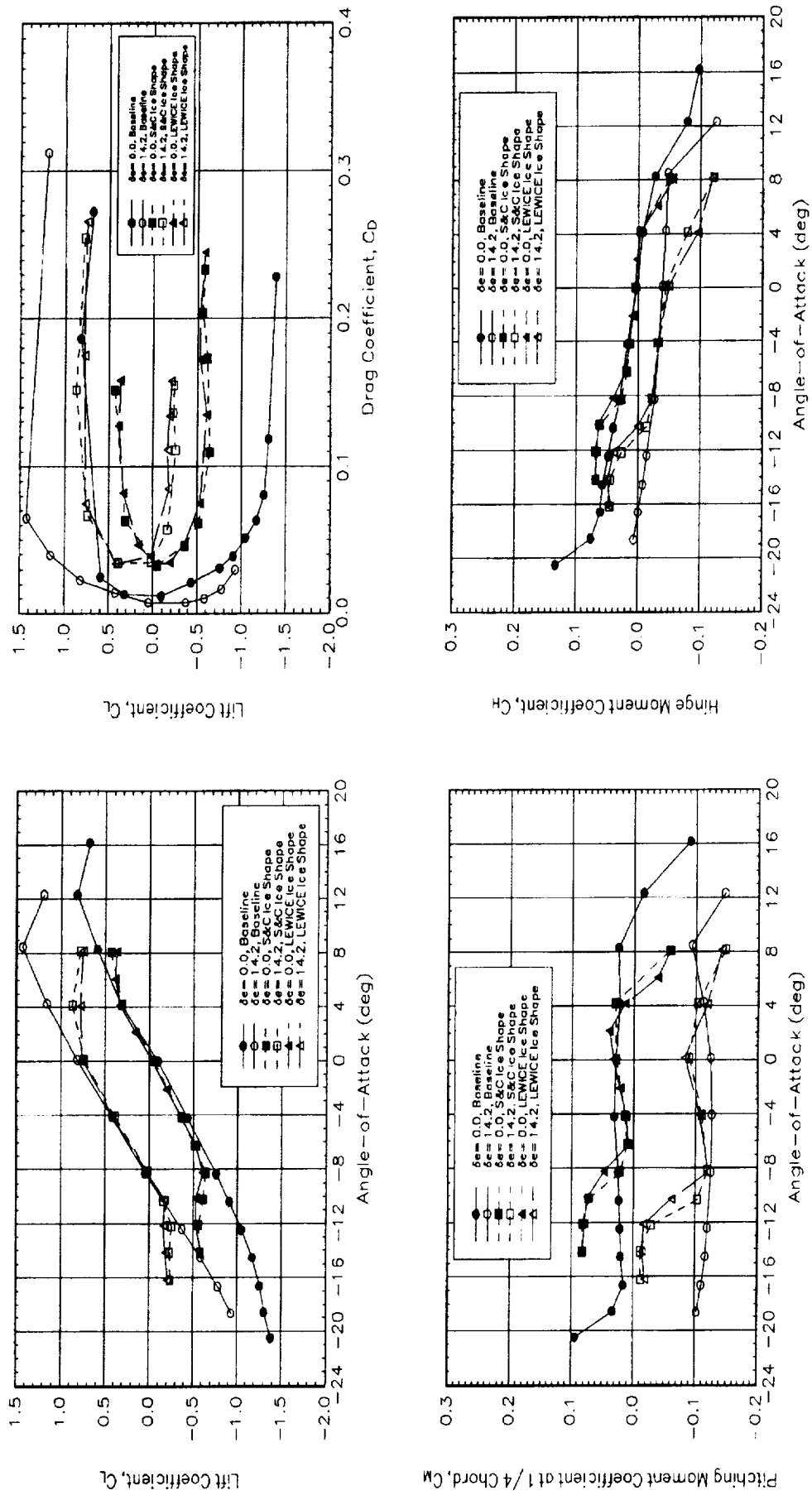

Figure F.13 Ice Shape Effects, 100 kts, Positive Elevator

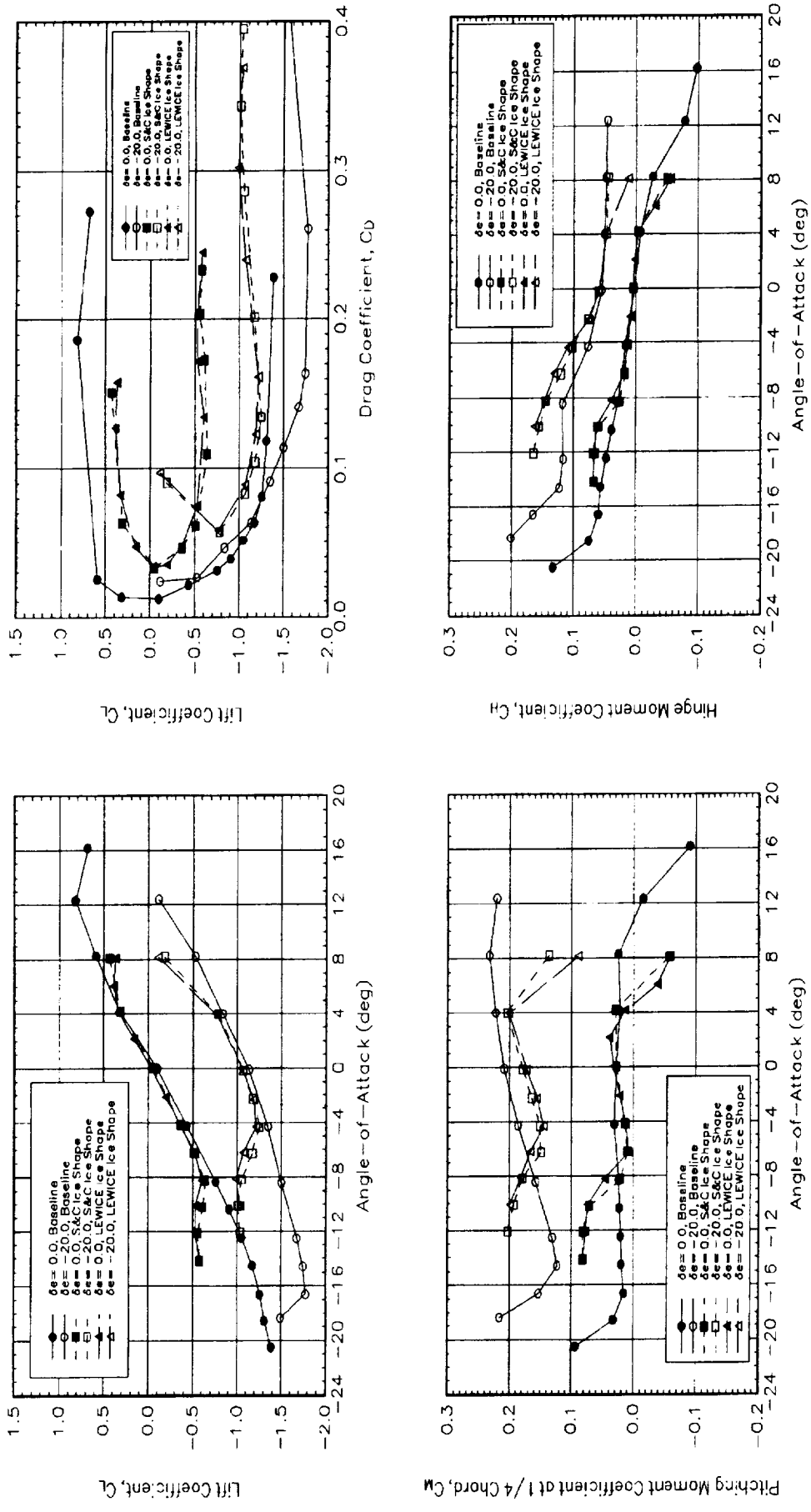

Figure F.14 Ice Shape Effects, 100 kts, Negative Elevator

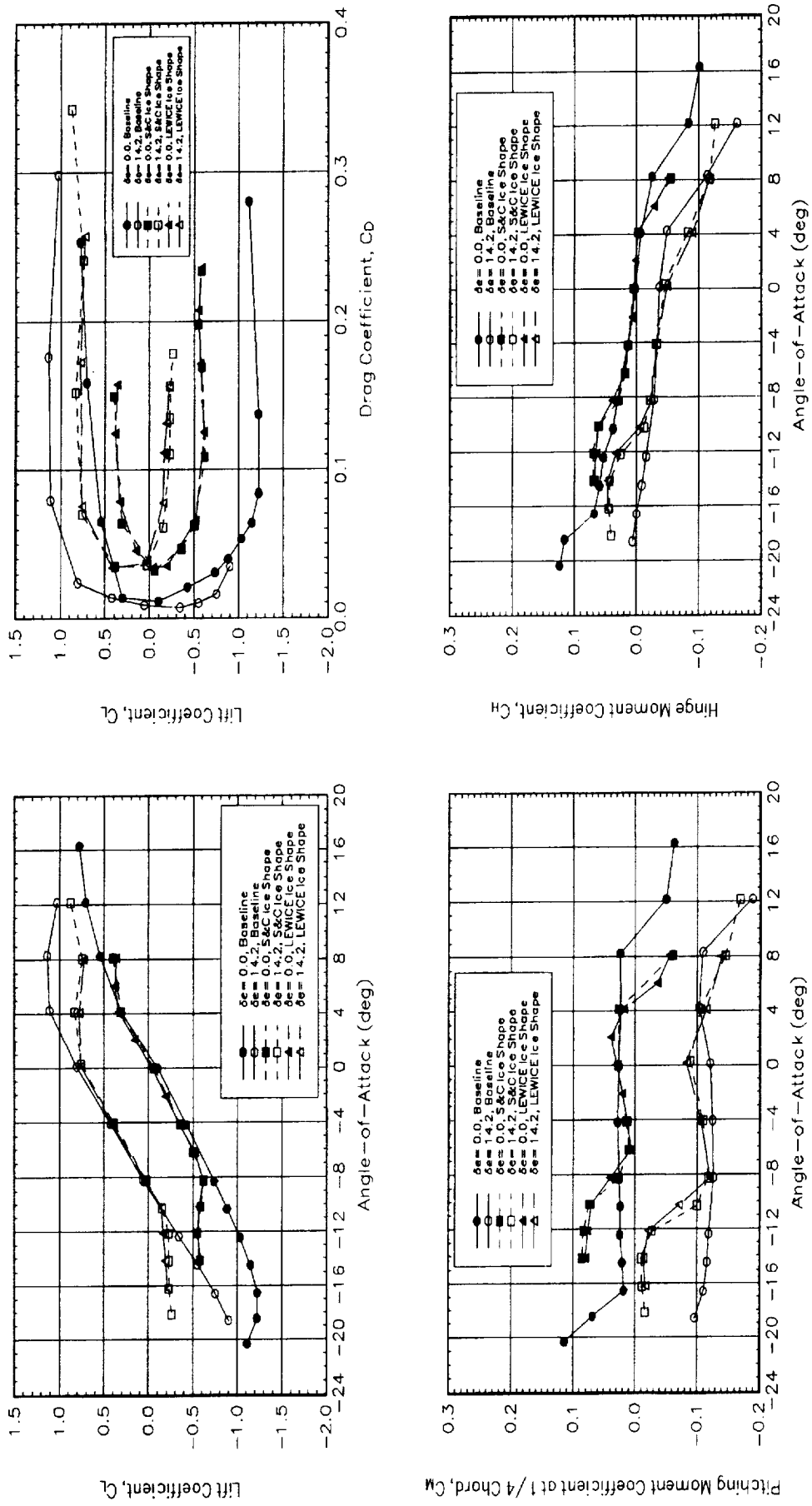

Figure F.15 Ice Shape Effects, 60 kts, Positive Elevator

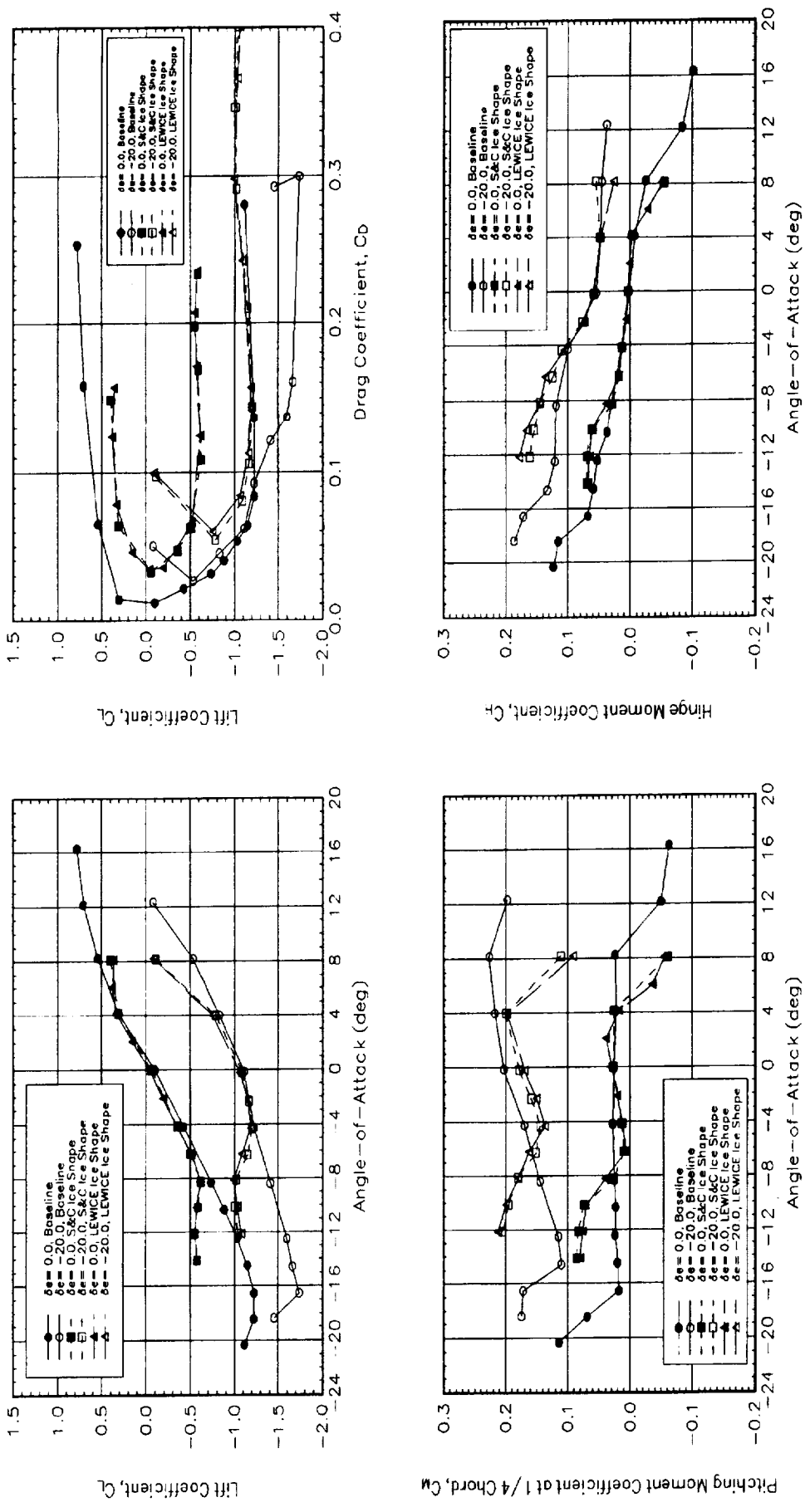

Figure F.16 Ice Shape Effects, 60 kts, Negative Elevator

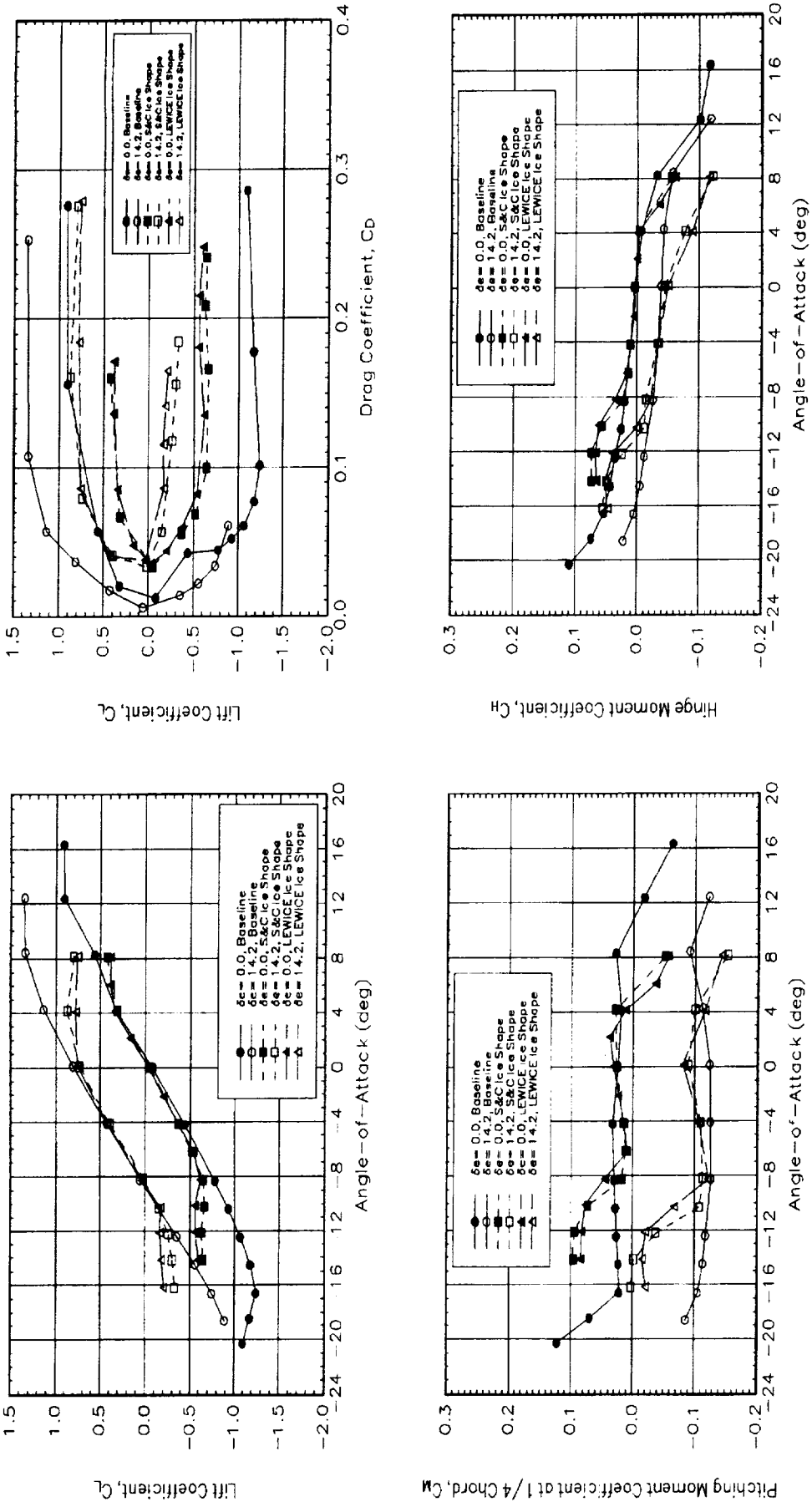

Figure F.17 Ice Shape Effects, Belt Taps, 100 kts, Positive Elevator

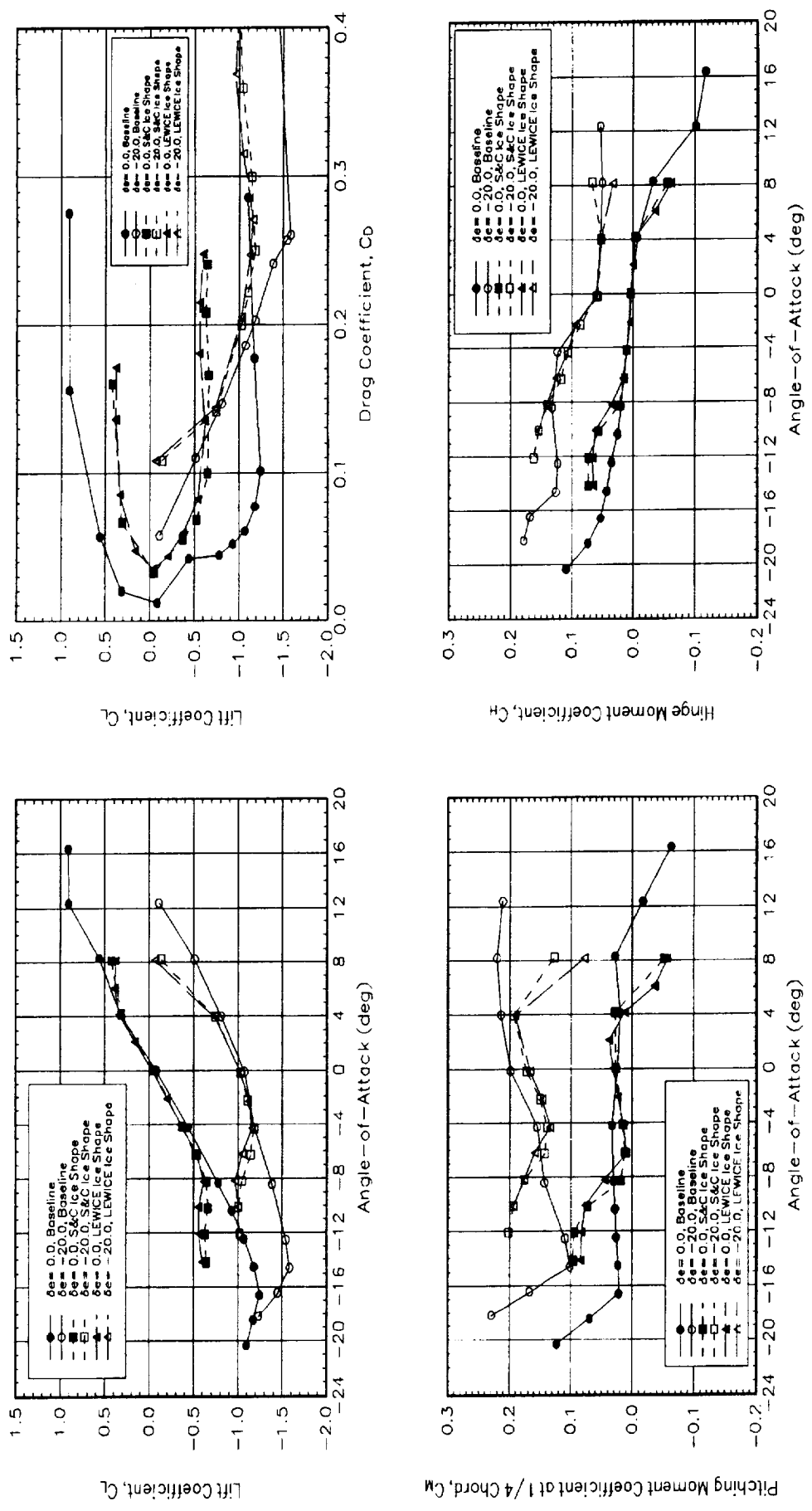

Figure F.18 Ice Shape Effects, Belt Taps, 100 kts, Negative Elevator

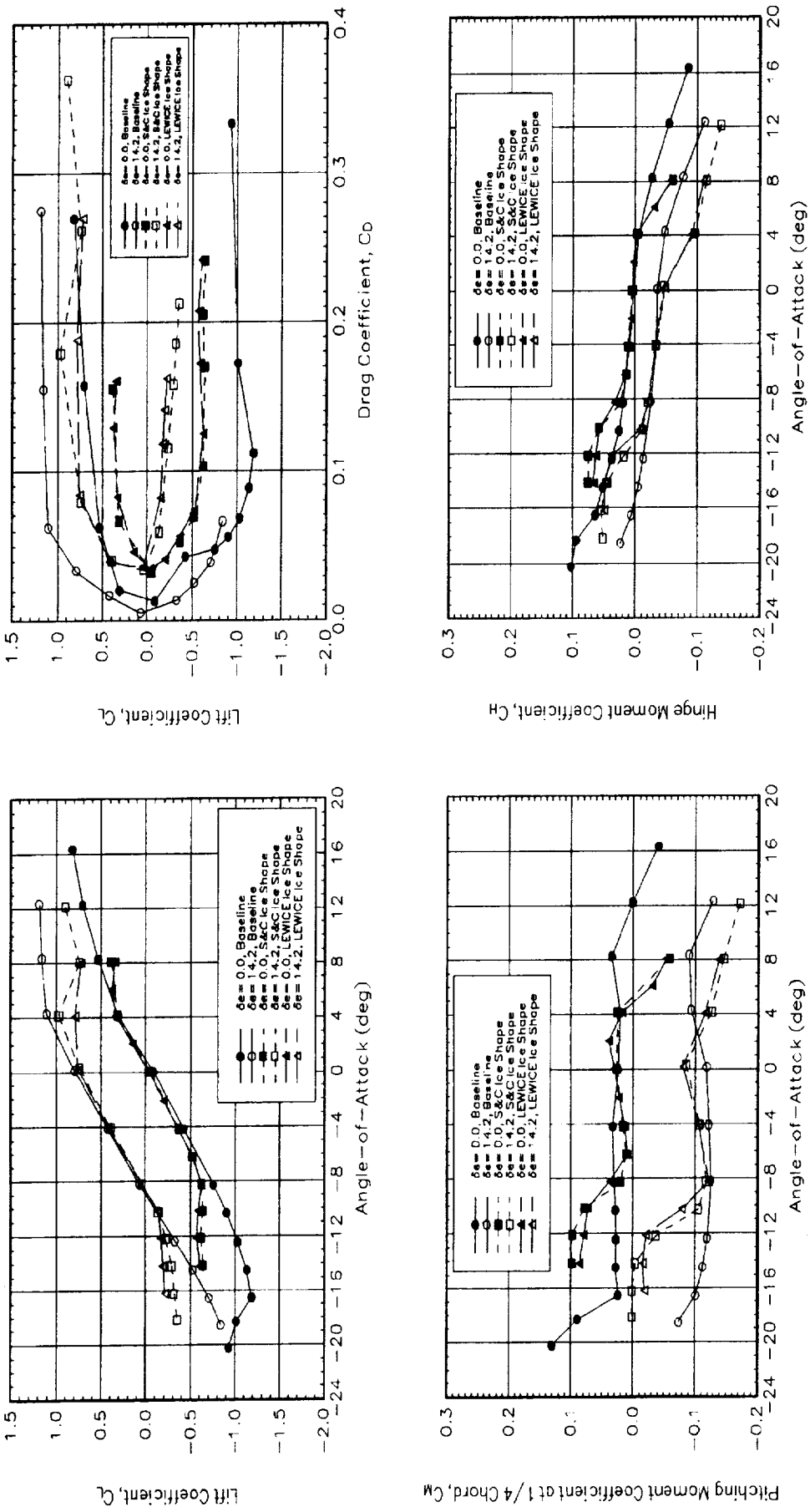

Figure F.19 Ice Shape Effects, Belt Taps, 60 kts, Positive Elevator

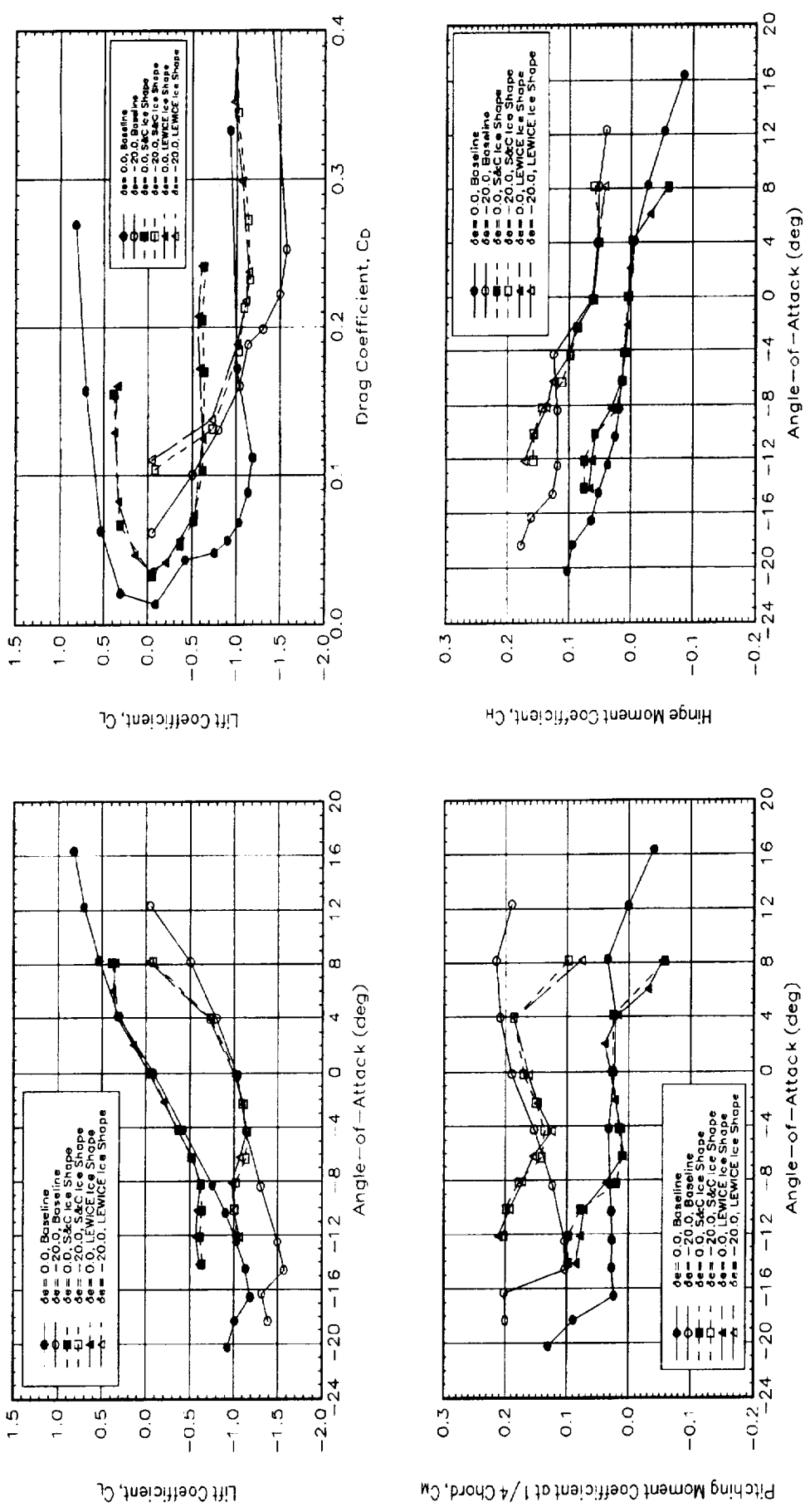

Figure F.20 Ice Shape Effects, Belt Taps, 60 kts, Negative Elevator

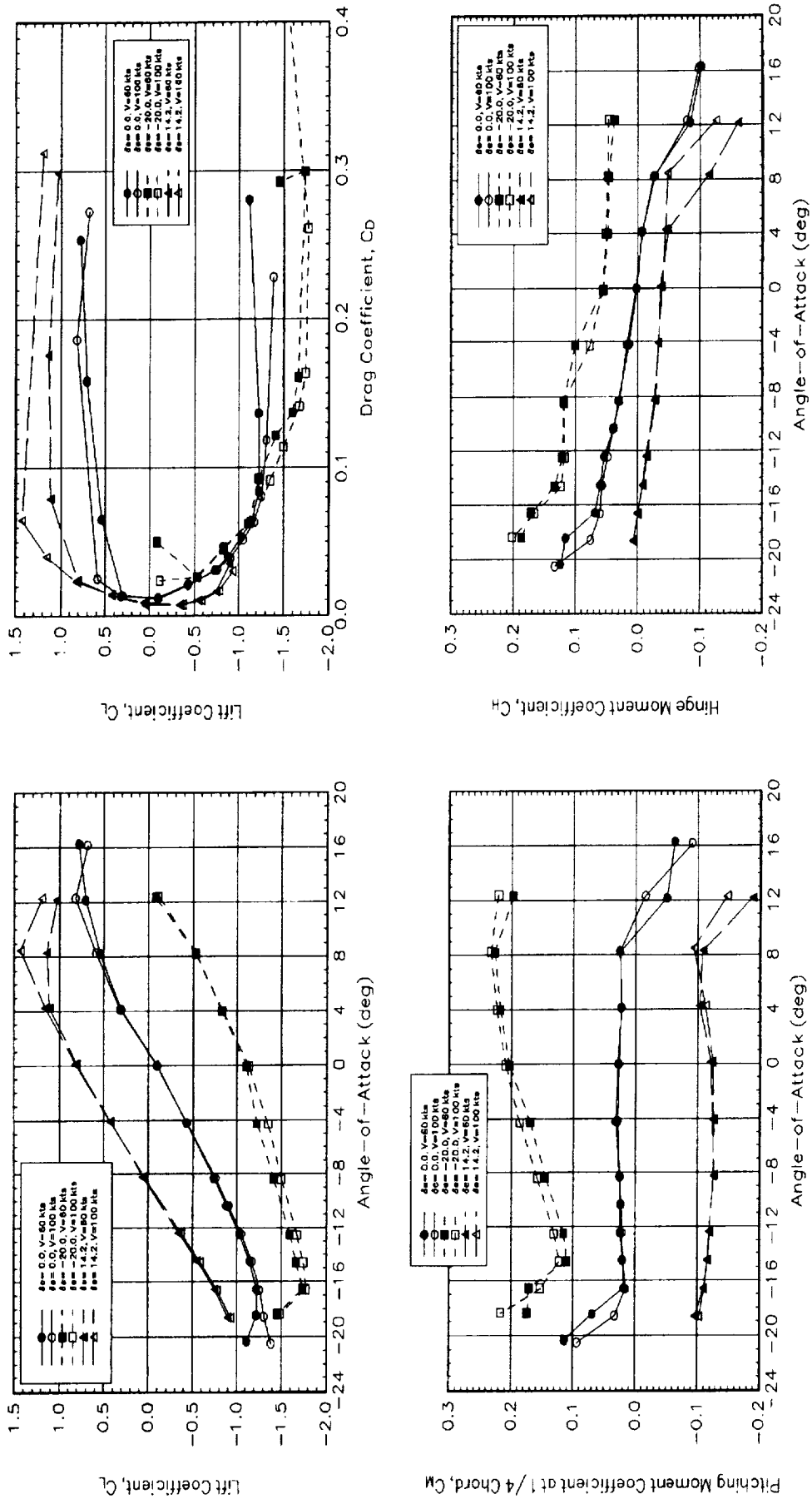

Figure F.21 Velocity Effects, Baseline

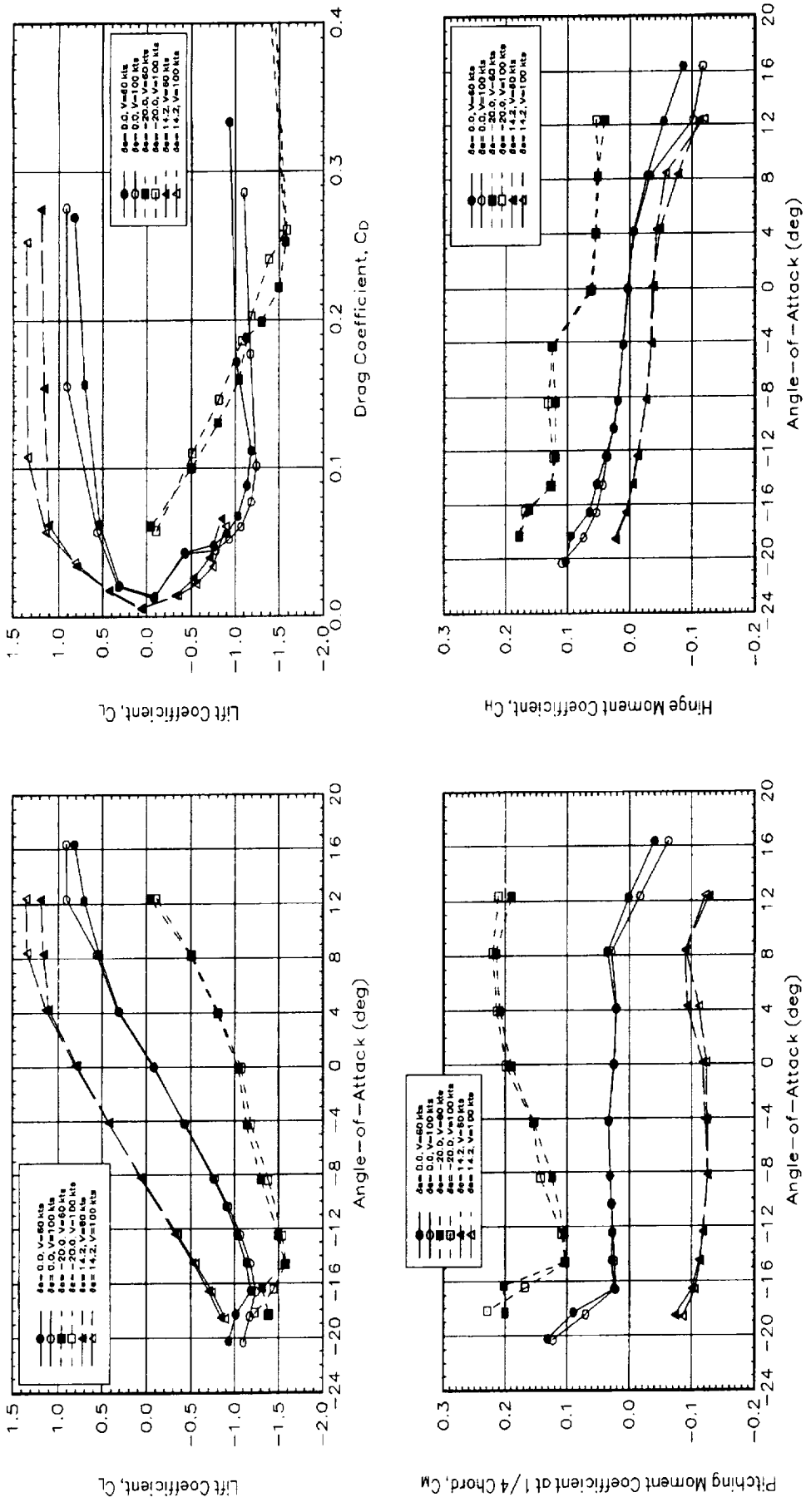

Figure F.22 Velocity Effects, Baseline, Belt Taps

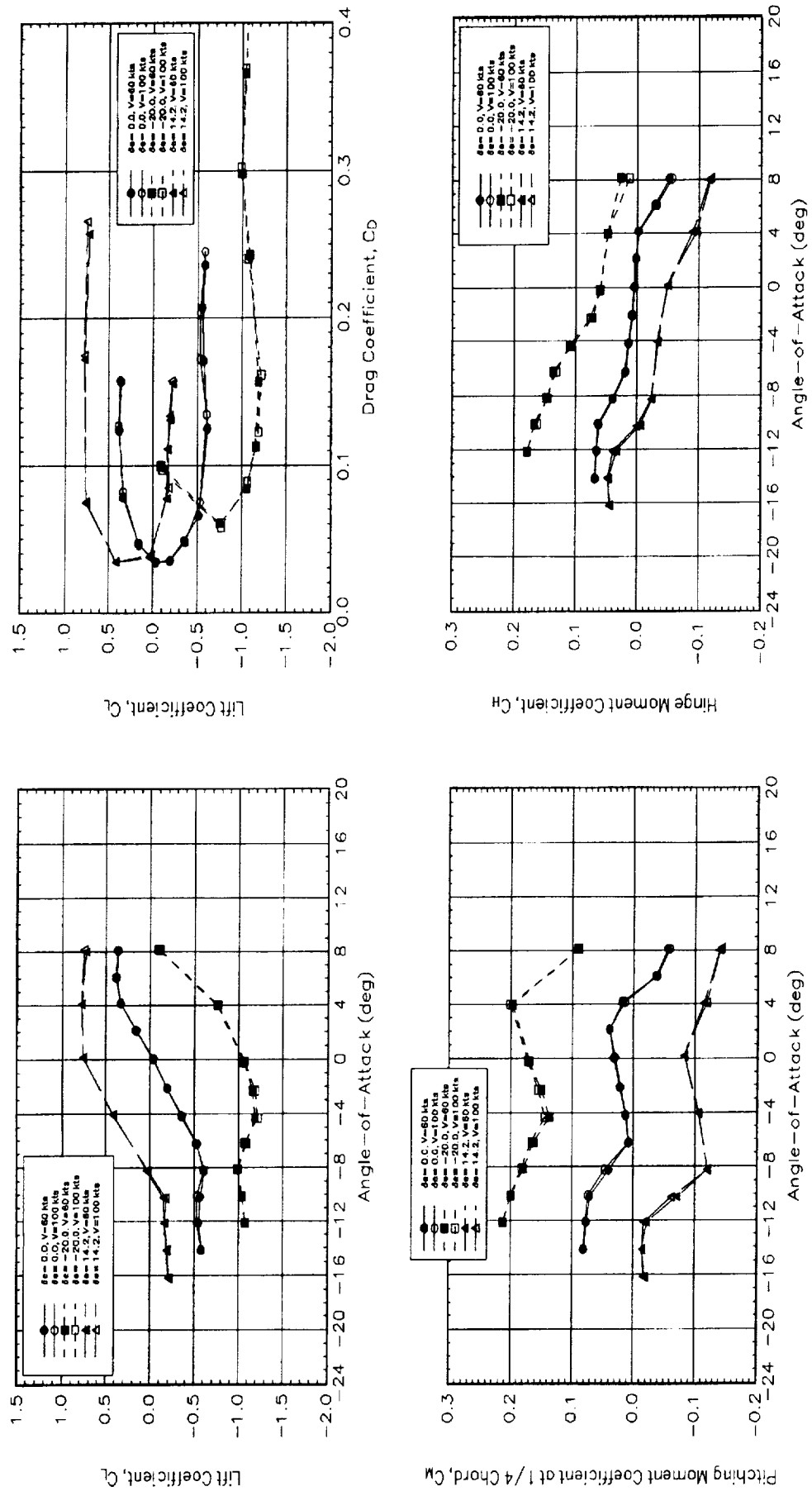

Figure F.23 Velocity Effects, Lewice Ice Shape

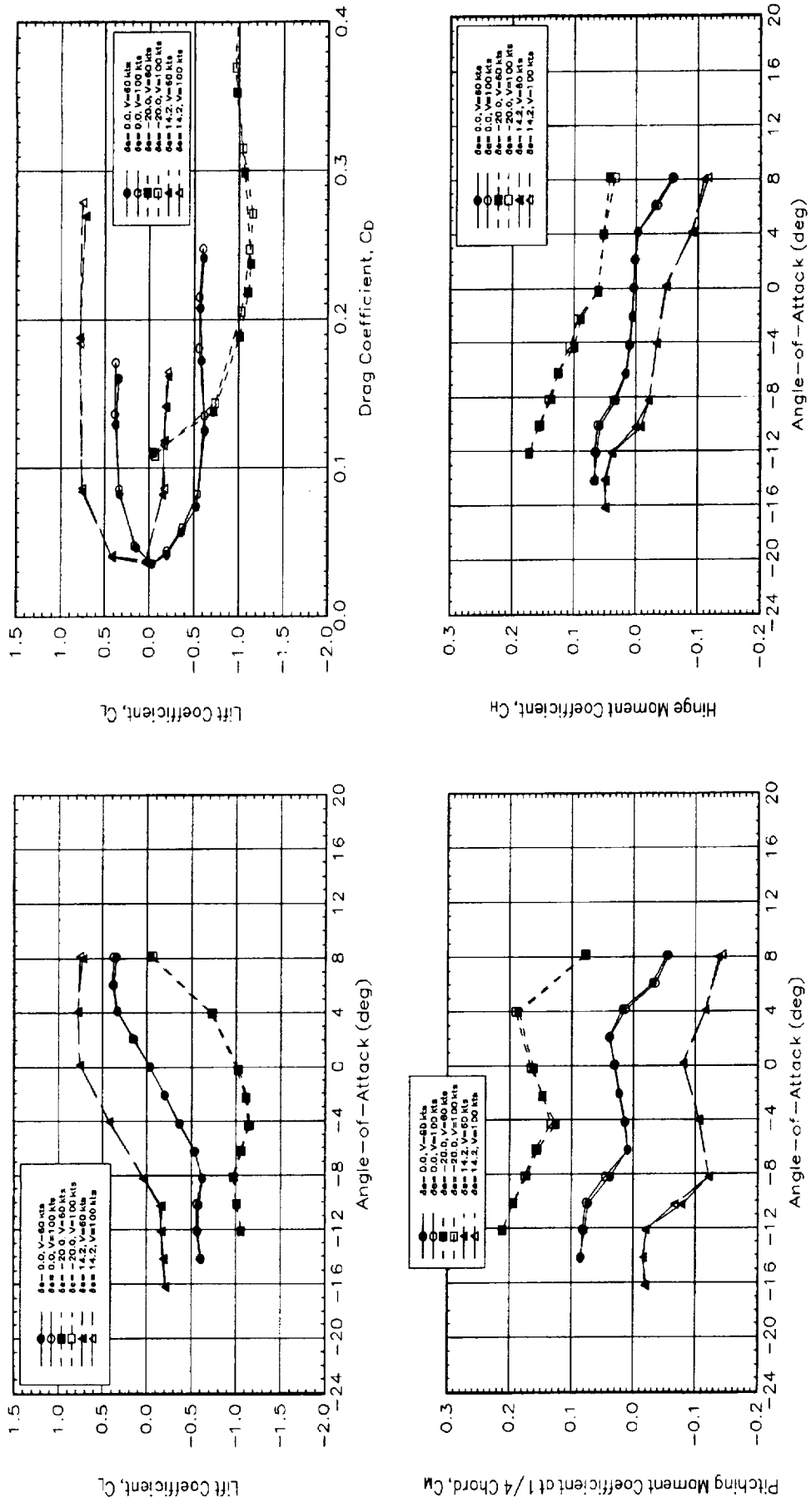

Figure F.24 Velocity Effects, Lewice Ice Shape, Belt Taps

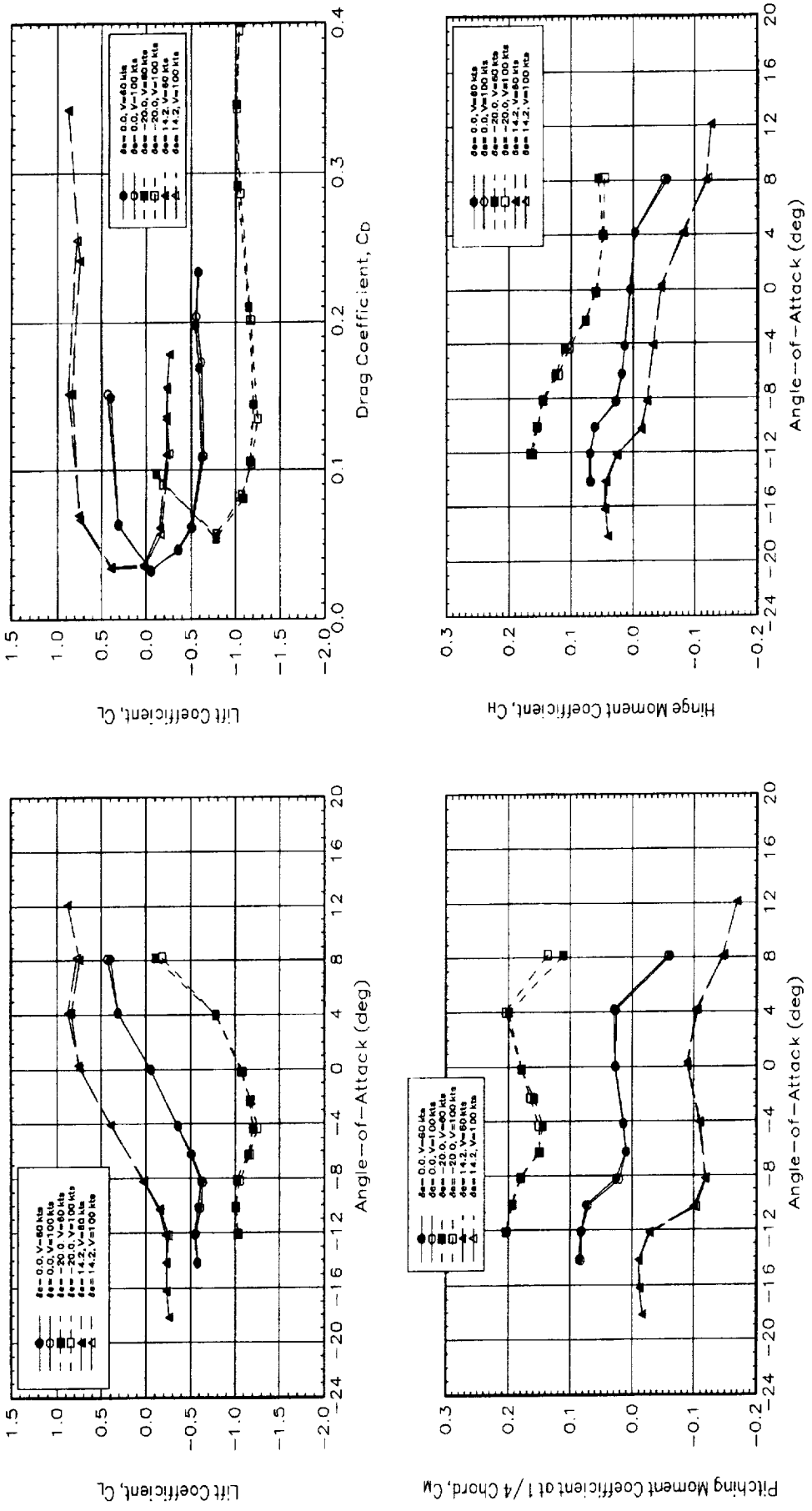

Figure F.25 Velocity Effects, S&C Ice Shape

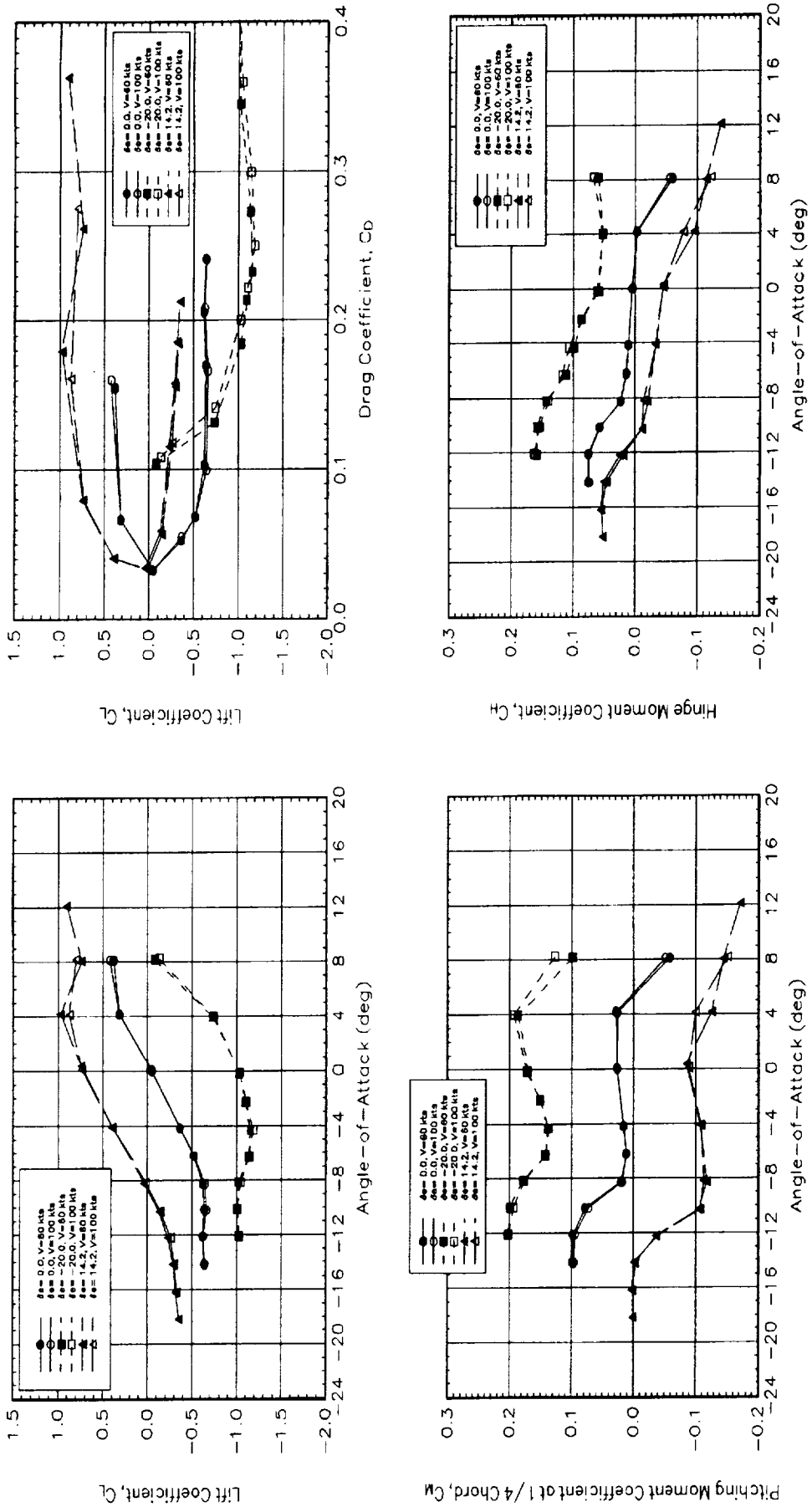

Figure F.26 Velocity Effects, S&C Ice Shape, Belt Taps

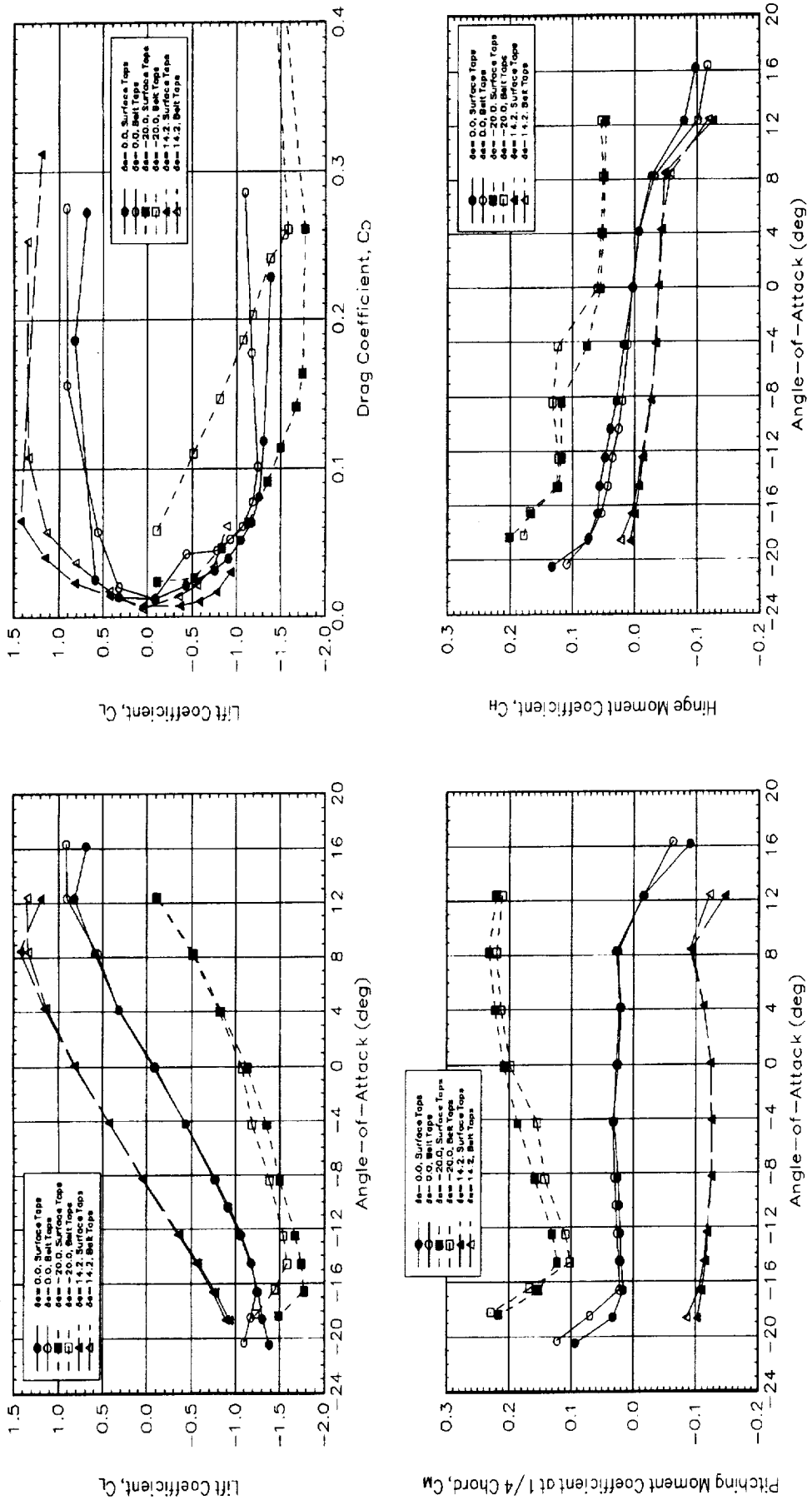

Figure F.27 Tap Line Effects, Baseline, 100 kts

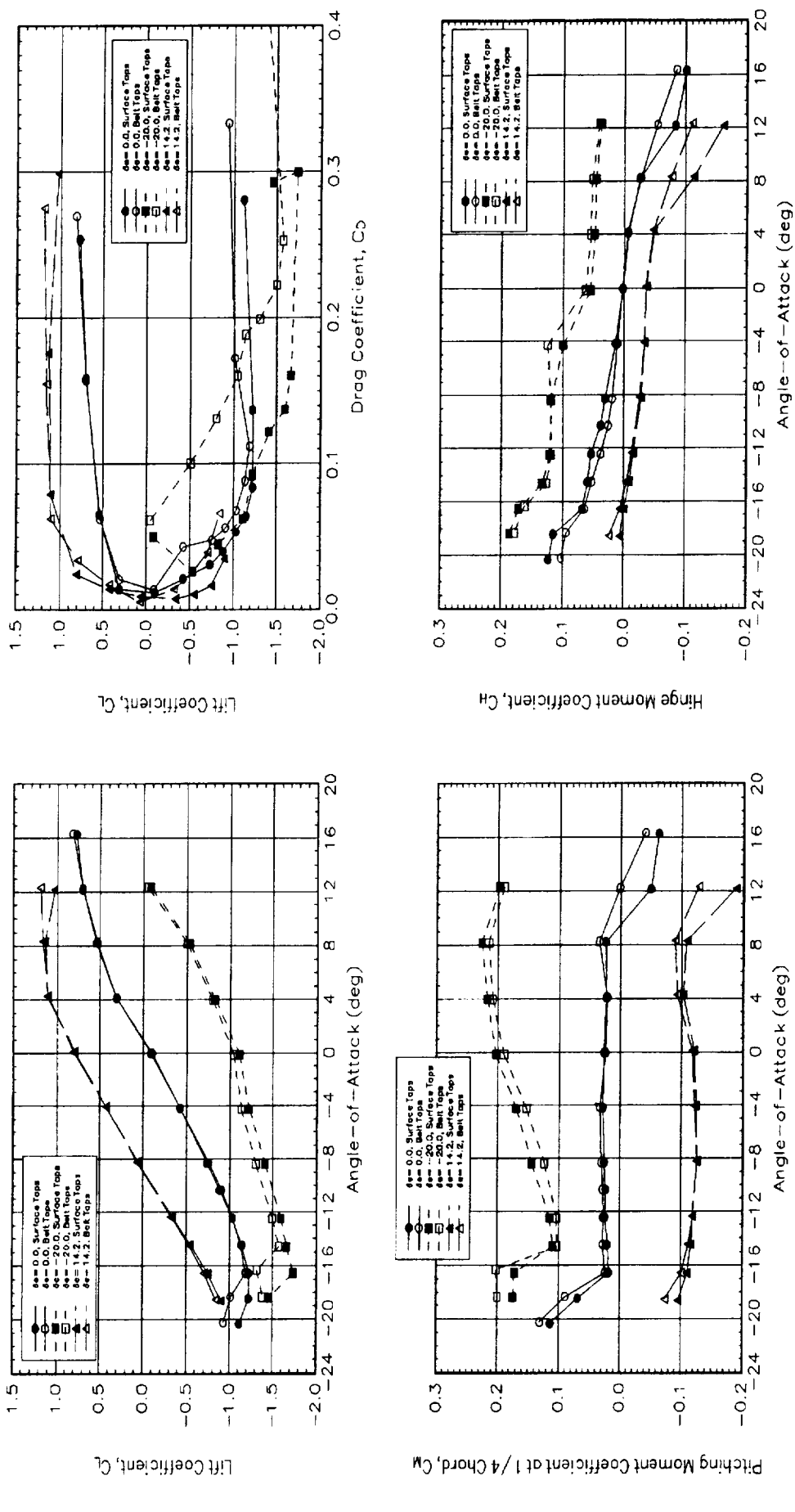

Figure F.28 Tap Line Effects, Baseline, 60 kts

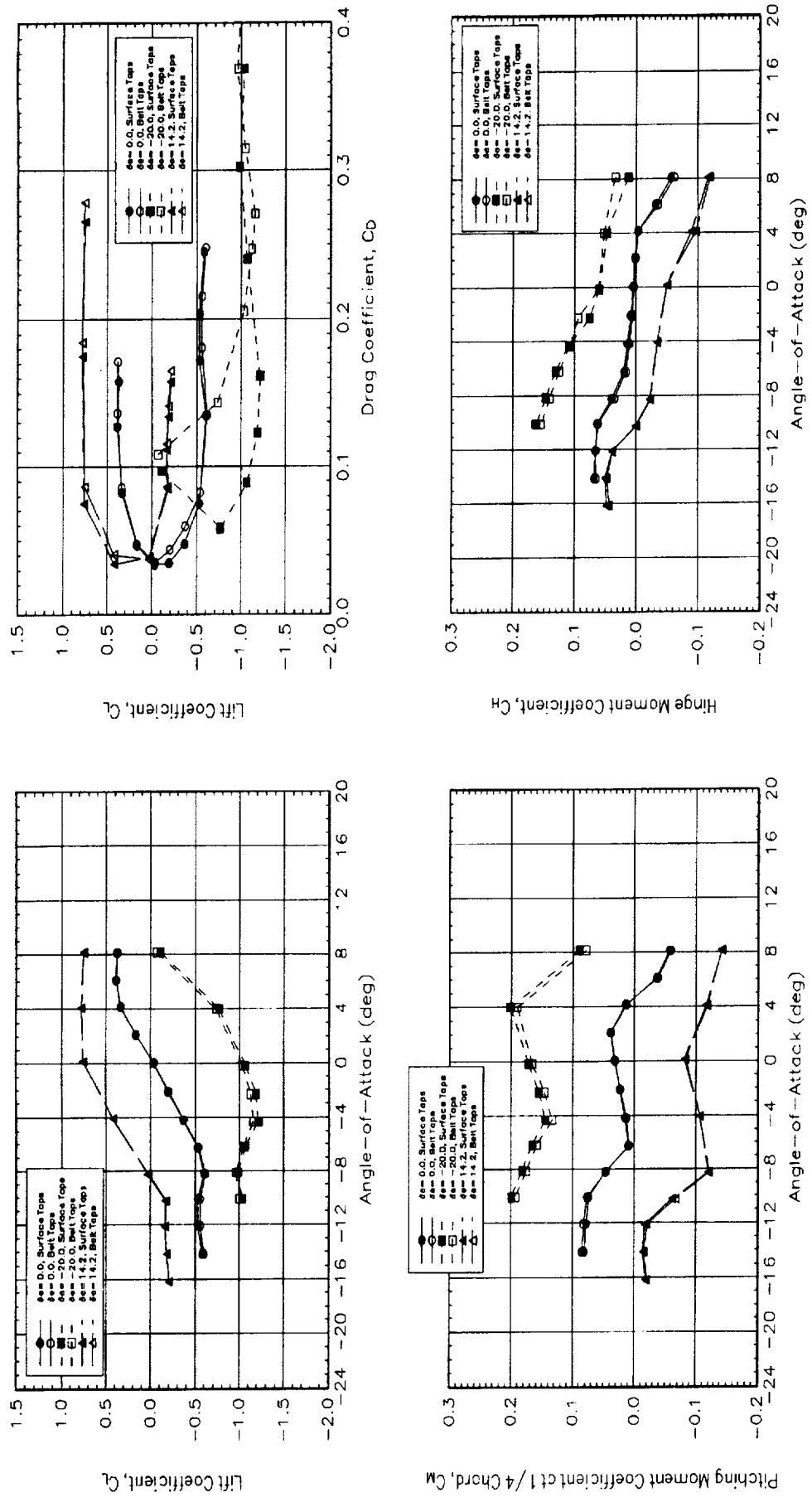

Figure F.29 Tap Line Effects, Lewice Ice Shape, 100 kts

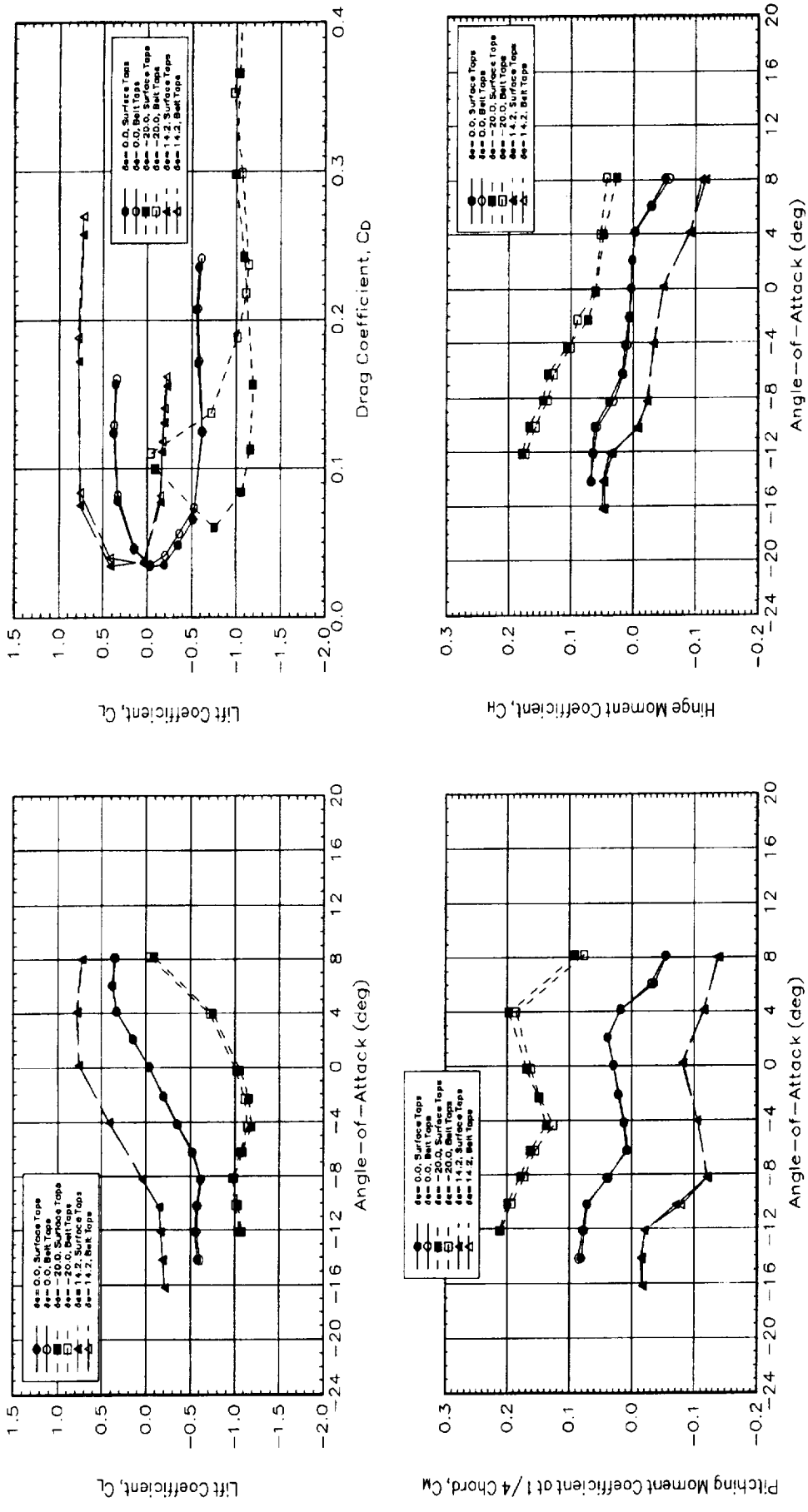

Figure F.30 Tap Line Effects, Lewice Ice Shape, 60 kts

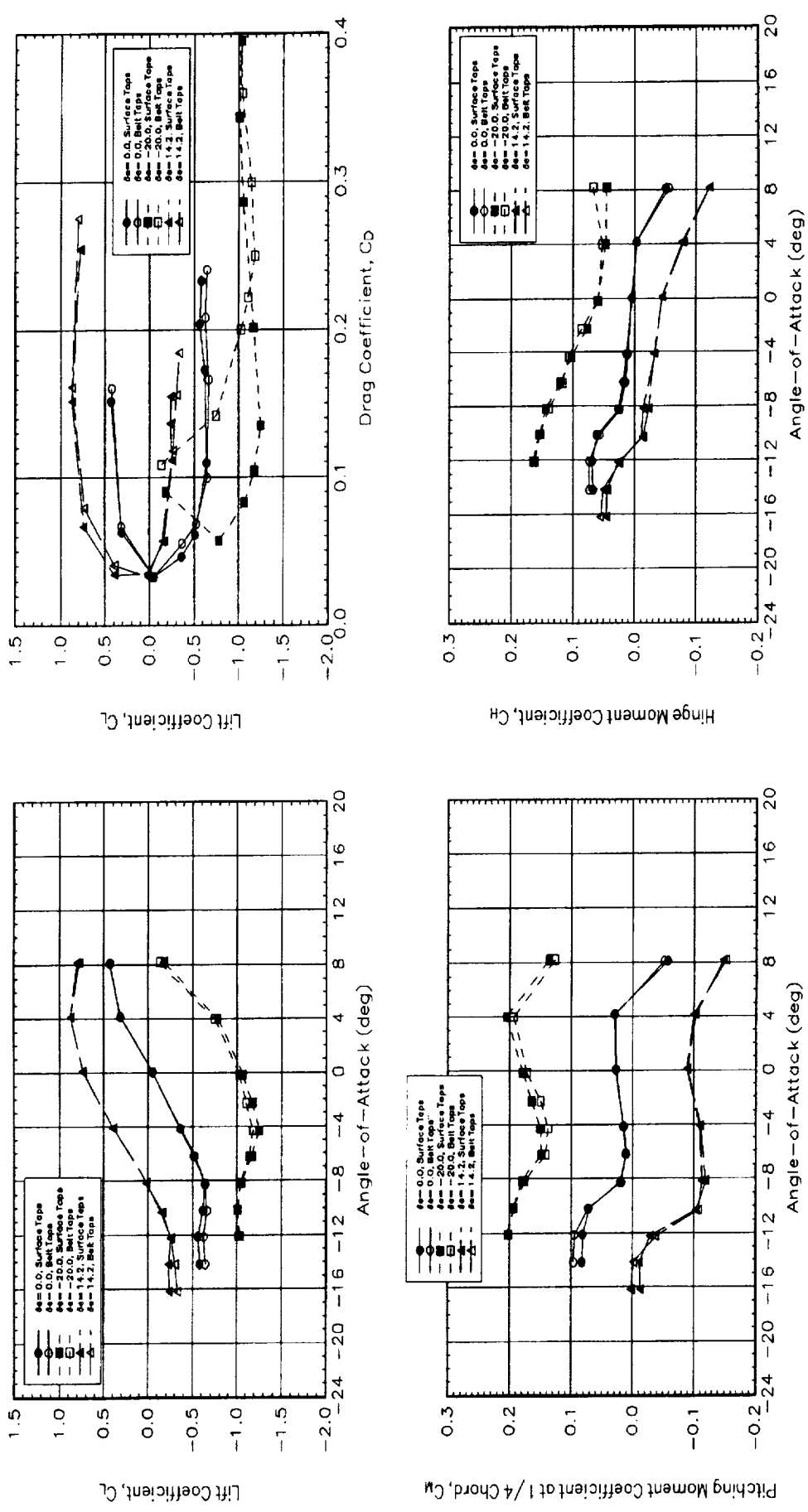

Figure F.31 Tap Line Effects, S&C Ice Shape, 100 kts

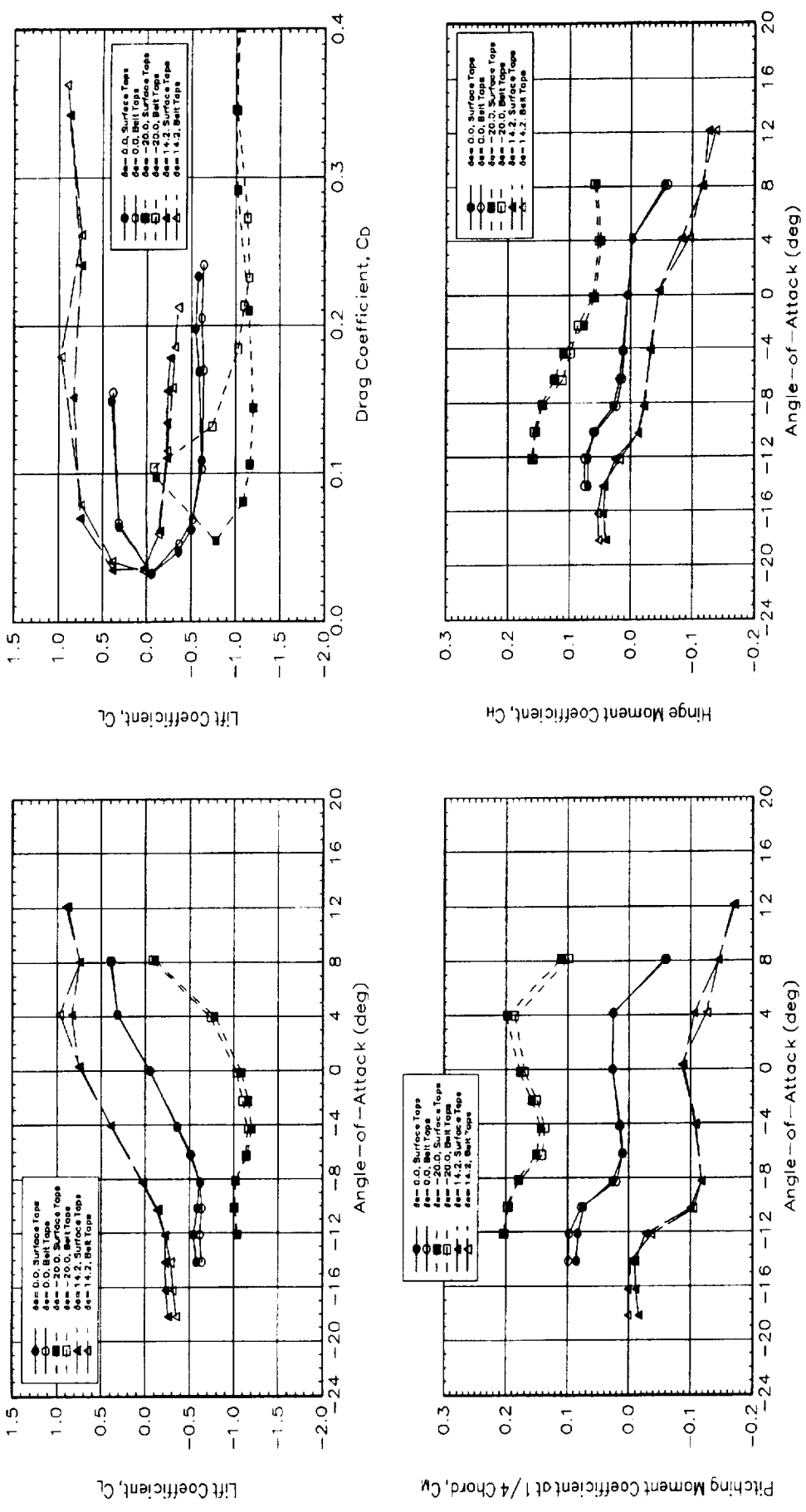

Figure F.32 Tap Line Effects, S&C Ice Shape, 60 kts

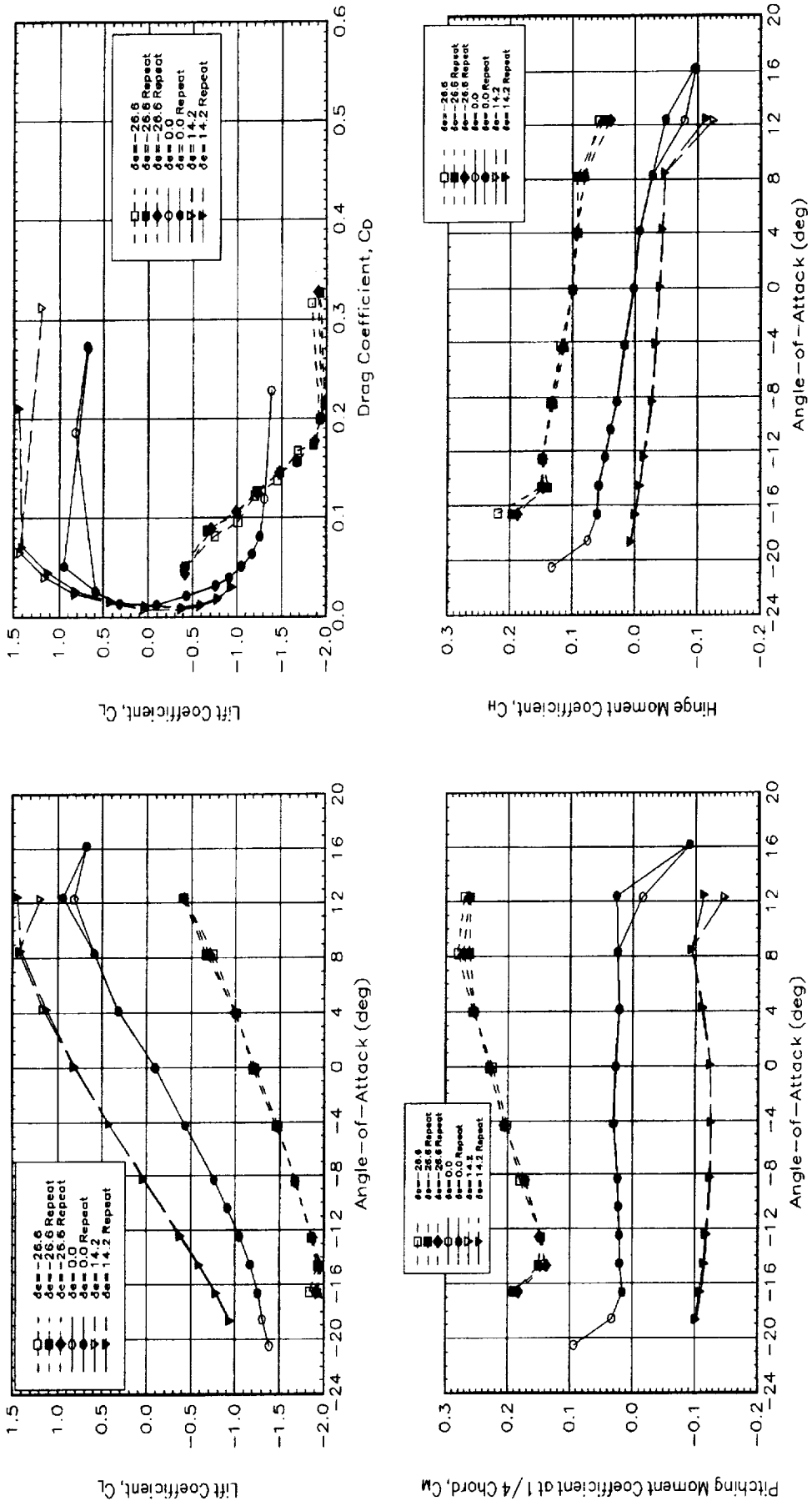

Figure F.33 Repeatability, Baseline

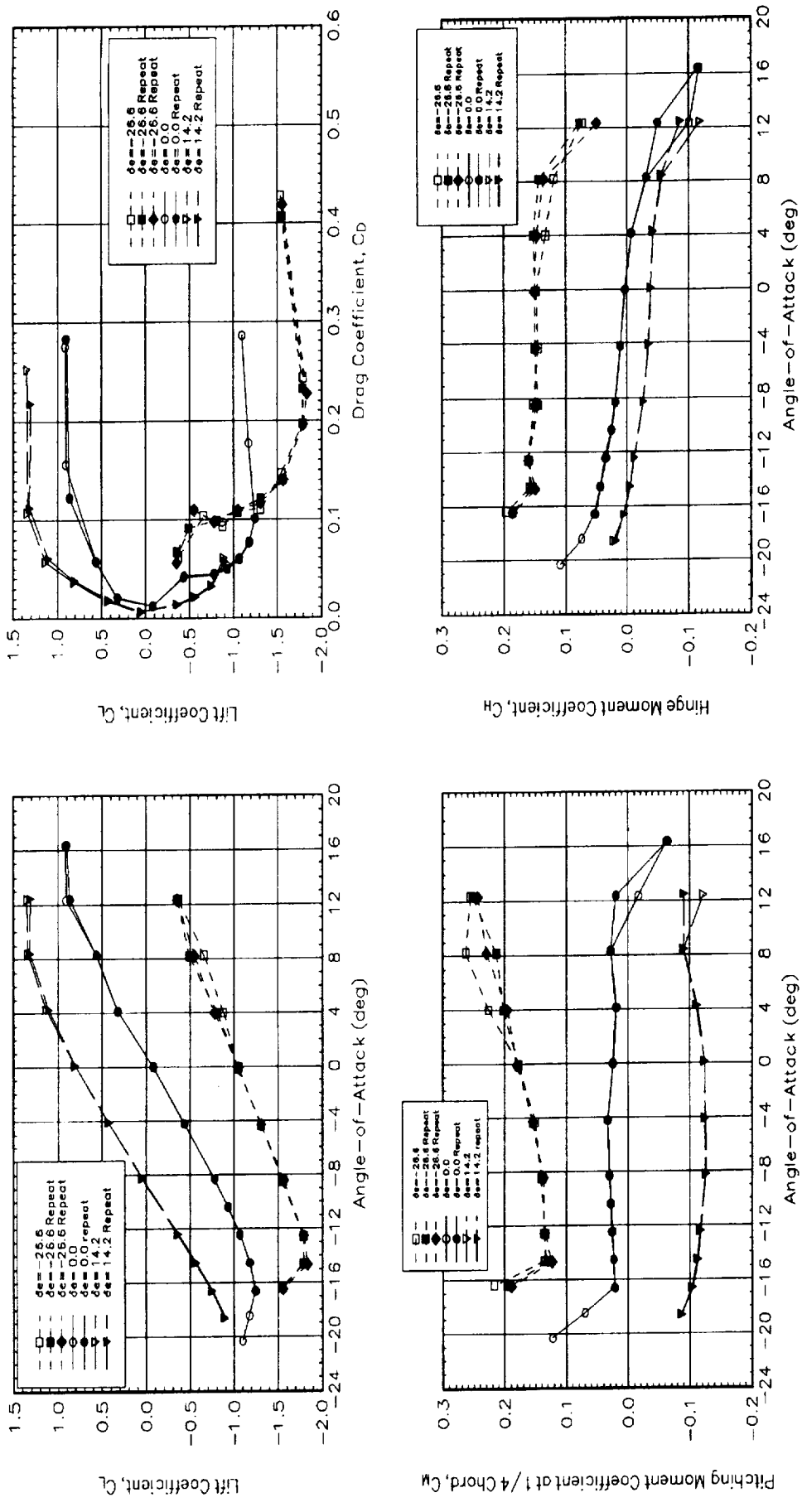

Figure F.34 Repeatability, Baseline, Belt Taps

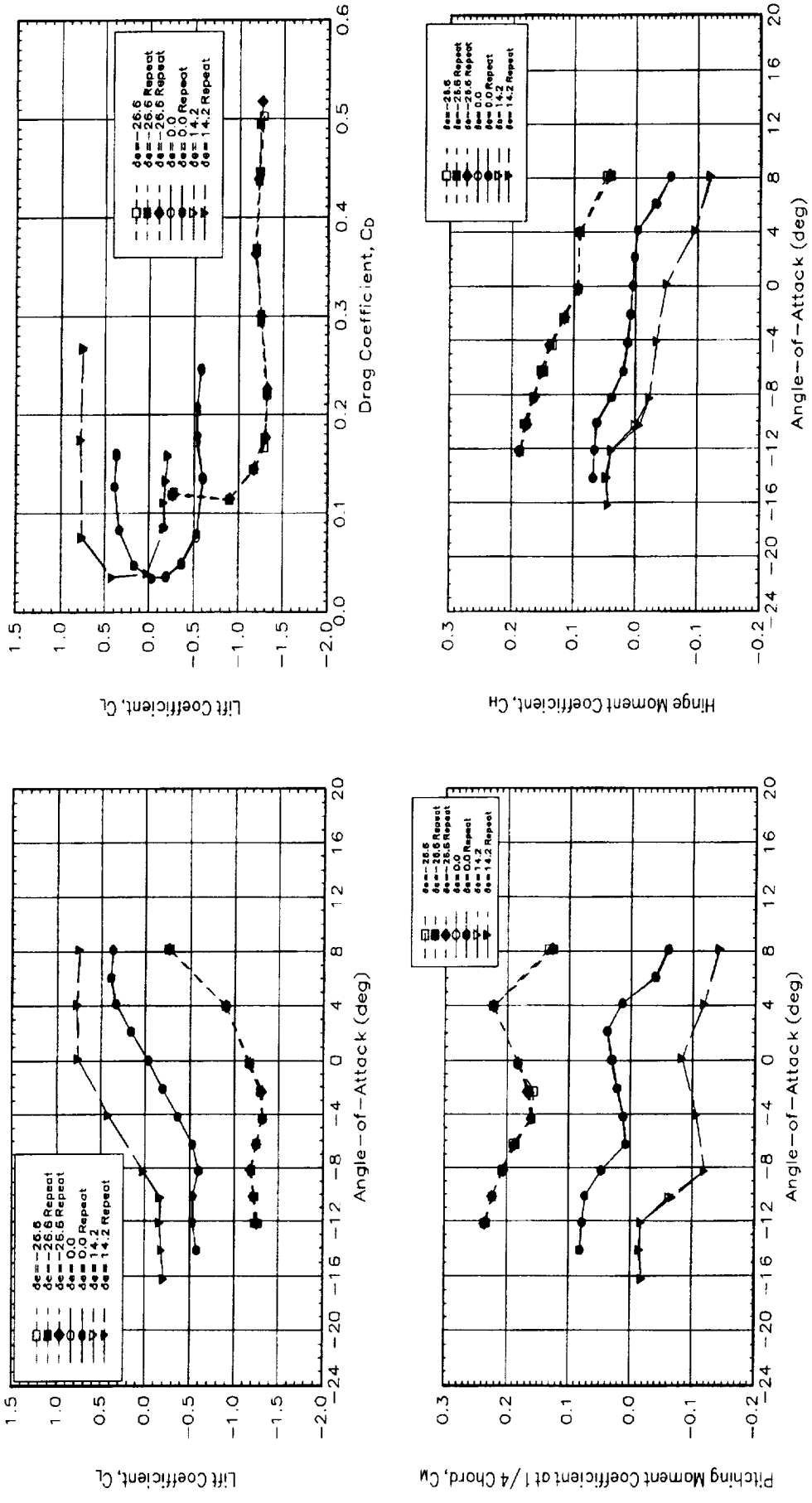

Figure F.35 Repeatability, Lewice Ice Shape

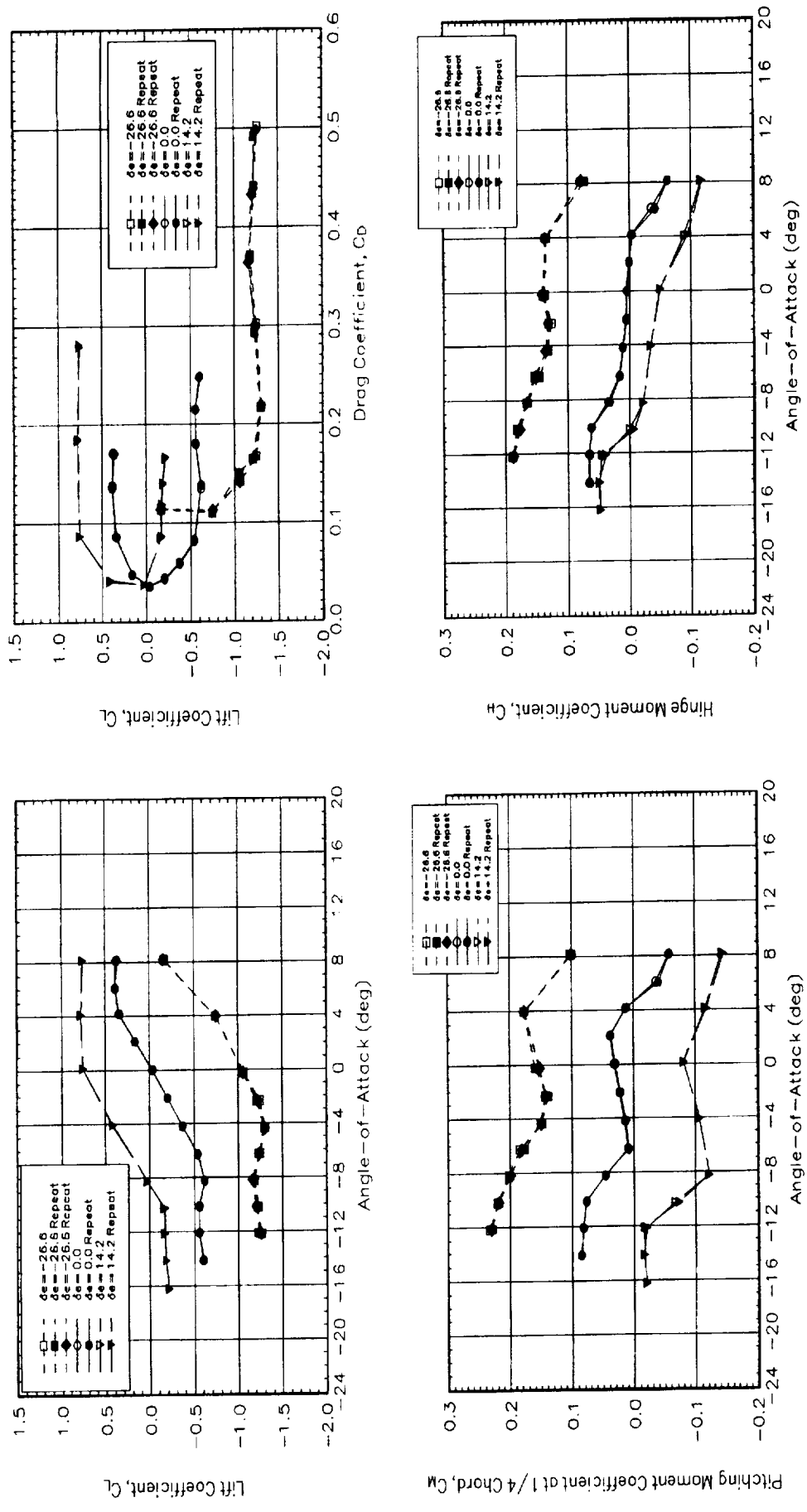

Figure F.36 Repeatibility, Lewice Ice Shape, Belt Taps

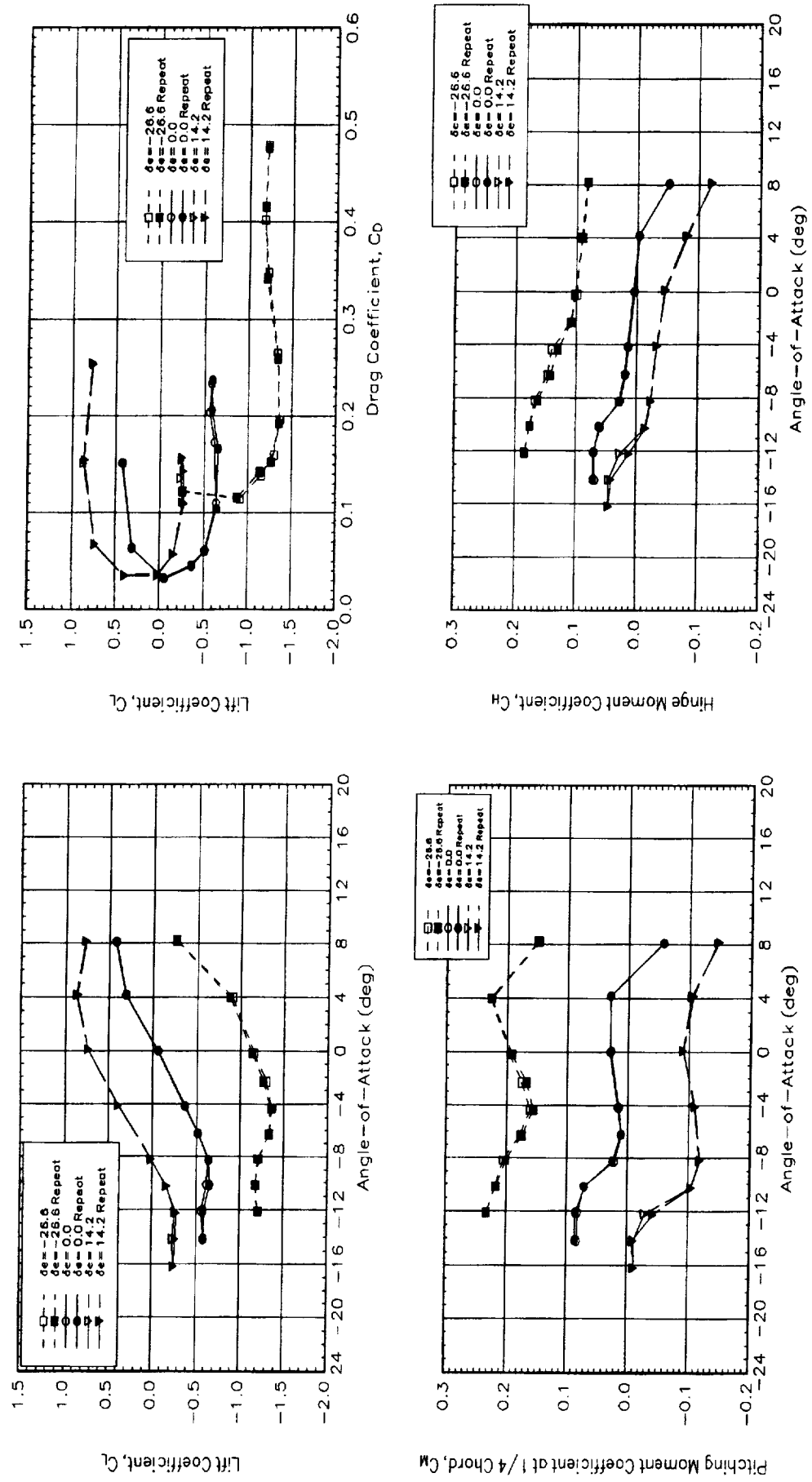

Figure F.37 Repeatability, S&C Ice Shape

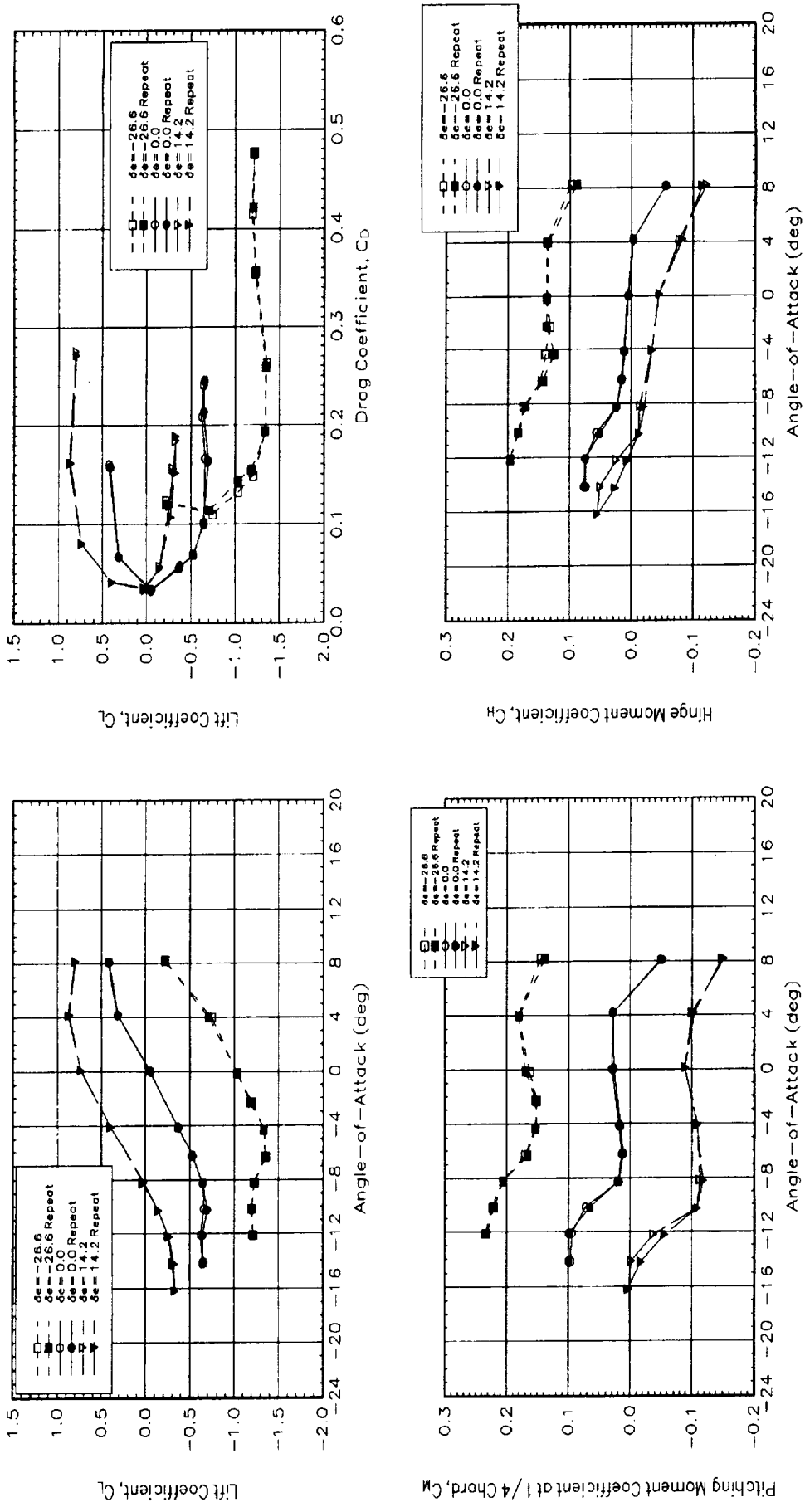

Figure F.38 Repeatability, S&C Ice Shape, Belt Taps

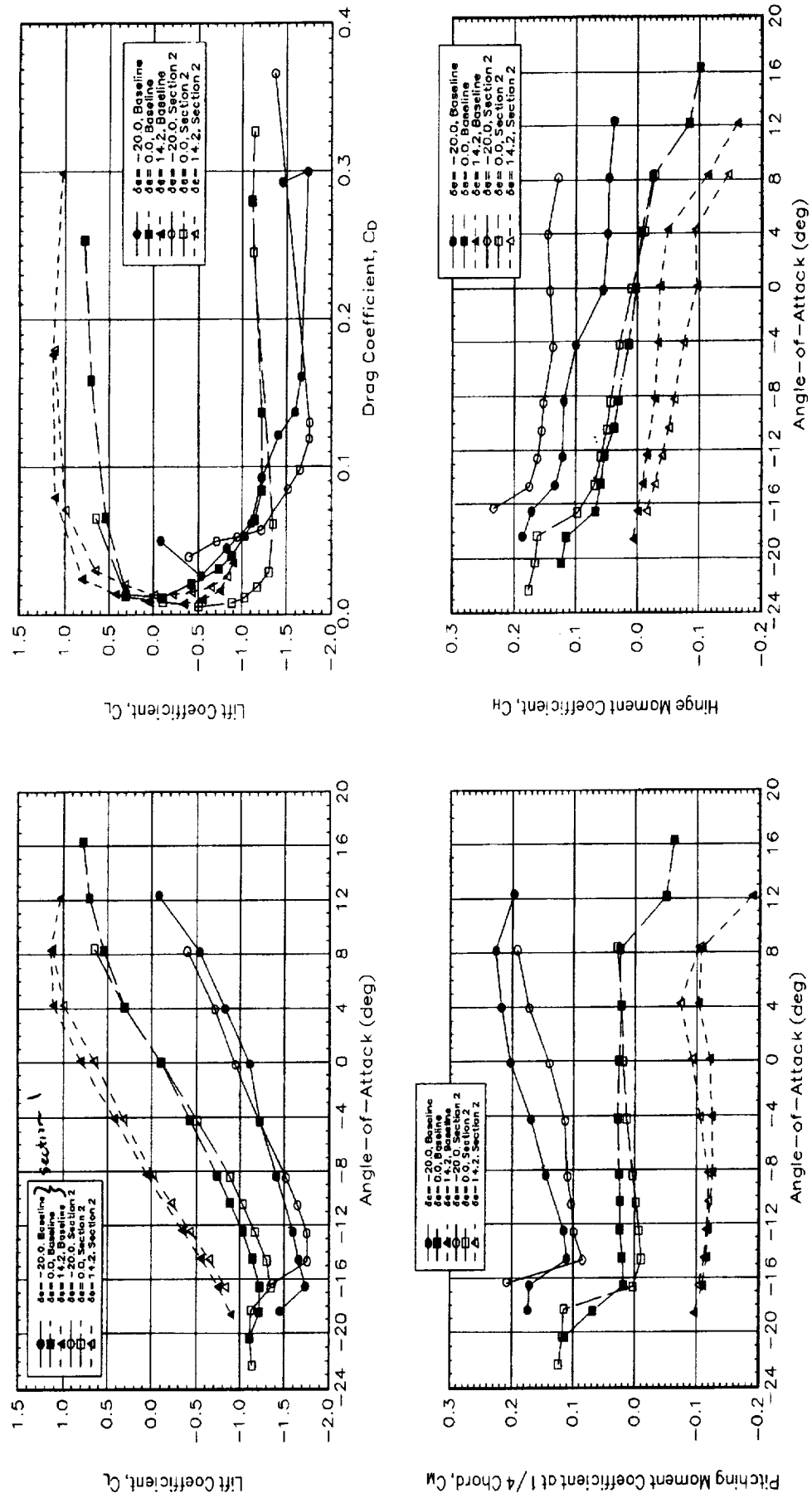

Figure F.39 Reference 2 Comparison, V=100 kts, Surface Taps

REPORT DOCUMENTATION PAGE

Form Approved
OMB No. 0704-0188

1. AGENCY USE ONLY (*Leave blank*)	2. REPORT DATE	3. REPORT TYPE AND DATES COVERED
	September 2000	Final Contractor Report

4. TITLE AND SUBTITLE

DHC-6 Twin Otter Tailplane Airfoil Section Testing in the Ohio State University 7x10 Wind Tunnel

5. FUNDING NUMBERS

WU–548–21–23–00
NAG3–1574

6. AUTHOR(S)

Dale Hiltner, Michael McKee, Karine La Noé, and Gerald Gregorek

7. PERFORMING ORGANIZATION NAME(S) AND ADDRESS(ES)

Ohio State University Research Foundation
1960 Kenny Road
Columbus, Ohio 43210–1063

8. PERFORMING ORGANIZATION REPORT NUMBER

E–12159–1

9. SPONSORING/MONITORING AGENCY NAME(S) AND ADDRESS(ES)

National Aeronautics and Space Administration
John H. Glenn Research Center at Lewis Field
Cleveland, Ohio 44135–3191

10. SPONSORING/MONITORING AGENCY REPORT NUMBER

NASA CR—2000-209921-VOL1

11. SUPPLEMENTARY NOTES

Project Manager, Thomas Ratvasky, Turbomachinery and Propulsion Systems Division, NASA Glenn Research Center, organization code 5840, (216) 433–3905.

12a. DISTRIBUTION/AVAILABILITY STATEMENT

Unclassified - Unlimited
Subject Categories: 02 and 05 Distribution: Nonstandard

This publication is available from the NASA Center for AeroSpace Information, (301) 621–0390.

12b. DISTRIBUTION CODE

13. ABSTRACT ***(Maximum 200 words)***

Ice contaminated tailplane stall (ICTS) has been found to be responsible for 16 accidents with 139 fatalities over the last three decades, and is suspected to have played a role in other accidents and incidents. The need for fundamental research in this area has been recognized at three international conferences sponsored by the FAA since 1991. In order to conduct such research, a joint NASA/FAA Tailplane Icing Program was formed in 1994; the Ohio State University has played an important role in this effort. The program employs icing tunnel testing, dry wind tunnel testing, flight testing, and analysis using a six-degrees-of-freedom computer code tailored to this problem. A central goal is to quantify the effect of tailplane icing on aircraft stability and control to aid in the analysis of flight test procedures to identify aircraft susceptibility to ICTS. This report contains the results of testing of a full scale 2D model of a tailplane section of NASA's Icing Research Aircraft, with and without ice shapes, in an Ohio State University 7×10 Low Speed wind tunnel in 1994. The results have been integrated into a comprehensive database of aerodynamic coefficients and stability and control derivatives that will permit detailed analysis of flight test results with the analytical computer program. The testing encompassed a full range of angles of attack and elevator deflections, as well as two velocities to evaluate Reynolds number effects. Lift, drag, pitching moment, and hinge moment coefficients were obtained. In addition, instrumentation for use during flight testing was verified to be effective, all components showing acceptable fidelity. Comparison of clean and iced airfoil results show the ice shapes causing a significant decrease in the magnitude of CLmax (from –1.3 to –0.64) and associated stall angle (from –18.6° to –8.2°). Furthermore, the ice shapes caused an increase in hinge moment coefficient of approximately 0.02, the change being markedly abrupt for one of the ice shapes. A noticeable effect of elevator deflection is that magnitude of the stall angle is decreased for negative (upward) elevator deflections. All these result are consistent with observed tailplane phenomena, and constitute an effective set of data for comprehensive analysis of ICTS.

14. SUBJECT TERMS	15. NUMBER OF PAGES
Aircraft icing; Tailplane icing; Airfoil performance	112
	16. PRICE CODE: A06

17. SECURITY CLASSIFICATION OF REPORT	18. SECURITY CLASSIFICATION OF THIS PAGE	19. SECURITY CLASSIFICATION OF ABSTRACT	20. LIMITATION OF ABSTRACT
Unclassified	Unclassified	Unclassified	